



UNIVERSITÀ DEGLI STUDI DI NAPOLI FEDERICO II

POLO DELLE SCIENZE E DELLE TECNOLOGIE

DOTTORATO IN RISCHIO SISMICO

-XVIII CICLO-

MECHANICAL BEHAVIOUR OF A NEAPOLITAN PYROCLASTIC SAND UNDER MONOTONIC AND CYCLIC LOADING

TESI PER IL CONSEGUIMENTO DEL TITOLO

ANGELINA PARLATO

RELATORE:

NAPOLI, DICEMBRE 2006

PROF. FILIPPO SANTUCCI DE MAGISTRIS

COORDINATORE DEL DOTTORATO:

PROF. PAOLO GASPARINI

CONTENTS

Chapter 1	1.2
1.1 Introduction.....	1.2
1.2 The triaxial chamber.....	1.3
1.3 The load application system	1.3
1.3.1 The axial load application system	1.3
1.3.2 The pressure application system	1.6
1.4 The Transducers	1.6
1.4.1 Measuring the deviator stress: the load cell.....	1.6
1.4.2 Measuring the pressure	1.7
1.4.3 Measuring the volume strain.....	1.9
1.4.4 On the importance of measuring axial strains locally	1.9
1.4.5 Measuring the axial strain.....	1.10
1.4.6 Data acquisition.....	1.14
1.4.7 Automatic control system	1.14
1.5 "MaTRIX" SOFTWARE	1.14
Chapter 2	2-1
2.1 Introduction.....	2-1
2.2 The Pyroclastic sand from San Pantaleone.....	2-3
2.3 – Grain size distribution and index tests.	2-5
2.4 Pre-treating of the material	2-9
2.5 Preparation Techniques for compacted specimens.....	2-10
2.5.1 Moist Tamping Method.....	2-10
2.5.2 Proctor.....	2-13
2.6 Specimen prepared in the Consolidometer.....	2-13
2.6.1 Water sedimentation and freezing	2-15
2.7 Specimen Trimming procedure	2-16
2.8 Dry Deposition Method	2-17
Chapter 3	3.1
3.1 Introduction.....	3.1
3.2 Specimen setting by the "dry setting method"	3.2
3.3 Saturation.....	3.4
3.3.1 Flushing.....	3.4
3.3.2 Connection to the loading system.....	3.5
3.3.3 Back Pressurization	3.5
3.4 Consolidation	3.5
3.5 Cyclic loading	3.6
3.6 Undrained shear.....	3.8
3.7 Triaxial data interpretation	3.9
3.8 Tests performed at very low confining stress	3.9
3.8.1 Latex membrane confining effect	3.10
3.8.2 Filter paper stiffness	3.11
3.8.3 Specimen self weight effect	3.12
3.8.4 Base friction	3.12

Chapter 4	4-1
4.1 The experimental program	4-1
4.2 Behaviour of the material under isotropic stress conditions	4-7
4.3 Shear tests	4-13
4.3.1 Behaviour of specimen reconstituted in the consolidometer	4-13
4.3.2 Behaviour of specimen prepared with Proctor.....	4-17
4.4 Undrained shear tests over specimen reconstituted with different techniques: flow liquefaction susceptibility	4-20
4.5 Undrained shear tests over specimen reconstituted with different techniques: critical state behaviour	4-27
Chapter 5	5-1
5.1 Introduction.....	5-2
5.2 Soil Stiffness	5-2
5.3 Young modulus	5-5
5.4 Experimental results	5-8
5.4.1 Small strain stiffness	5-8
5.4.2 Influence of the load frequency	5-12
5.4.3 Young modulus evaluated during shear: influence of the mean deviator stress	5-13
5.4.4 Influence of cyclic load amplitude	5-14
5.4.5 Pore pressure development	5-15
5.5 Cyclic strength of San Pantaleone Pozzolana.....	5-19

Conclusion

Appendix 1

Introduction

0.1 Objective and outline of the research

In the evaluation of seismic risk impending on a site, various scientific figures and capabilities are involved. Geotechnical engineers, in particular, are involved in the evaluation of the local amplification of a site.

To this end it is important to know the parameters that characterize the dynamical properties of a soil, from the deepest layers up to the superficial layers.

The behaviour of superficial soil is important in the study of the dynamic response of a site. Superficial soils, being very loose and thus very compressible, play an important role in the local amplification of the seismic input. Moreover, while studying the stability of natural slopes, the mechanical properties of the superficial soil, generally prone to landslide risk, is very important. Furthermore, the superficial, loose layer is the one involved in the evaluation of liquefaction susceptibility.

The authors' opinion on the soil behaviour at very low confining stress is quite discordant. Whilst Ponce and Bell (1971) found a marked variation of the friction angle and of the material compressibility, Fukushima and Tatsuoka (1984) sustain that no variation in the friction angle and in the compressibility takes place at low confining stress. Koseki et al.(2001), on the other way, studying the effect of confining stress on liquefaction susceptibility, show that the sand they studied has a more dilatative behaviour at low confining stress. Henkel and Gilbert (1952) have measured significant variation of the stress-strain behaviour of clays at very low confining stresses.

In the course of this Phd thesis, the mechanical behaviour of a Neapolitan pyroclastic soil, under monotonic and cyclic loading condition, has been studied. The soil was prepared, using different reconstitution techniques, in loose and dense samples, and was tested at very low to medium confining stress.

In the following are listed the topics that main have been investigated in the course of this doctoral thesis:

1. influence of the reconstitution technique on the mechanical behaviour of soil samples;
2. the mechanical behaviour of San Pantaleone Sand at very low confining stress;
3. the mechanical behaviour of San Pantaleone Sand from small strain up to failure;
4. Influence of state parameter on soil stiffness;
5. the mechanical behaviour of San Pantaleone Sand in cyclic loading tests, in order to evaluate cyclic strength.

0.2 Layout of the thesis

The structure of this Phd thesis can be summarized as follows:

- In the first chapter the experimental apparatus used has been described; in particular, emphasis has been put in the description of the triaxial apparatus MaTRIX: in the description of his functioning parts and of the machine set up during tests.
- In the second chapter the material tested in this doctoral thesis ha been described, together with the various experimental procedures adopted to reconstitute the soil specimen.
- In the third chapter the procedure used for setting up the specimens in the triaxial machine have been described step by step. The Saturation phase by dry setting method has been illustrated in details. The procedures related with the execution of the consolidation phase and the shear phase are also discussed.
- In the forth chapter the mechanical behaviour, in terms of compressibility and pre-failure behaviour of the material has been analyzed.
- In the fifth chapter, San Pantaleone sand small strain stiffness has been studied, together with stiffness degradation. Moreover, its cyclic strength has been studied.

Chapter 1

The triaxial testing system “MaTRIX”

1.1 Introduction

All the tests executed in the course of this PhD thesis have been realized on stress path controlled automated triaxial cells. In particular, two apparatus owned by the soil dynamic laboratory of the University of Naples have been used.

Tests performed on 1D consolidated specimens were executed mainly in the Bishop and Wesley triaxial machine (Bishop and Wesley, 1975). This apparatus will not be described in this thesis, since it is already well known (Santucci de Magistris, 1992).

The other tests were executed on MaTRIX triaxial cells: the Department of Geotechnical Engineering of the University of Naples Federico II, has recently bought four automated triaxial apparatus, designed at the University of Tokyo (Tatsuoka et al., 1994, Santucci de Magistris et al., 1999). This advanced machine is widespread in Japan, but very uncommon in Europe, where only a few machines have been adopted.

The basic components of which MaTRIX is made up are: a triaxial cell, a unique mechanical axial loading system and several transducers, connected through A/D and

D/A cards to a microcomputer that controls the tests and records the data (Tatsuoka 1988). In Figure 1-10 is illustrated a scheme of the machine.

In the course of this chapter the main parts that constitute MaTRIX will be described in detail.

1.2 The triaxial chamber

The triaxial chamber, (in which the soil specimen is placed) is put inside an iron frame, which supports the motor and contrasts the advancement of the ram in its application of the deviator stress.

The pressure cell has a cylindrical shape, and is made up of Plexiglas, reinforced with aluminium bands at its ends. The interposition of two o-rings makes the cell water proof.

The internal steel structure is constituted by a frame made up of two horizontal plates held by three tie rods. On the lower plate is placed a cylinder that acts as the specimen pedestal. Over the specimen is set out the top platen (cap), a steel cylinder integral with the loading shaft.

The specimen assembling stage can seriously spoil the results of tests performed in conventional apparatus. The MaTRIX triaxial cell was designed to reduce the disturbance in the soil specimen during this stage. The operator can work with the cell open: he can put easily the specimen in place, and can put the cap over the specimen by hand, allowing for a correct alignment between the loading piston, the sample cap, and the sample.

A drainage is placed both on the upper and on the lower base: this expedient has two major advantages: it helps reducing specimen consolidation time, and it allows the specimen saturation to be performed inside the cell.

MaTRIX can house cylindrical specimens with a diameter of 50mm and a height that is typically of 100 mm.

1.3 The load application system

For an accurate control of the stress path, this machine is equipped with an advanced axial loading device and an electro-pneumatic pressure regulator system.

1.3.1 The axial load application system

The system adopted for MaTRIX allows one to :

- Maintain a constant strain rate;
- Execute very small unload-reload cycles with an axial strain amplitude of the order of 0.001% or less, without a noticeable time lag when reversing the loading direction.

The loading device was designed to automatically switch the motor on and off and select the upward and downward loading shaft direction through a personal computer and a D/A card.

By means of a simple control loop, it is then possible to maintain a constant deviator stress during transient stages like consolidation processes or creep tests, by setting the prescribed axial displacement rate to be higher than that at which the specimen would tend to axially deform under the imposed stress state.

The motor is connected through a series of speed-reduction gear boxes to the axial loading shaft (Figure 1-1). The peculiarity of the system is the way the loading shaft can change his direction. In fact, the motor always rotates in the same direction, and transmits his movement to the gears G2, G3, G4 and G5. The electromagnetic friction EMC has the task to connect the shaft alternatively to G2 or G5: in fact these two gears rotate in opposite directions, thus transmitting an opposite movement to the shaft. Thanks to this system, the movement of the specimen cap results to be very sharp in the changing of loading direction.

The loading device is driven by an a-c servo motor (Wako Giken Co. Ltd., model 002C) equipped with a digital servo driver (Wako Giken Co. Ltd., model AFS-4). The high performances of this loading device are mainly due to the feedback system of the a-c servo motor: an electrical encoder is attached to the motor body in order to measure the position and the rotation rate of the rotor; the digital servo driver compares the current status with the target condition and updates the driving signal of the motor, if required. The motor can control the rotation rate, the position of the rotor or the torque. For the test results described later, the rotation rate control was adopted.

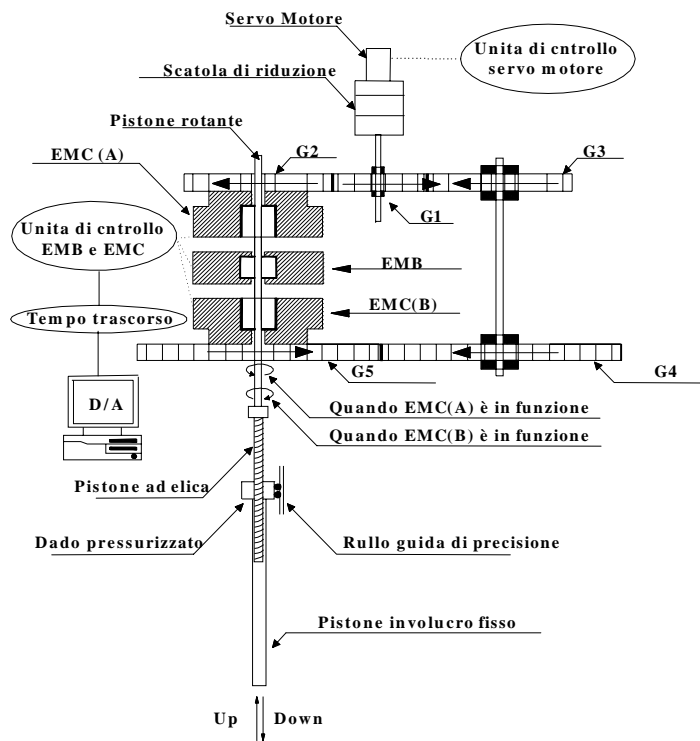


Figure 1-1 A scheme of the axial load application system.



Figure 1-2 Axial load application system.

1.3.2 The pressure application system

A high pressure line from an air compressor is fed into a 800 kPa pressure regulator to maintain steady the pressure of the air supplied.

The cell pressure is regulated by an electro-pneumatic transducer (Fujikura Transducer Mod. RT: E/P) that receives the commanding signal from a computer. Alternatively, cell pressure can be controlled by a manual regulator (Fairchild).

By now, the pore pressure is controlled only through a manual regulator.

1.4 The Transducers

1.4.1 Measuring the deviator stress: the load cell

The load cell used in the present study, designed at the University of Tokyo is pressure-insensitive; i.e., the reading (output voltage) from the load cell does not change with changes in the cell pressure. Moreover, to eliminate the effects of piston friction, it is placed inside the triaxial cell.

This load cell is made of a very stiff material (i.e., phosphor bronze) and is essentially non-compressible when subjected to changes in the cell pressure σ_c within the range in the present study (i.e., $\sigma_c=0\sim600\text{Kpa}$), which is negligible compared to the compressive strength of the load cell material.

The effects of the self-weight of the load cell on the signal can be trimmed off by reading the initial state with zero output when the top cap is connected to the bottom of the load cell and placed in the triaxial cell as in the triaxial compression tests.

Forces applied on the load cell induce deformation in the top weakened part of the transducer, to which four electrical resistance (ER) strain gauges in a full Wheatstone bridge are attached (Figure 1-3). Thus the load cell deformation is directly connected both to the output voltage and to the axial force.

Through calibration, it is possible to correlate each voltage variation to the relative axial load increment.

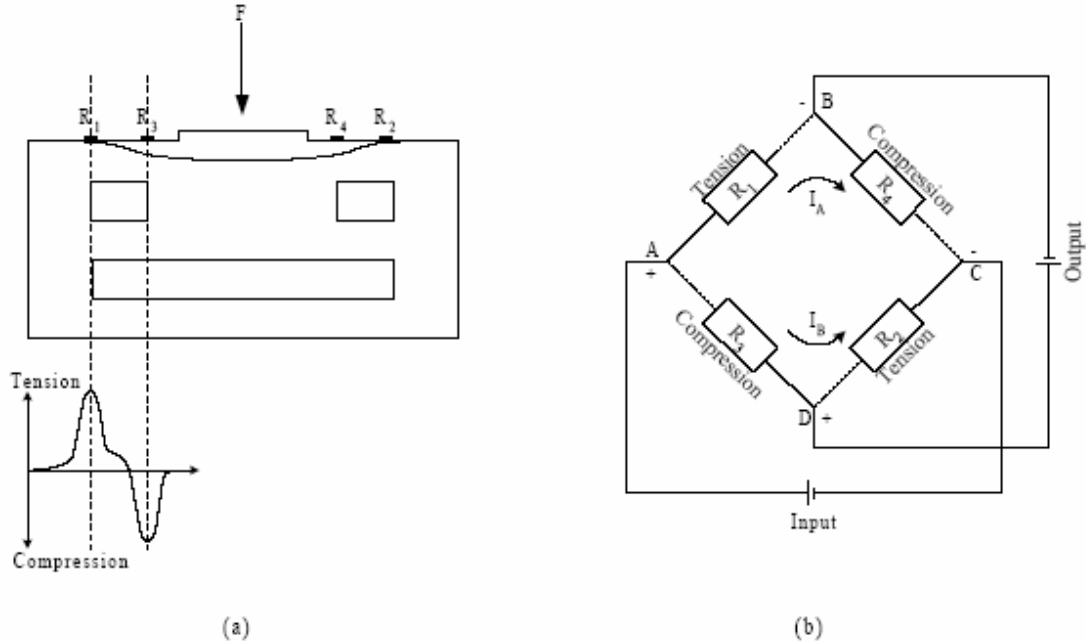


Figure 1-3 a)The axial load induces a deformation in the load cell; b) strain gauges glued to the load cell.

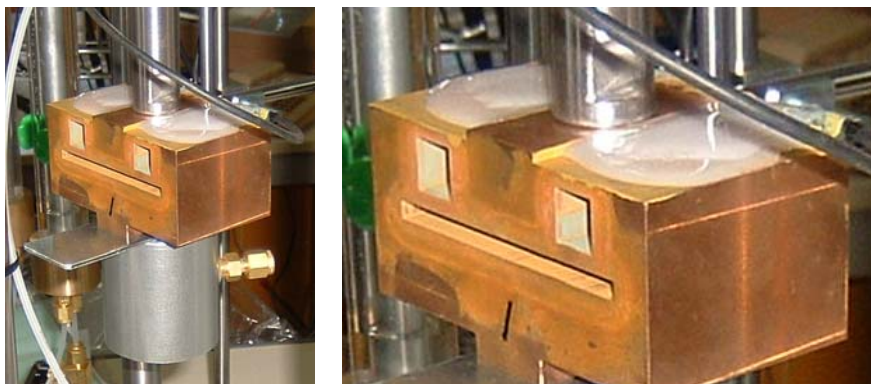


Figure 1-4 A picture of the load cell installed in MaTRIX cell 1.

The measures performed with strain gauges arranged in a full weathstone bridge are not being affected by load eccentricity and by temperature variations.

1.4.2 Measuring the pressure

The effective confining pressure is measured accurately and directly through a liquid-liquid High Capacity Differential Pressure Transducer (HCDPT) produced by Fuji Electric (FCX-A type FCH/I).

The two channel of HC-DPT are connected respectively to the pore pressure water and to the cell pressure water (Figure 1-5).

The generalized equation for the evaluation of the effective confining pressure acting at every level in a saturated sample is given by:

$$\sigma'_r = p_h - u + \Delta\sigma_{rm}$$

Equation 1-1

where:

- $p_h = \sigma_c + (h_{cl} + h_{DP}) \gamma_w$

Liquid pressure applied on the high pressure face of the HC-DPT

- σ_c

Cell air pressure

- h_{cl}

Height of cell water from the sample bottom

- h_{DP}

Distance of HC-DPT down form the specimen bottom

- γ_w

Unit weight of water

- $u = \sigma_{BP} + (h_B + h_{DP}) \gamma_w$

Pore water pressure applied on the low pressure face of the HC-DPT

- σ_{BP}

Back air pressure

- h_B

Height of burette water surface from the sample bottom

- $\Delta\sigma_{rm}$

Stress correction for membrane forces

On the other end, the pressure measured by HCDPT is :

$$\Delta P = p_h - u$$

Equation 1-2

Consequently, the value of σ'_r is obtained as:

$$\sigma'_r = \Delta P - \Delta\sigma_{rm}$$

Equation 1-3

This measuring method is very effective especially for a test at a high back pressure and small confining pressure, because the resolution in the output of DPT is independent of the back pressure whereas the accuracy of measured value of σ'_r decreases when the pressures p_h and u are measured separately.

MaTRIX, in the present configuration, is equipped to measure only the effective confining stress. It is not possible to measure pore pressure and cell pressure separately.

1.4.3 Measuring the volume strain

The volume change measurement method adopted is illustrated in Figure 1-5. It utilizes a low capacity differential pressure transducer (LCDPT) from Fuji Electric (FCX-A type FHC/I). This instrument is directly connected to a double burette system: a very useful trick to compensate for water evaporation assuming that the rate of water evaporation is probably the same in the two burettes.

One burette is used to give a reference level for the reading of LCDPT, the other one is directly connected with the specimen pore water.

A back pressure is applied to water inside burettes. The pressure helps dissolving air (if present) in the pore water fluid, thus improving the quality of the measure, and helps reducing the evaporation phenomenon.

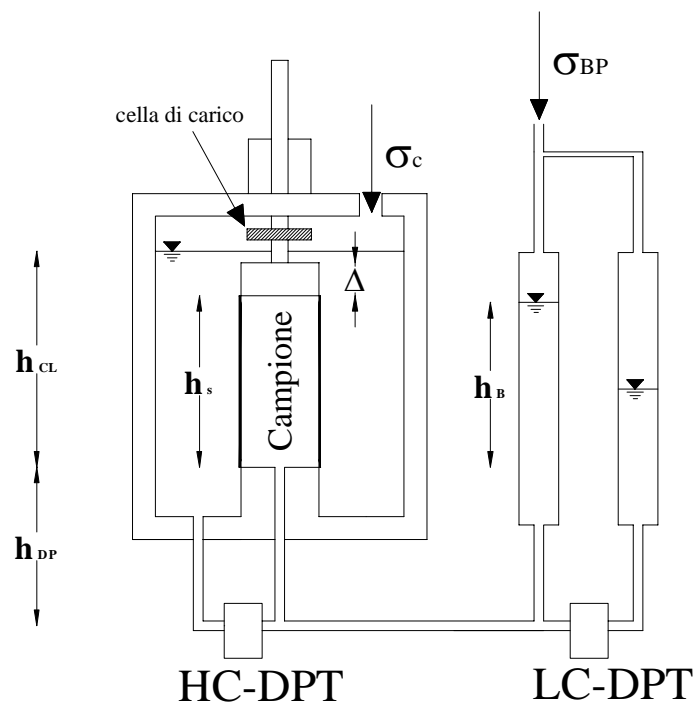


Figure 1-5 HCDPT and LCDP working scheme.

1.4.4 On the importance of measuring axial strains locally

The importance of measuring axial strains locally is widely recognized in the geotechnical community.

It is almost 20 years since it has been proved that external axial strain measurement is subjected to many experimental errors. In Figure 1-6 Figure 1-6 are schematized the main error source that can affect external axial strain reading. Because of these errors, the axial strain resulting from conventional external axial strain measures is

bigger than the real axial strain. Therefore, stiffness measured in the conventional way results is lower.

Experimental errors can be caused by axial loading system deformation, from load cell deformability or from filter paper and porous stones settlement. But the principal cause of errors are bedding errors, that are due to imperfect setting of the specimen between pedestal and top cap.

To avoid these experimental errors, it is necessary to measure axial strain directly on specimen lateral surface.

In many research works (Tatsuoka and Shibuya, 1992; Tatsuka and Kohata, 1995) it has been underlined that the use of a local deformation transducer bring to the evaluation of higher Young modulus, close to those measured in situ.

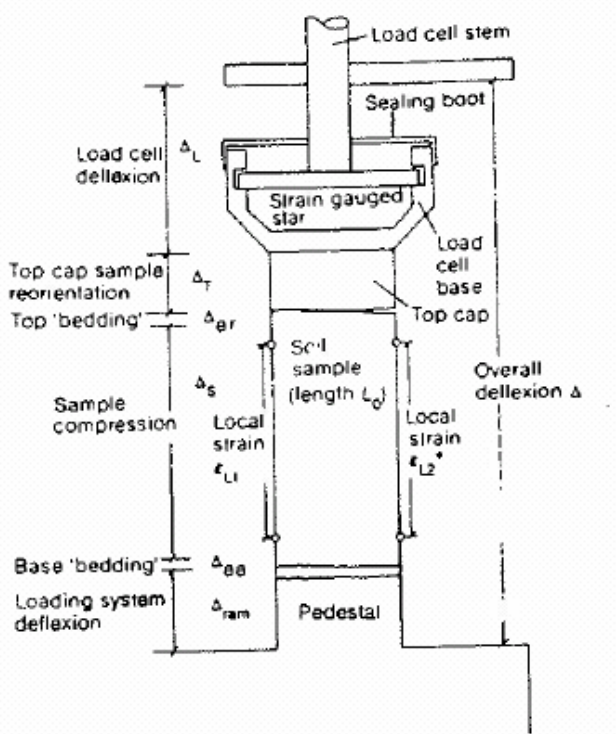


Figure 1-6 Main error sources in external measure of axial strain (from Jardine et al., 1984).

1.4.5 Measuring the axial strain

MaTRIX is endowed with three different devices to measure axial strain.

- LVDT (Linear Vertical Displacement Transducer)

Produced by Kanetec, this instrument has a maximum measuring range of 40 mm; its output voltage is ± 5 Volt.

- Gap Sensor

A proximity transducer AEC-5509 (Applied Electronics Corporation) placed in opposition with a steel target integrated with the top cap; The electromagnetic field produced by the instrument changes with the changing in its distance from the target.

The Gap Sensor MaTRIX is equipped with, has a maximum measuring range of 2 mm.

- LDT (Local Deformation Transducer)

In triaxial specimens it is crucial to measure "local" strain in order to exclude the bedding error from the measurement. The term "local" herein implies a sort of averaged strain determined over a certain length of the soil specimen (Goto et al., 1991).

In this study Local Deformation Transducers (LDTs) designed and realised in the geotechnical engineering laboratory of the University of Tokyo have been used.

Each LDT consists of a thin, flexible strip of heat-treated phosphor bronze on which are attached electrical resistant strain gauges. The strip is held in place by a couple of pseudo-hinged attachments.

Since the working principle of LDT is based on the elastic buckling deformation of the carrier strip, a heat-treated phosphor bronze strip was used, according to its highly elastic behaviour (cf., Young's modulus is 1.2×10^6 kgf/cm²). This treated phosphor bronze can withstand axial buckling without permanent deformation. The strain gauges currently in use have a resistance of 120 W with the grid dimension of 0.68 mm wide and 1 mm long and the elastic limit strain of 5% (Kyowa KFG-1N-120-C1-16).

Each LDT is hold at both ends of the strip by a pair of pseudo hinges aligned on the surface of the specimen. The distance between the two hinges has to be slightly shorter than the length of the strip, so that the strip will be hold in place by its own elastic force against the hinges. Before starting the further procedures of the test, LDTs were kept in place on the specimen for at least 45 minutes, i.e. until the rate of creep deformation at the hinges would become negligible.

Connecting the strain gauges in a full Wheatstone bridge theoretically minimizes the effect of temperature fluctuation on the change of the gauge strain. However, the temperature fluctuation inside the triaxial cell, caused by the change in room temperature or by introducing water into the cell, can affect dimension of the

specimen and also of the LDT strip. This change, usually, cannot be correctly detected by LDTs (Hoque et al., 1997). By the way, the tests described within this thesis were performed in a controlled room temperature (i.e., the room was air conditioned with no severe fluctuation of the temperature).

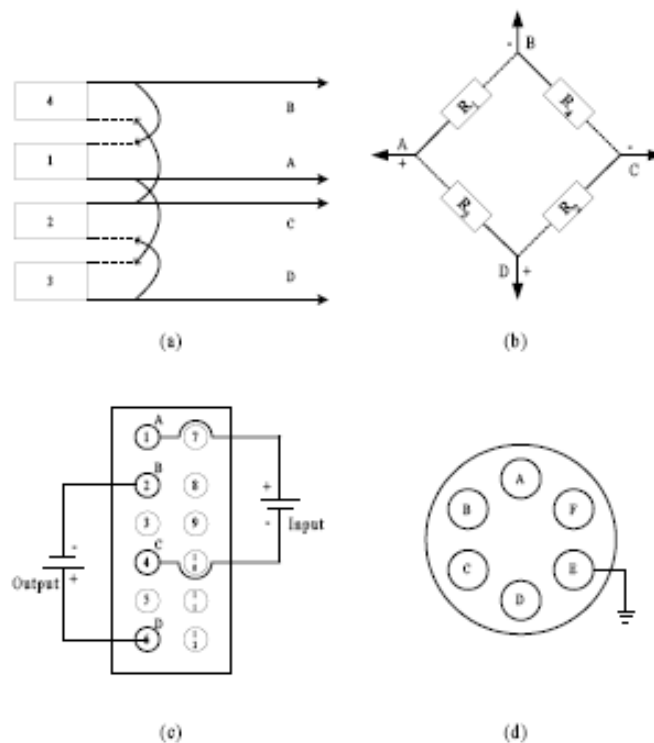


Figure 1-7 A circuit of a full Wheatstone bridge for longitudinal LDTs; (a) & (b) four strain gauges were connected in circuit; (c) & (d) the connection between LDT and the amplifier.

The concept of using the electrical resistance strain gauges connected in a circuit of a full Wheatstone bridge, attached on LDT, is similar to that in the case of the load cell. The electric circuit of connected strain gauges of LDT are shown in Figure 1-7 four strain gauges were attached on both sides of the bronze strip (two strain gauges on each side). Two additional electrical resistors of 120W were used in place of the other two strain gauges to form a circuit of a full bridge. These two additional electrical resistors, in this case, were attached on the lead wires of the LDT.

When the specimen buckles, the distance between the two LDT ends changes and the strain gauges deform, resulting in a change of the output voltage. Going this way, the specimen strain can be associated to the detected output through calibration.

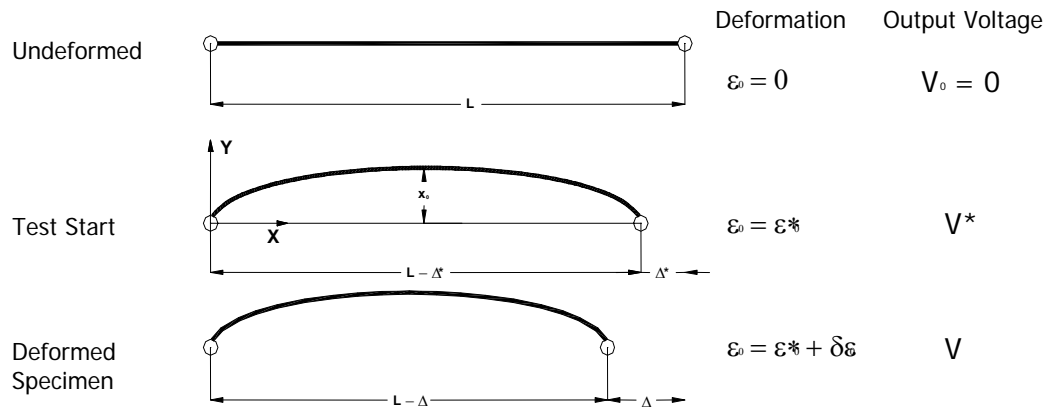


Figure 1-8 LDT deformation sequence.

In Figure 1-8 is illustrated the deformation sequence that LDTs undergo. Here:

- L is the LDT length, in undeformed conditions
- Δ is the relative strain

Referring to a Cartesian system centred in one of the elastic strip end, the curvature can be expressed by the equation:

$$\varepsilon_0 = (\pi / l) \sqrt{(\Delta / l)} \sin\{\pi x_0 / l\} \quad \text{Equation 1-4}$$

Where t is the thickness of the strip. In the case of LDT, ε_0 is to be calculated over $x_0 = l/2$; the deformation Δ is connected to ε_0 by the relation (Goto et al., 1991):

$$\Delta = \left\{ (L - \Delta)^3 / (\pi t)^2 \right\} \varepsilon_0^2 \quad \text{Equation 1-5}$$

The specimen axial deformation, ε_a , can be obtained by:

$$\varepsilon_a = -\ln\left\{1 - (\Delta - \Delta_1) / GL\right\} \quad \text{Equation 1-6}$$

where:

Δ_1 is the value of Δ when $\varepsilon_a = 0$

$GL = L - \Delta_1 - B$, where B is the initial distance between the two hinges.

The calibration curves of the eight LDTs used in this study are shown in Appendix II. It was observed that the LDTs calibration curves are not linear. However, all of the curve could be fitted by second order polynomial regression with the statistically satisfaction of a correlation coefficient, R^2 , of in between 0.99 and 1.

1.4.6 Data acquisition

The transducers "Matrix" is equipped with, have various output voltage. The output signal is sometimes connected to an external amplifier, sometimes is directly amplified by the instrument itself. In this way the output signal can be fitted in a range (± 5 Volt) consistent with the A/D card used.

LDTs, Load cell and LVDT use an external "Strain Amplifier-Kyowa" (mod. DPM 601-A). Instead, Gap sensor and DPT have an internal amplifier.

1.4.7 Automatic control system

MaTRIX control and data acquisition system is based on a computer on which is installed an A/D 16 bit (Contec AD 16-16(PC)EH) card and a D/A 8 bit (Contec AD 12-6(LC)PC) card. both cards are endowed with 8 differential or 16 absolute channels.

1.5 "MaTRIX" SOFTWARE

The software used for controlling "Matrix" has been developed during the present Phd Thesis. It has been written in Visual Basic, an object language very easy ad friendly.

The programme is capable of transforming the voltage output from transducers in physical data, passing through the calibration constants. Basing on the data received from the machine, it is able to run the load application system and the pressure application system in order to obtain the desired stress path.

The data acquisition speed is subjected to the frequency of computer internal clock, and in the present case is around 1/10 sec.

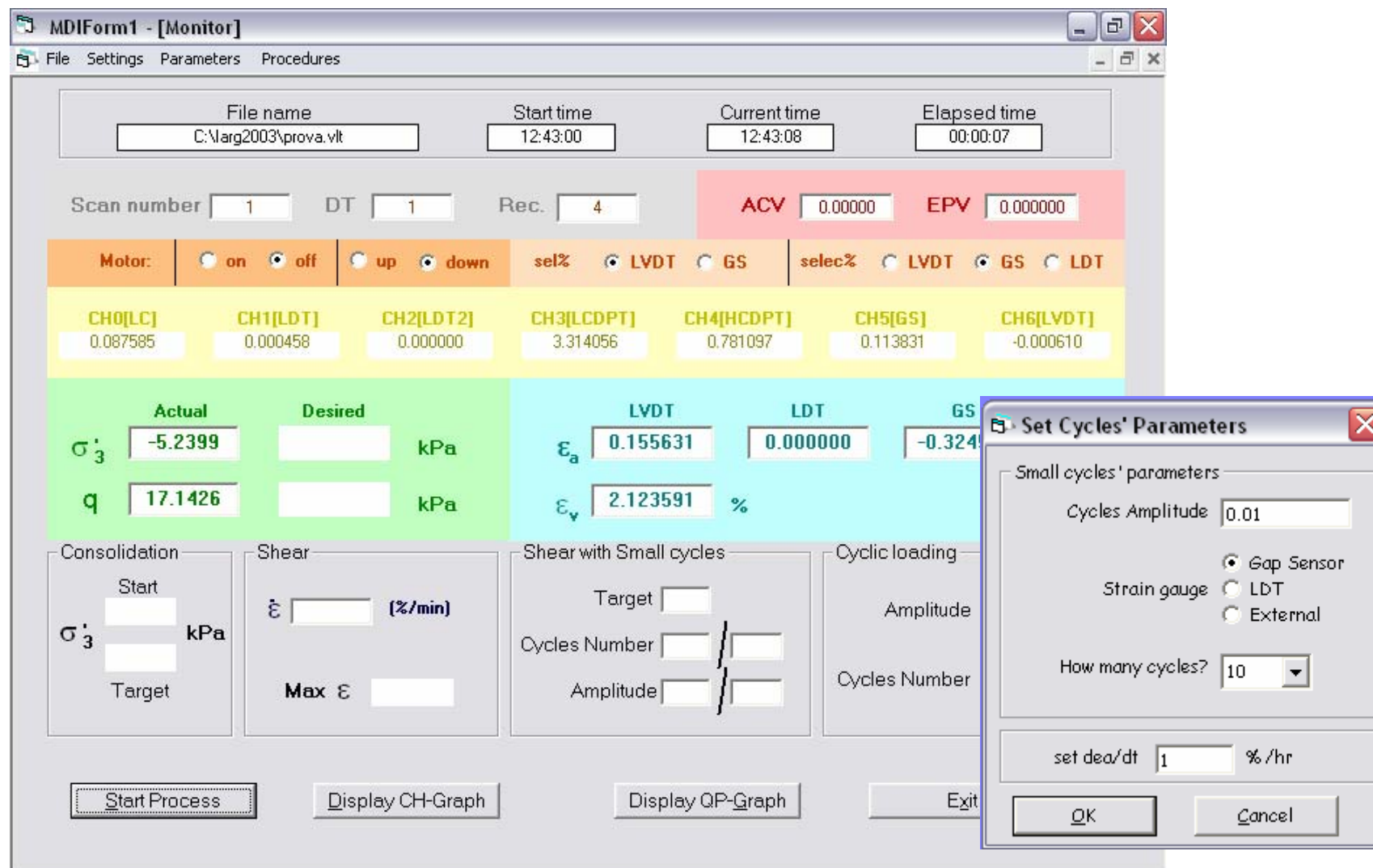


Figure 1-9 The matrix computer programme as it appears in phase of execution.

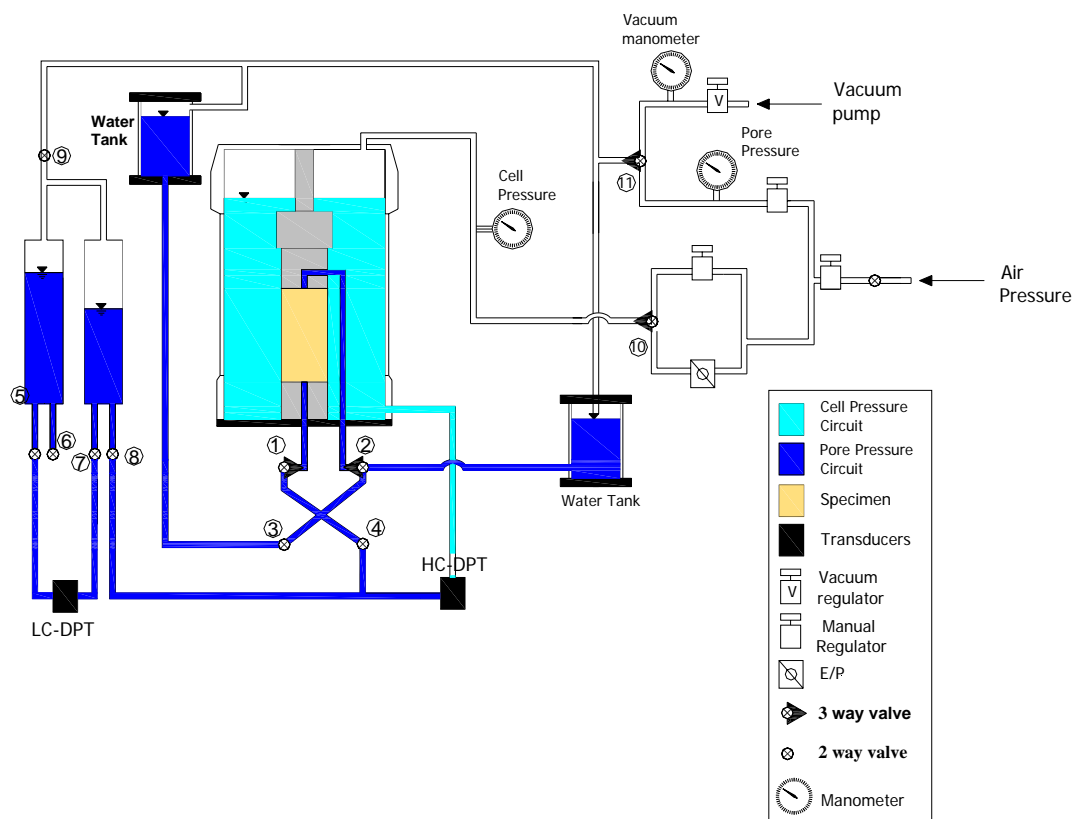


Figure 1-10 Functioning scheme of triaxial cell "MaTRIX"

REFERENCES

- Aversa, S. e Vinale, F.(1995), **Improvements to a stress-path triaxial cell**, ASTM Geotechnical Testing Journal, 18(1), 116-120.
- Bishop, AW. e Wensley, LD.(1975), **Hydraulic triaxial apparatus for controlled stress path testing**, Geotechnique, 25(4), 657-670.
- Goto S., Tatsuoka F., Shibuya S. Kim YS, Sato T. (1991), **A simple gauge for local small strain measurement in the laboratory**, Soils And Foundation; 31(1):169-180.
- Jardine R.J., Symes M.J. and Burland J.B. (1984), **The measurement of soil stiffness in the triaxial apparatus**, Geotechnique; 34(3): 323-340.
- Kongsukprasert, L.(2000), **Effects of ageing on stress-strain behaviour of cement-mixed sand**, Tesi di Master, Tokyo University.
- Parlato, A. e Santucci de Magistris, F. (2003), **Confronto tra una cella triassiale a stress path controllato ed una cella "TXJ"**, IARG incontro nazionale dei ricercatori di geotecnica, Potenza 2003.
- Santucci de Magistris, F. (1992): **Una cella triassiale a stress path controllato: messa a punto e primi risultati sperimentali**, Bachelor Thesis, Università degli studi di Napoli Federico II. (In Italian).
- Santucci de Magistris, F., Koseki, J, Amaya, M, Hamaya, S, Sato, T, Tatsuoka, F (1999), **Triaxial testing system to evaluate stress-strain behaviour of soils for wide range of strain and strain rate**, ASTM Geotechnical Testing Journal, 22(1), 44-60.
- Tatsuoka, F. (1988), **Some recent developments in triaxial testing systems for cohesionless soils**, Keynote lecture, ASTM special Technical Publication No.977, pp.7-67.
- Tatsuoka, F. Shibuya, S. (1992): **Deformation characteristics of soil and rocks from field and laboratory tests**, Report of the institute of Industrial science, The University of Tokyo Vol. 37 No. 1-235.
- Tatsuoka, F, Sato, T, Park, CS, Kim, YS, Mukabi, JN, Kohata, Y (1994), **Measurements of elastic properties of geomaterials in laboratory compression tests**, ASTM Geotechnical Testing Journal, 17(1), 80-94.

Tatsuoka, F. and Koata, Y.(1995): **Stiffness of hard soils and soft rocks in engineering applicatons**, Report of the institute of Industrial science, The University of Tokyo, 38(5): 235.

Chapter 2

Material and Reconstitution techniques

2.1 Introduction

The description of the material tested in this doctoral thesis, and the various experimental procedures adopted to reconstitute the soil specimen, will be the subject of this chapter.

When using laboratory reconstituted specimen, the choice of the preparation technique is of great importance. In fact, the mechanical behaviour (in terms of compressibility and stiffness) of the specimen is strongly influenced by the preparation technique.

In this study, many different reconstitution techniques have been used. Moreover, some tests were performed on natural samples.

In the course of this chapter, some attention will also be paid to the description of the saturation techniques used.

2.2 The Pyroclastic sand from San Pantaleone

The soil tested in the course of this thesis has a pyroclastic nature. This material is very common in the outskirts of Naples (south Italy), since it derives from the activity of the Vesuvius Volcano.

The material used in this experimentation was taken from a site interested by a flow slide that took place in 1997 (Fenelli, 1997). The flow slide triggered at level with one of the upper hairpin bend of a street that climbs up a hill that stands on the Nocera tollbooth of Napoli-Salerno Highway.

Two experimental campaign have been undertaken in order to borrow the material needed for the characterization of San Pantaleone Soil. The sites interested by the investigation are indicated in Figure 2-1

Undisturbed samples were taken using cylindrical samplers ($\phi=20\text{cm}$, $H=20\text{cm}$), pressed horizontally in an exposed trench (Figure 2-1) constituted of soil that underwent one of the flowslides cited above. In particular, the soil was part of the deposition zone of the slide.

The remoulded material utilized to evaluate the physical properties of the soil and to prepare reconstituted specimens, was taken by the same working face (Figure 2-2).

In order to reconstruct the stratigraphy in correspondence of the working face from which the specimen were taken, the outcropping trench has been analyzed.

From the bottom to the top the following layer have been singled out:

- fractured calcareous rocks;
- volcanic ashes (A) fine grain size, homogeneous, colour from light brown to yellow;
- pumices (B) lightly disturbed, grain size close to gravel;
- pozzolana (C) colour light brown, containing some roots apparatus;
- pyroclastic layer(D), containing a thick roots network, deriving from shrubs growth.

The ashes layer, thanks to its grading curve in which the fine content prevails, is capable to preserve its water content almost unchanged also on summer.

The pumices layer, is not present everywhere along the slope: not in the steepest zones, were the flowslide is triggered.

The disturbed soil comes from the loose soil layer that covers the calcareous soil, while the undisturbed soil was taken from the ashes layer (A).

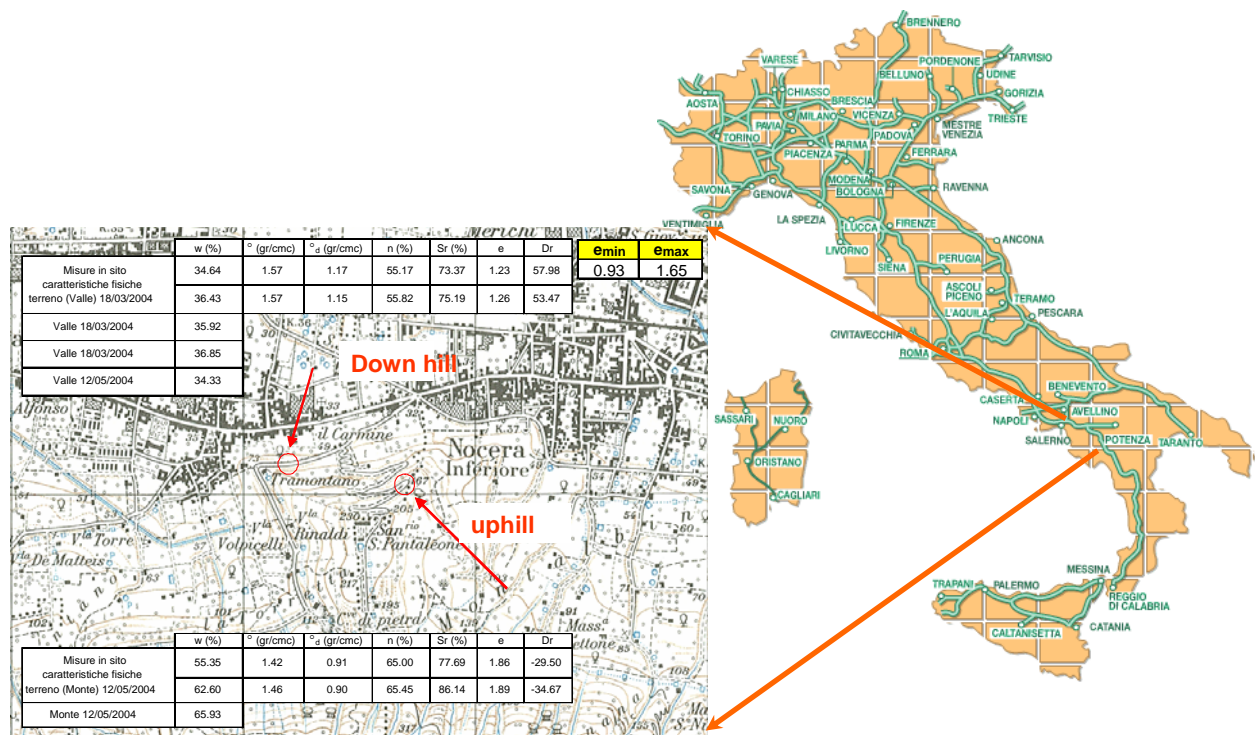


Figure 2-1 Identification on a topographic map of the working faces where the material for the experimentation was withdrawn.

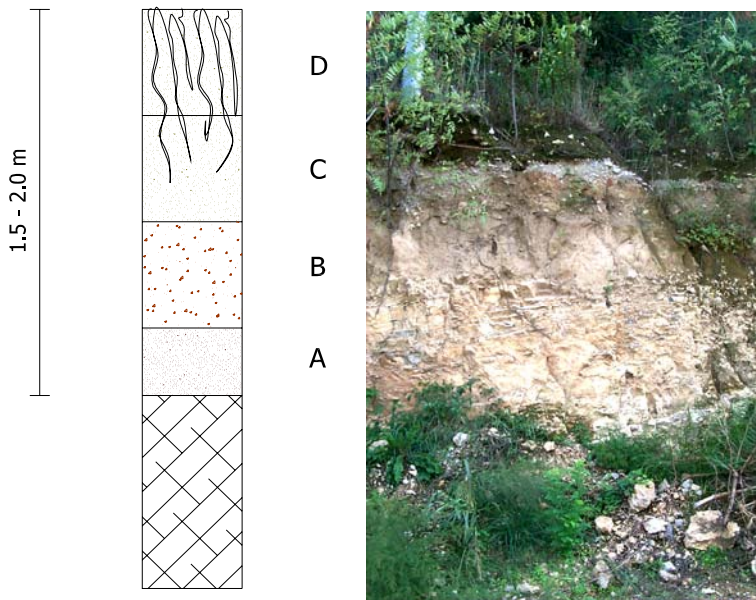


Figure 2-2 The Soil profile and the working face from which the material was drawn .

2.3 – Grain size distribution and index tests.

The soil taken was subjected to laboratory analysis to define its grading curve and determine its index properties.

The results of the grading curve analysis are shown in (Figure 2-3); you can see how the fine content of specimen taken from the upper side of the hill (curve plotted with continuum line) is very different from the one of samples taken from the lower side of the hill (dashed curves). In fact, in the first case the sand matrix prevails over the clayey matrix, whilst in the second case the silty content is prevalent. This distribution is coherent with the material exchange mechanism that take place during the soil movement, between the soil mass and the sliding layer.

In fact, during the sliding, the soil flow is not strong enough to carry downs the bigger particles, that set down along the way. Instead, the finest particles stay suspended in the soil mass, and set down only at the tip of the slump.

The sliding mass was composed by a silty sand. The soil particle specific weight is equal to 2.66 g/cm^3 .

The soil plasticity of the soil is barely zero, except for the specimen taken from the downslope zone (Figure 2-1), in which the higher fine content manifests itself in a $Ip=10.9\%$, obtained thanks to a liquid limit $w_L = 45.11\%$ and a plasticity limit $w_P = 34.20\%$. An organic fraction of 5% was found. The soil can be plotted in the Casagrande Chart Figure 2-4, resulting in an organic silt.

Looking at the data reported, the material utilized in this experimentation can be classified as a silty sand (ASTM D2487-00).

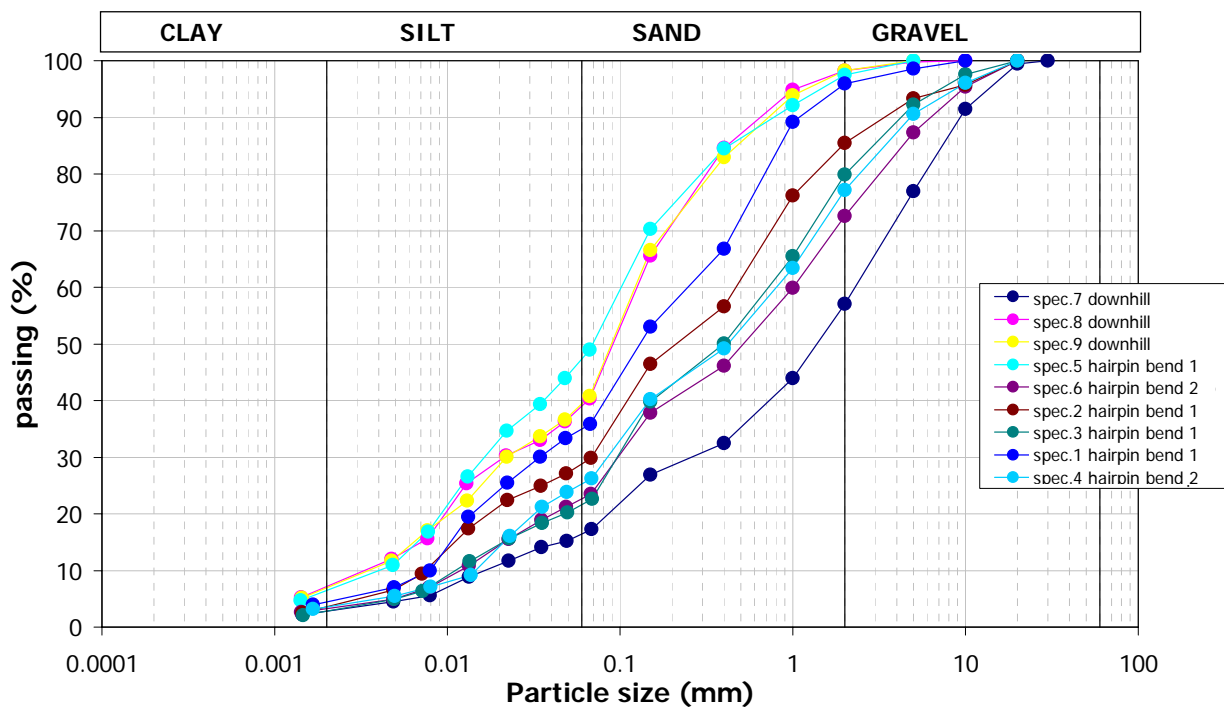


Figure 2-3: San Pantaleone Soil grading curves.

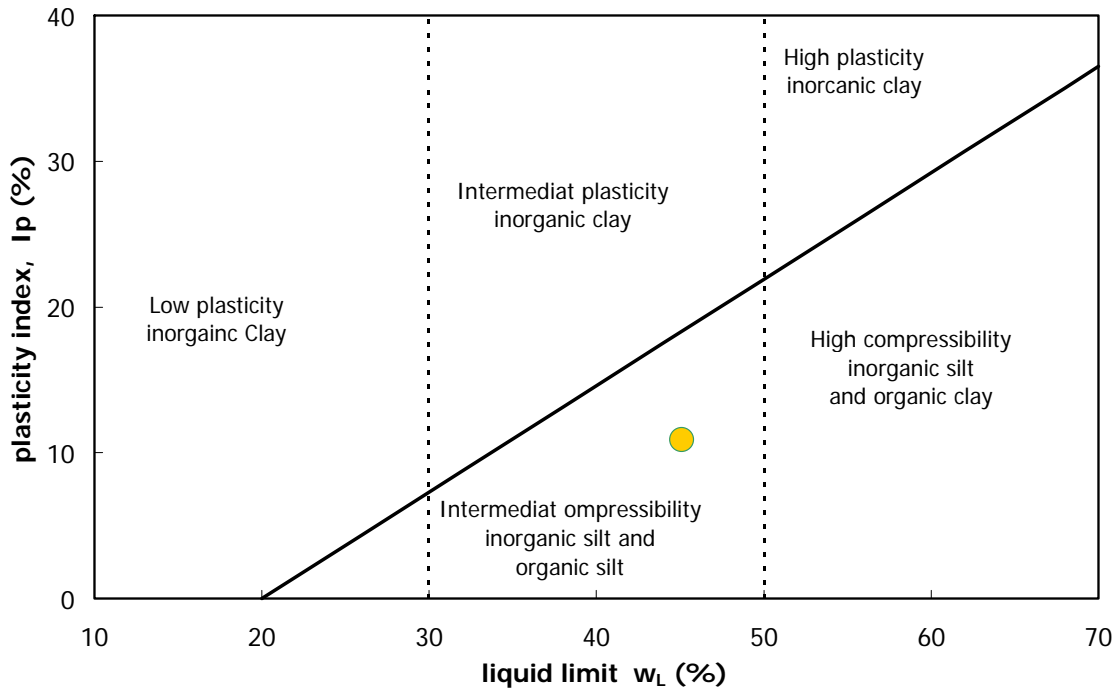


Figure 2-4: Casagrande Chart.

To evaluate the relative density for in situ soil, the minimum and maximum porosity (e_{min} , e_{max}) have been identified using the standard techniques ASTM D4254-00 and ASTM D698-00. The porosity ranger between 0.97 and 1.65.

The Proctor compaction tests, executed coherently with the Proctor standard technique (ASTM D698-00) let us determine the value of the optimum water content $w_{opt}=31\%$ (Figure 2-5).

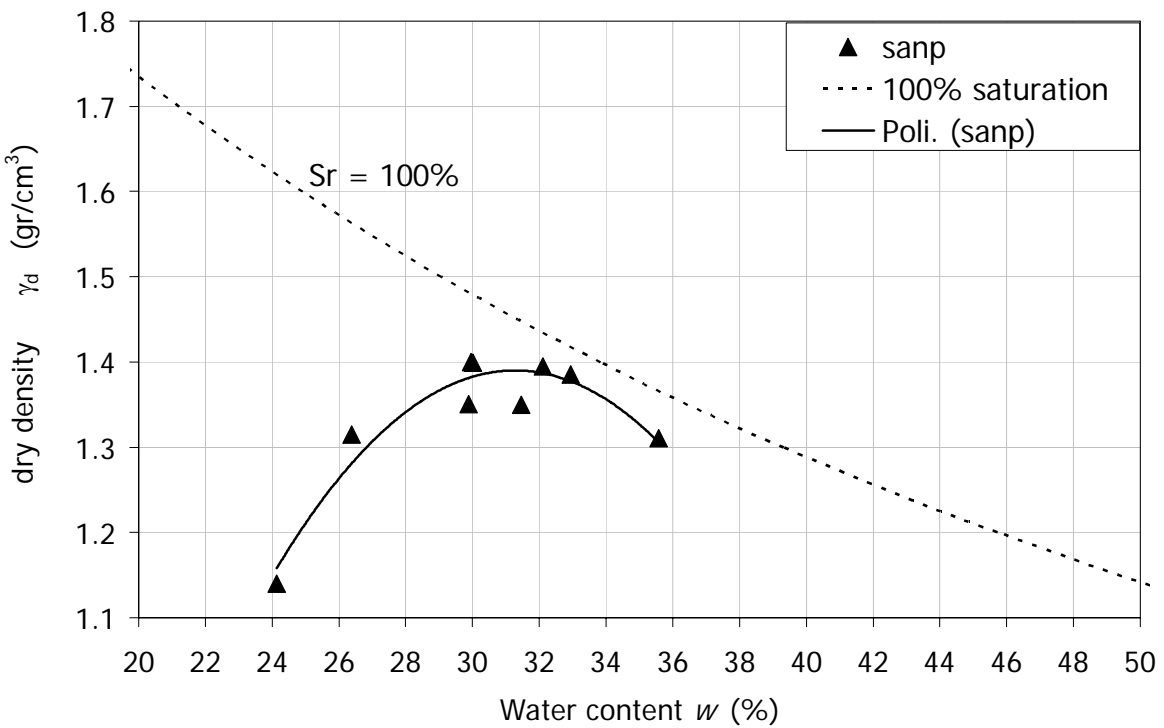


Figure 2-5: Proctor curve.

In Figure 2-6 some measures of in situ density and water content are plotted and compared with the Proctor standard compaction curve. These data were taken along the slope at different times of the year: all the specimens tested have a low density. Specimens deriving from the upper side of the slope were taken after a rainy period, and have the highest water content and the lowest density.

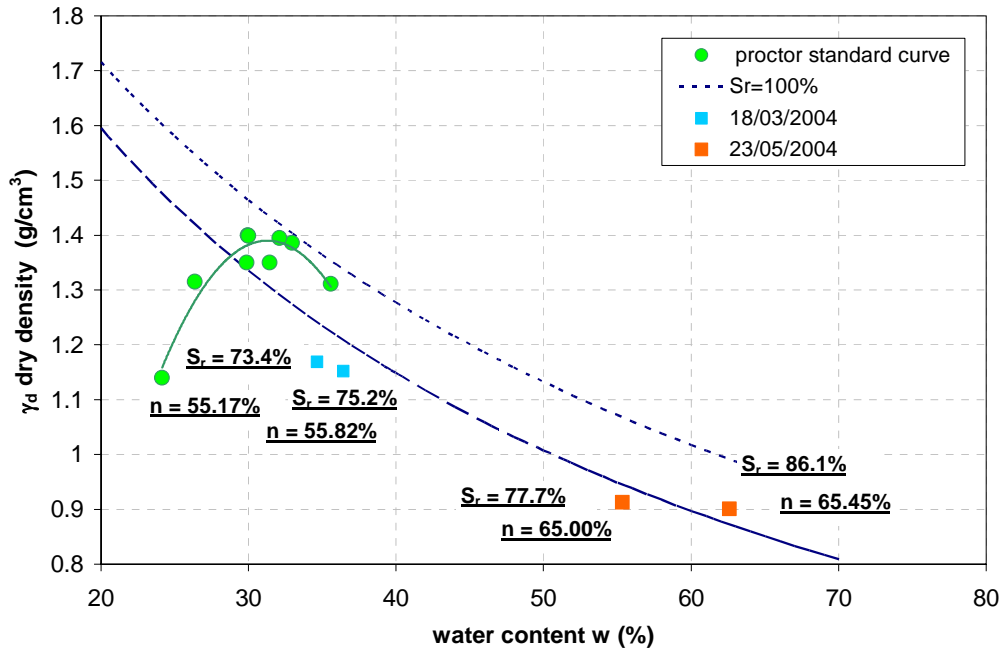


Figure 2-6: Some values measured in situ.

Synthesizing the information reported above, resulting from laboratory analysis of the physical properties of the tested soil, it is possible to characterize the geotechnical properties of the San Pantaleone Soil: it is a gravelly sand, lightly silty, with a porosity index ranging from 0.97 to 1.65.

2.4 Pre-treating of the material

The natural material has to be pre-treated before being used for the triaxial tests:

- First, the operator has to perform a gross breakage of the particle aggregates, by lightly tamping the soil with a rubber pestle. It is better not to use a marble pestle, since its hardness could cause the breakage of single soil particles.
- The material is passed through the 2mm sieve, thus cutting the gravel-size particles. This step was performed in order to obtain a uniform specimen: in fact, the soil specimen has to be treated as a single element, analyzed as a simple contour problem (Muir Wood, 1989), and big particles could cause a non-uniformity in the specimen.
- The soil is dried for at least 12 hours in a 110° oven.

- If the target is to prepare the soil for compaction, the dry soil is mixed with water to obtain the desired water content. The soil-water mixture is then left in a humidity controlled room for at least 12 hours (ASTM D 1557-00), to obtain a more homogeneous compound.
- If the soil has to be prepared for the consolidometer, the soil is mixed with the desired amount of water (in this experimentation equal to $1.2 w_L$) and then is put into a kneading machine to obtain a well blended mixture.



Figure 2-7: some stages of the soil pre-treating: a) the soil taken from the site is kept in big plastic tanks; b) the first stage is to dry the soil in the oven; c) then, with a plastic hammer, the particle aggregates have to be broken; d) the material is sieved at the 2mm sieve

2.5 Preparation Techniques for compacted specimens

Two are the main criteria for the preparation of compacted specimens: the first is to fix the target density for the soil (through parameters like the dry density or the porosity index). Once you have fixed the desired density, and knowing the specimen dimensions, it is the easiest way to proceed.

The second criteria is to fix the compaction energy. In this case it is essential to pursue one of the standardized procedures, since they are intimately connected with the density obtained.

2.5.1 Moist Tamping Method

This reconstitution method has been widely used in the study of static liquefaction related phenomena, especially for clean sands. Ishihara (1993) suggests to dispose : "Five or six equal preweighed oven-dried portions of soil, mixed with de-aired water at a desired water content. Each portion of the soil is strewn by hand to a predetermined

height in five to six lifts, as shown in Figure 2-8. At each stage of the lifts, tamping is applied lightly with a small flat bottom tamper. Because of capillary effects between particles, the moist sand can be placed at a very loose structure well in excess of the maximum void ratio of the dry sand, which is determined by the procedures stipulated in the ASTM or JSSMFE standard test method. An optimum amount of energy for preparation of the loose initial structure of the sample is a matter to be decided on for the individual sand used for the test. If the tamping energy is small, the sample is placed so loose that the volume contraction on subsequent saturation becomes unduly large and consequent reduction in sample diameter tends to create vertical wrinkles in the membrane. If a denser sample has to be prepared, a larger amount of energy needs to be applied, for example by increasing the number of tampings during compaction at each stage of the lift. By this procedure, a state of sand with any combination of void ratio and confining stress can be produced by the use of a varying amount of compacting energy during tamping, as shown in Figure 2-9. One of the advantages of this method is its versatility, permitting any sample to be prepared within a wide range of void ratio. The sample can therefore be very loose and highly contractive or dilative in subsequent loading, depending on the void ratio at the time of sample preparation."

In the opinion of many researchers (Yamamuro e Lade, 1997), this reconstitution technique, is not representative of the in situ condition of clean specimen, since at low density it would bring to a "metastable" structure, a structure that would easily bring to the instable behaviour that characterizes the static liquefaction of soils. Instead, at higher density, "the tamping process may overconsolidate portions of the specimen by compacting grains together at fairly high stresses" (Yamamuro e Lade, 1997).



Figure 2-8 Specimen prepared using wet tamping method.

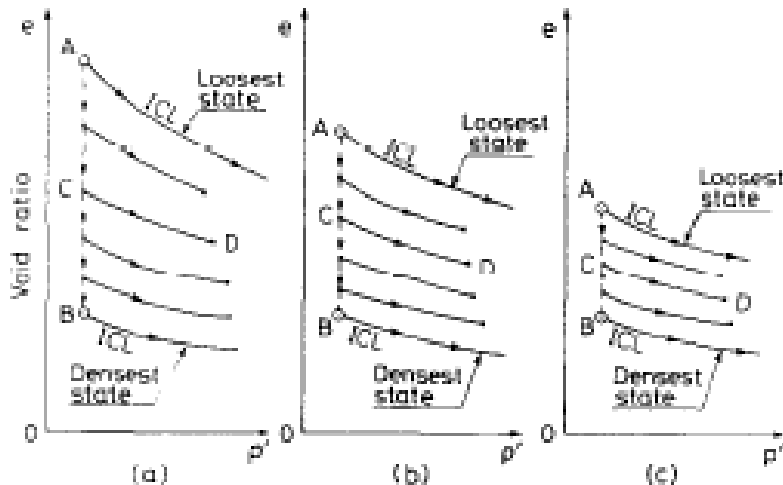


Figure 2-9 Consolidation characteristics of samples prepared by: (a) moist placement; (b) dry deposition; (c) water sedimentation

What stated before is especially suited for a naturally water deposited soil. Instead, in the case of pyroclastic soils put in place through aeolic deposition, it seems that the moist tamping technique can simulate well the natural behaviour. This also considering that aeolic ashes deposits can be very loose, and this is also the case for San Pantaleone Slope.

2.5.2 Proctor

This compacting procedure, proposed by R.R. Proctor in the thirties (Engineering News Record, 7 September 1933) is nowadays one of the most utilized in the common practice.

The criterion on which Proctor procedure is based is simple: the energy is transferred to soil sample through an iron rod, that falls from a fixed height. The material is prepared in an iron mould: it is placed in three layers with a known water content; each layer receives 25 to 26 hits from a hammer of the weight of 24.4 N, falling from an height of 30.5 cm.

With this procedure (standardized by ASTM 698/91) the soil receives always the same fixed energy of 600 kN/m^3 .

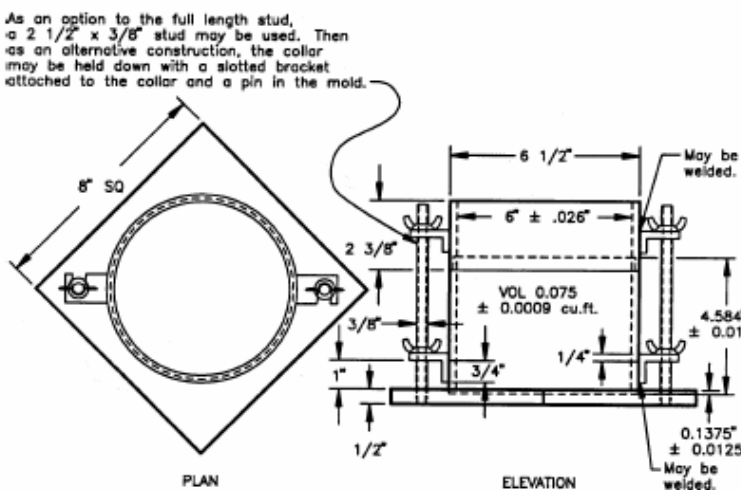


Figure 2-10 Scheme of a mould standardized by ASTM.

The ASTM standard 698/91 describes the procedure to obtain the "Proctor curve" of the soil. This procedure was used also for San Pantaleone Sand, for determining its optimum water content and its maximum dry density.

2.6 Specimen prepared in the Consolidometer

A slurry was prepared mixing about 3 kg of oven dried soil from San Pantaleone, and an amount of water equal to about 1.2 times the limit water content of the soil (an higher water content can result in a too liquid soil, too difficult to handle). The slurry was

stirred for at least 0.5 hr, in order to avoid particle segregation and every kind of disuniformity. The slurry was then transferred into the consolidometer. To reduce the air bubbles, the lateral surface of the consolidometer was hit several times with a hammer. Then the a water soaked filter paper disc was carefully put on the surface of the slurry, the piston was put in place and filled with some water; he bottom drainage tubes were connected. Then the consolidometer was put under an hydraulic press, equipped with a servo-controlled system capable of maintaining the desired deviator stress.



Figure 2-11 Various stage of the preparation of the slurry



Figure 2-12 The consolidometer under the hydraulic, servo controlled press.

2.6.1 Water sedimentation and freezing

Frozen specimen were prepared to obtain loose saturated specimen to test in Bishop cell. They were prepared putting the dry material in a mold filled with distilled water. The mold was made with an overhead transparent sheet folded in a cylindrical shape, having an inner diameter equal to 38 mm and an high of around 100 mm. The lower base of the mold was closed with a cap and then the soil was gently poured with a teaspoon. Then, the mold with the soil was frozen at – 30°C.

Before starting the mechanical test, the two bases were trimmed to have a specimen of 76 mm in high that was placed in the triaxial cell, after removing the folded overhead sheet. To avoid a quick defrosting of the specimen and its subsequent collapse, the reservoir of de-aired water used to fill the triaxial cell with and the triaxial chamber itself were packed with ice. Once the setup was completed the specimen was left for at least 24 hours under an effective isotropic stress state of 10 kPa before starting the consolidation stage, in order to allow for complete thawing of the material.

2.7 Specimen Trimming procedure

The procedure described herein, is part of the traditional procedures adopted at the Geotechnical laboratory of the University of Naples. This procedure was used in the course of this sperimentation, to cut natural samples, Proctor reconstituted samples and consolidometer samples. Instead, air pluviated samples and moist tamping samples were prepared directly in their final shape.

The soil sample is put inside an hand press (Figure 2-13, left). On the sample is put an iron cylinder, with its inner dimension (diameter and height) equal to the required specimen dimensions (50mm and 100mm). The cylinder is slowly pressed into the sample through the hand press, while the operator cuts the exceeding soil, giving the sample a conical shape, in order to reduce the lateral friction (Figure 2-13, right). The operator has to be very sharp and careful, in order not to induce high disturbance in the specimen.



Figure 2-13 The hand press to cut specimen from a natural (photo on the left); the specimen during the trimming procedure (photo on the right).

2.8 Dry Deposition Method

The dry deposition method is frequently used in the study of static liquefaction.

"Oven-dry sand is filled in a cone-shaped slender funnel with a nozzle about 12 mm in diameter, as shown in Figure 2-15. This funnel is the same as that used for determining the maximum void ratio of sand based on the JSSMFE method. The sand is spread in the forming mould with zero height of fall at a constant speed until the mould becomes filled with the dry sand. Tapping energy is applied by hitting the side of the mould to obtain a desired density. Any state of a sample can be produced by this method, as shown in Figure 2-9, by adjusting the tapping energy during the process of sample preparation. The sample is generally denser than that prepared by the moist placement method. Even if it is prepared in its loosest state without any tapping, the sample may be only slightly contractive in its behaviour in the subsequent application of shear stress. Therefore, this method is not adequate for the preparation of samples with highly contractive characteristics" (Ishihara, 1993).

The method described above was used in this experimentation to obtain very loose samples. In fact, in this work specimen were prepared without any tapping. Moreover, the funnel used was not compatible with the JSMFE standard.

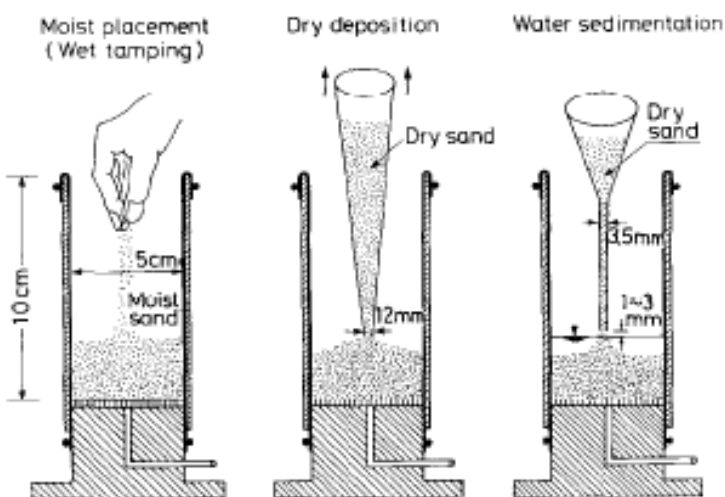


Figure 2-14 Methods of sample preparation

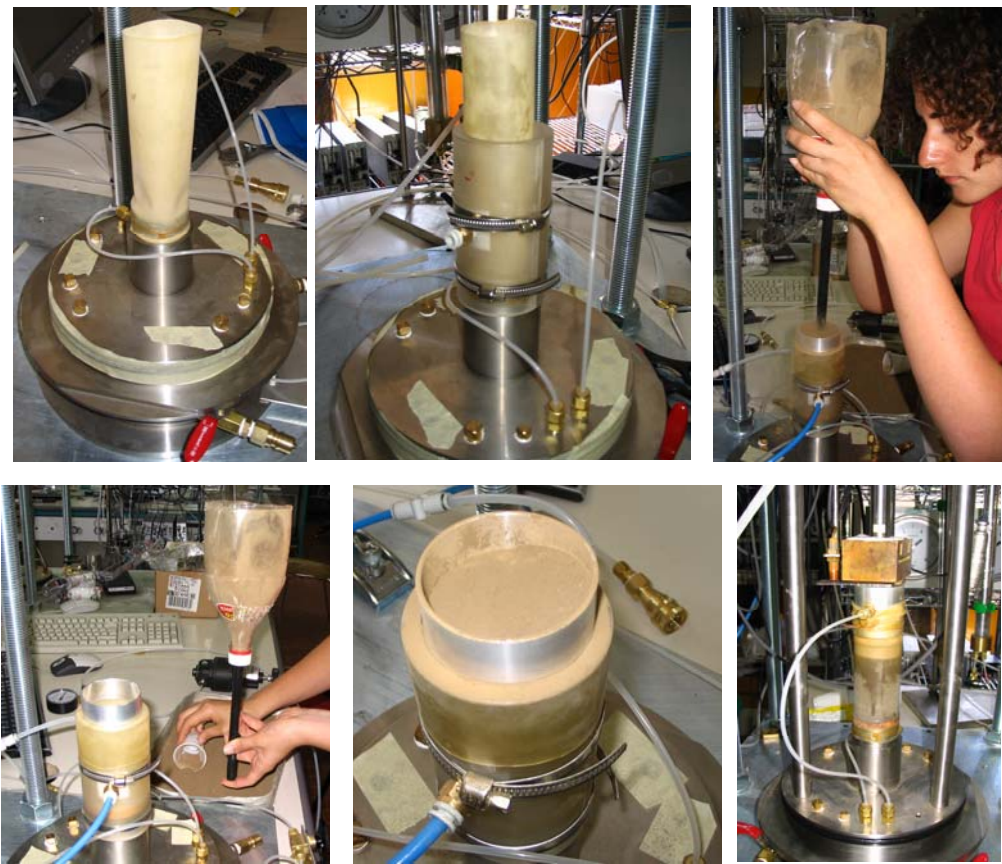


Figure 2-15 A specimen prepared with air pluviation method.

REFERENCES

ASTM: D 698-00, **Standard Test Methods for Laboratory Compaction Characteristics of Soil Using Standard Effort (12,400 ft-lbf/ft³(600 kN-m/m³))**, ASTM International, West Conshohocken, PA.

A.S.T.M. D 2487-00, **Standard Practice for Classification of Soils for Engineering Purposes (Unified Soil Classification System)**, ASTM International, West Conshohocken, PA.

ASTM: D 4254-00, **Standard Test Methods for Minimum Index Density and Unit Weight of Soils and Calculation of Relative Density**, ASTM International, West Conshohocken, PA.

A.S.T.M. D 4318, **Test Method for Liquid Limit, Plastic Limit, and Plasticity Index of Soils**, ASTM International, West Conshohocken, PA.

Burland, J. B. (1990), **On the compressibility and shear strength of natural clays**, Géotechnique 40(3), 329-378.

Hight, D. W. & Georgiannou, V. N. (1995), **Effects of sampling on the undrained behaviour of clayey sands**, Géotechnique 45(2), 237-247.

Ishihara, K. (1993), **Liquefaction and flow failure during earthquakes**, Géotechnique 43(3), 351-415.

Lampitiello, S. (2003), **Resistenza non drenata e suscettibilità alla liquefazione di ceneri vulcaniche della Regione Campania**, Phd Thesis.

Skempton, A. W. and V. A. Sowa, V. A. (1963), **The behaviour of saturated clays during sampling and testing**, Géotechnique 13(4), 269-290.

Yamamuro, J. A. and Lade, P. V. (1997), **Static liquefaction of very loose sands**. Canadian Geotechnical Journal 34, 905-917

Vaid, Y. P., Sivathayalan, S., and Stedman, D. (1999), **Influence of specimen-reconstituting method on the undrained response of sand**, Geotechnical Testing Journal 22(3), 187-195.

Wood, D. M. (1989), **Evaluation of material properties**, General report on Proc. Of Pre-failure deformation of geomaterials. IS-Hokkaido 397-417.

Chapter 3

Experimental procedures and interpretation of the results

3.1 Introduction

In this chapter, the procedure used for setting up the specimens in the triaxial machine will be described step by step. The Saturation phase by dry setting method will be illustrated in details, since this procedure is not commonly used in Italy. The procedures related with the execution of the consolidation phase and the shear phase are also discussed in detail.

3.2 Specimen setting by the “dry setting method”

1. The air-dried filter paper, cut into vertical strips, is first wrapped around the specimen (only for natural samples, proctor reconstituted samples and consolidometer samples)¹. Round discs of air-dried filter paper are also put between the specimen and the porous stone. The filter paper accelerates the drainage during saturation and consolidation, and accelerates equalization of pore pressure during shearing.

¹ Specimens prepared with air pluviation method were set up without filter paper: the specimen preparation method was not compatible with the paper. Specimens prepared with wet tamping at very low density and tested at very low confining stress were set up without filter paper: otherways the paper tended to wrinkle, causing problems in the evaluation of volumetric strain and of effective confining stress.

2. Using the membrane stretcher, the external latex membrane is set around the specimen, and folded back at the ends. Great care is taken in this operation, in order not to damage the membrane.
3. The specimen, wrapped in the filter paper and still inside the membrane stretched on the membrane former, is placed on its base inside the triaxial cell. Great care was paid in checking the alignment between the specimen and its base.
4. The top cap is carefully placed on the specimen, trying not to apply a deviator stress on the specimen. This operation is performed by hand, carefully checking the q value on the computer screen. Once the deviator stress is around 0.5 kPa (that meant that the top cap was really in contact with the specimen cap) the tie rod was clamped in this position.
5. The membrane ends are unfolded, to wrap the top and bottom base of the specimen. Two strips of latex membrane for sealing the outer membrane are firmly tied around the top and base pedestal.
6. A vacuum of around -5 kPa is applied to the specimen, in order to make the membrane adhering to the lateral surface of the specimen. At this stage, the specimen (especially if it is not much dense) tends to shrink. In order not to make the deviator stress increasing too much, the operator has to be careful in bringing the top cap nearer to the specimen.
7. All the inner and local displacement transducers are set and adjusted.
 - a. The 2mm capacity proximity transducer (gap sensor) is set.
 - b. A pair of LDTs, if the specimen was not too weak².
8. The readings of the displacement transducers were recorded to memorize their zero value and the specimen was then ready for saturation.

² In weak specimens, the deformation during the saturation stage is already too much for LDTs range.



Figure 3-1 Two stages of specimen set up: 1) the specimen is put between filter paper and porous stones, 2) the latex membrane is placed around the specimen.



Figure 3-2 two images of the specimen already set up in the machines, with LDT on.

3.3 Saturation

In this testing program, the specimen was saturated by a combination of vacuuming, flushing with distilled water, time lag and back pressurization in a procedure called "Dry Setting Method". This procedure has been shown (Ampadu, 1989) to be equally effective in saturating specimens as the conventional procedure, that uses porous stone and filter paper already saturated (and consequently wet). The main idea in this procedure is to allow free water to come into contact with the specimen surface only after an effective pressure has been applied to the specimen. This way the water intake which is known to soften the specimen (especially if overconsolidated)

is reduced. Moreover, this methods avoids the difficulties of handling wet thin strips of filter paper.

3.3.1 Flushing

Flushing with distilled water is done to ensure that water fills all the pores inside the specimen, and all the drainage line including the spaces between the membrane and the specimen, and all the drainage tubes.

1. The vacuum was slowly increased so that the back pressure was reduced to - 10 kPa, at zero cell pressure.
2. Water tank 1 was raised about 70 cm above the level of tank 2. This establishes a pressure difference of 7 kPa between the bottom and the top of the specimen and allows the water to flow from the bottom to the top. In this work, flushing at $\sigma_{bp} = -10$ kPa and $\sigma_c = p_0 = 0$ kPa was continued for at least 2 hours. In this stage, the specimen shows the strongest tendency to shrinking: the operator makes manually the job to bring the top cap nearer to the specimen, thus keeping the deviator stress constantly equal to zero.
3. At the end of flushing under vacuum condition, the operator can read the specimen dimensions manually: using a digital calibre, he can read the specimen height and diameter from outside the latex membrane. MaTRiX is not equipped for measuring directly the radial strain: only in case of saturation degree equal to 100%, it is possible to obtain the radial strain through the value of the volumetric strain. From now to the beginning of the consolidation stage, the radial strain will be supposed to be equal to zero (Sladen & Handford, 1987, Vaid & Sivathayalan, 1996). This approximation probably is suited to the specimen behaviour in this stage.

3.3.2 Connection to the loading system

1. The pressure cell was assembled. The drainage valve was closed and the cell was carefully moved into its position, co-axial with the loading ram.
2. The loading ram was brought close tot the loading piston.
3. The external displacement transducers were then set in place.
4. The saturation continued, but the vacuum was reduced until $\sigma_{bp} = 0$ and $\sigma_c = 10$ kPa. In this condition, the specimen was kept overnight.

3.3.3 Back Pressurization

The idea of back pressurizing is to force any air bubbles still remaining to go into solution. The set up for back pressurizing is described below.

1. The differential pressure transducers (HCDPT and LCDPT) were flushed with distilled water to remove any air bubbles entrapped.
2. The vacuum source for pore pressure was replaced with a positive pressure source (the manual pressure regulator described in chap.2). The back pressure was slowly increased, together with the cell pressure; the isotropic stress condition being assured by a servo-assisted procedure (q -control) that imposes a zero deviator stress condition.
3. After back-pressurization, the degree of saturation as defined by the Skempton's B parameter achieved, was determined.

3.4 Consolidation

In this testing program, the consolidation program was automated. The basic idea of automatic consolidation is to subject the specimen to a pre-determined stress path whose control is fully automated. Automation is necessary to ensure reproducibility of consolidated specimens for undrained shear, since:

- Automation ensures that the consolidation stress path is continuous and follows the desired stress path almost exactly. This eliminates any chances of large deviations from the intended stress path, which could lead to irrecoverable strains
- Automation ensures that the stress path can be reproduced from test to test.
- The automatic program controlling matrix allows one to perform also creep stages and cyclic loading while performing consolidation.

In this testing program, only isotropic consolidation was performed.

In some cases, when the purpose of the operator was to measure the variation of small strain stiffness with the confining pressure, the isotropic compression was staggered with q constant creep ($q=0$) and cyclic loading. The q constant creep stage was necessary to reach the secondary compression stage (for the confining pressure reached), and stabilize the pore pressure distribution inside the specimen.

In the course of the experimental program on San Pantaleone sand, it was found that, for a consolidation rate of 10 kPa/hr, the minimum time to wait for performing a cyclic stage was 0.5 hours.

3.5 Cyclic loading

Since the main target of this work was the study of the dynamic properties of the soils involved in this experimental campaign, many cyclic loading phases were scheduled in the course of each test.

Cyclic loadings stages can be performed both in a q -controlled and in a a -controlled way. In the course of this experimental program, cyclic loadings stages were performed in a q -controlled way. This means that the cycles' amplitude was assigned and controlled through the deviator stress read by the load cell. In this way, the smallness of the cycle was directly connected to the load cell electric resolution, and with the electric noise of its output. In the case of the 1 ton load cell, the minimum amplitude to obtain significant load cycles was 3.5 kPa (for specimen 5 cm in diameter). In the case of the 100 kg Load cell, it was possible to obtain cycles with an amplitude as small as 0.35 kPa. (for specimen 5 cm in diameter). (see

Figure 3-4).

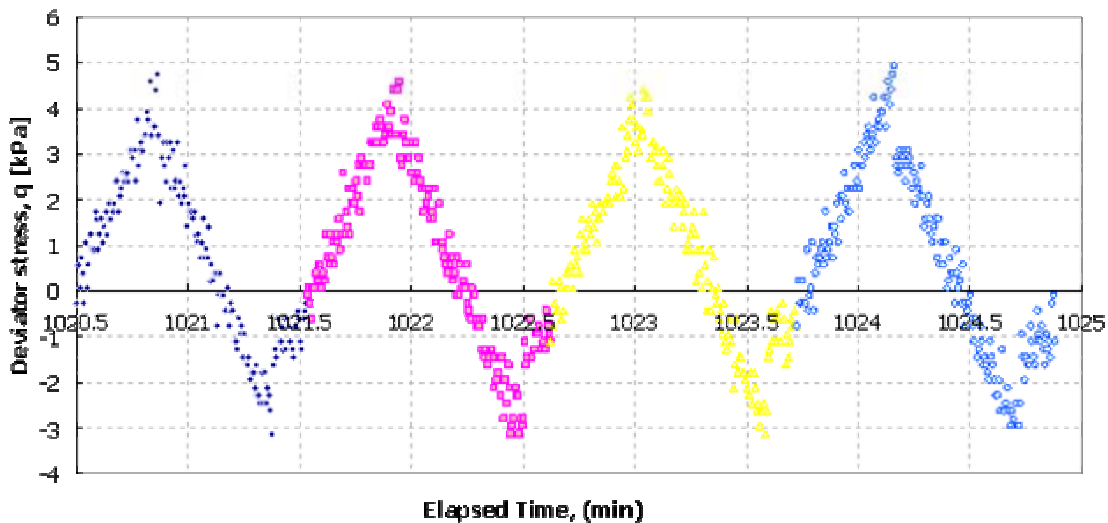


Figure 3-3 Cyclic loading test performed with the 1 ton load cell.

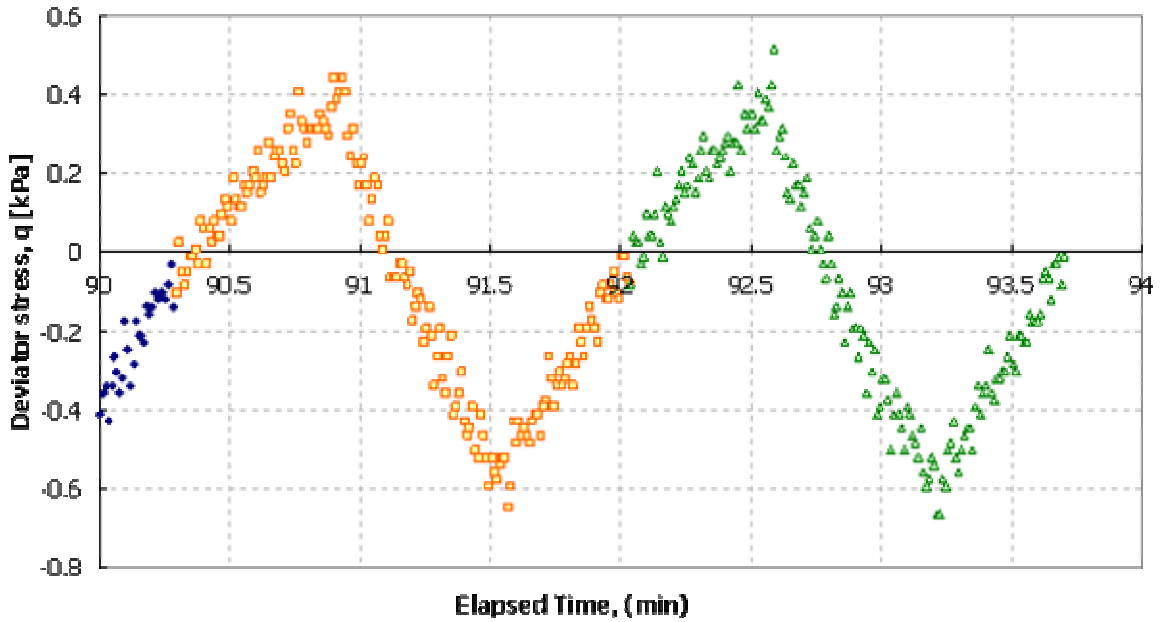


Figure 3-4 Cyclic loading test performed with the 100 kg load cell.

3.6 Undrained shear

This stage can be performed through an automated procedure, that allows also for the change of the motor speed and for the execution of small unload-reload cycles for the evaluation of the elastic properties of the specimen during the shear phase.

Before leaving to the computer the job of conducting the shear phase, there are a few operation that have to be conducted manually:

1. The drainage valve of the specimen has to be closed.
2. The 2 mm gap sensor in the cell has to be reset to the appropriate initial value. This was made possible by the support on which the transducer was mounted to allow manipulation from outside cell.
3. If necessary, the LVDT has to be adjusted in order not to go out of his reading scale.
4. At the end of testing the pressures has to be slowly released and the specimen was carefully taken out of the system and its water content together with the volume of water expelled during consolidation was used to back calculate the initial water content w_i .

3.7 Triaxial data interpretation

The interpretation of triaxial data is not difficult. However, for a better understanding of the results presented in the next chapter, a few notes are necessary.

1. In the execution of stress path controlled triaxial tests, the specimen dimensions are continuously monitored in order to know the real time value of stress and strain invariants. In particular, the deviator stress q is evaluated from the axial deviator load and the specimen transversal area A_c . The A_c value can be evaluated assuming a cylindrical deformation shape for the specimen. In this hypothesis, A_c can be evaluated from:

$$A_c = A_0 (1 - \varepsilon_v) / (1 - \varepsilon_a) \quad \text{Equation 3-1}$$

2. In low confining pressure tests the correction described in chapter 1 have been adopted. For all the other tests no correction was used: In fact, trying to adopt the same stress corrections as used for lower confining stress, the difference between corrected and uncorrected results was irrelevant.

3.8 Tests performed at very low confining stress

Looking at the geotechnical literature, only a few articles have been written on soil behaviour at low confining stresses. The specimens tested were most of all sand specimens.

This is very surprising, considering that laboratory tests at low confining stresses are useful for example:

- 1) in soil dynamic and in geotechnical engineering in general, to characterize superficial soils, that often have poor mechanical properties,
- 2) to characterize the soil used in 1g models,
- 3) in marine geotechnics.

The authors' opinion on the soil behaviour at very low confining stress is quite discordant. Whilst Ponce and Bell (1971) found a marked variation of the friction angle and of the material compressibility, Fukushima and Tatsuoka (1984) sustain that no variation in the friction angle and in the compressibility takes place at low confining stress. Koseki et al.(2001), on the other way, studying the effect of

confining stress on liquefaction susceptibility, show that the sand they studied has a more dilatative behaviour at low confining stress. Henkel and Gilbert (1952) have measured significant variation of the stress-strain behaviour of clays at very low confining stresses.

In the following a brief list of the difficulties of executing tests at low confining pressures is reported.

Several special efforts are necessary to obtain reliable results:

- Use of an accurate pressure-independent load cell placed inside the triaxial cell
- Measurement of the effective confining pressure with a high-precision differential pressure meter (DPT)
- Correction of stresses for membrane force
- Rigorous control of specimen density: effects of gravity force limits the lowest effective confining pressure for meaningful 'element' tests.(Fukushima & Tatsuoka, 1984; Tatsuoka et al. 1986b)

3.8.1 Latex membrane confining effect

Henkel and Gilbert (1952) have studied the confining effect of latex membrane for normal consolidated clays. In the author's opinion, the membrane confining effect is independent by the specimen strength and cell pressure, but is proportional to membrane stiffness.

The membrane contribution to the overall confining pressure can be evaluated in two ways:

a) Compression shell theory:

in this theory latex membrane has the shape of a thin walled cylindrical shell, and during deformation it stays completely adherent to the specimen:

$$\Delta\sigma_{am} = -\frac{8}{3} \cdot \frac{E_m \cdot t(2\varepsilon_{am} + \varepsilon_{\theta m})}{d} \quad \text{Equation 3-2}$$

$$\Delta\sigma_{rm} = -\frac{4}{3} \cdot \frac{E_m \cdot t(\varepsilon_{am} + 2\varepsilon_{\theta m})}{d} \quad \text{Equation 3-3}$$

where $\Delta\sigma_m$ and $\Delta\sigma_r$ are adjustments to axial and radial stress, E_m and t are Young Modulus and the actual membrane thickness, and $\Delta\sigma_{am}$ e $\Delta\sigma_{ar}$ are the mean axial strain and the mean radial strain of the membrane, that are supposed equal to specimen strain. In the equation is supposed $v = 0.5$.

a) "Hoop tension" theory

the contribute to axial stress of the membrane is considered to be zero, for the formation of wrinkles.

$$\Delta\sigma_{am} = 0$$

Equation 3-4

$$\Delta\sigma_{rm} = -\frac{2E_m \cdot t \cdot \varepsilon_{\theta m}}{d}$$

Equation 3-5

the equations written above in this paragraph, are similar to those obtained by Henkel e Gilbert (1952), but are taken from a paper by Fukushima and Tatsuoka (1984).

3.8.2 Filter paper stiffness

Duncan and Seed (1967) suggest a correction for the load sustained by filter paper ($\Delta\sigma_{afp}$). In their opinion, it should be:

$$\Delta\sigma_{afp} = -k_{fp} \left(\frac{P}{A_s} \right)$$

Equation 3-6

In which k_{fp} is the load per unit length bearable by filter paper, P is the specimen perimeter, and A_s is the specimen cross area.

In the authors opinion, this correction should be applied for axial strain larger than 2%: beyond this target, the filter paper contribution would reach its maximum, maintaining this value until the end.

In the calculation reported in this PHD thesis, the filter paper stiffness was not taken into account: in fact, filter paper was applied only in tests performed on specimen prepared with proctor compaction and on specimens prepared in the consolidometer: specimen prepared with this techniques were tested under conventional confining pressure. Specimen tested under low confining pressure (air pluviated specimen,

specimen prepared with wet tamping and natural specimens) were set up without filter paper.

3.8.3 Specimen self weight effect

At very low confining stress, specimen self weight has a not negligible effect on the deviator stress that bring the specimen to its failure (Ponce e Bell, 1971).

In the opinion of Fukushima and Tatsuoka (1984) a not homogeneous stress distribution takes place inside the specimen due to self weight, σ_v varying with the height reached inside the specimen, whilst σ_r is a constant along the specimen, not varying with specimen height.

3.8.4 Base friction

To reduce friction at specimen base and to keep the specimen deformation plane at the base, it is commendatory to reduce base friction and to use top and pedestal bigger specimen diameter.

REFERENCES

- Ampadu S. I. K, Tatsuoka F.(1989): **The dry versus the wet Methods of setting clay specimens for triaxial testing**, 28th National Conference of the Japanese Society of Soil Mechanics and Foundation Engineering, Tokyo, June 1989
- Ampadu, S. I. K. (1991): **Undrained Behaviour of Kaolin in Torsional simple shear**, Phd Thesis, Institute of Industrial Science, University of Tokyo.
- Ampadu S. I. K, Tatsuoka F.(1993): **Effect of Setting Method on the Behaviour of Clays in Triaxial Compression from Saturation to Undrained Shear**, Soils and Foundations 33(2), 14–34.
- Sladen, J. A. and Handford, G. (1987): **A potential systematic error in laboratory testing of very loose sands**, Canadian geotechnical journal 24, 462-466.
- Vaid, Y. P., and Sivathayalan, S. (1996): **Errors in estimates of void ratio of laboratory sand specimen**, Canadian geotechnical journal 33, 1017-1020.

Chapter 4

The Mechanical Behaviour

4.1 The experimental program

In Table 4-1 are briefly reported the tests performed on natural and reconstituted specimens. Tests on reconstituted specimens are intended to obtain a clear reference scheme for the analysis of the behaviour of soil in situ, and at the same time help assessing the repeatability of physical proprieties of the soil.

Overall 43 triaxial tests have been performed, 18 of which were performed in a Bishop cell, at medium confining pressure (between 100 kPa and 400 kPa) on remoulded samples reconsolidated under 1-D conditions starting from a water content equal to $1.2 w_L$. These tests were used to determine the mechanical parameter useful to model the stress-strain behaviour of the soil, taking apart the natural history of the material. In fact, specimen prepared in consolidometer are much homogeneous, and do not suffer influence of the structure.

The remaining 25 tests were performed in the MaTRIX cell, on specimen reconstituted with different systems, aiming at looking into the effect of the specimen reconstitution technique on their stress-strain behaviour.

Finally 13 out of the 25 tests performed in MaTRIX were executed at low confining stress, (between 15 an 30 kPa), over very loose specimens . These kind of tests are useful to simulate the behaviour of superficial soil layers.

Test id.	Reconstitution technique	Initial density γ_d [t/m ³]	Initial porosity e_0	Test description	Triaxial apparatus
SP1	wet tamping, w=36%	1.129	1.357	Sat. at p'=30 kPa, U.L.C. and C.I.U.	MaTRIX
SP2	Natural specimen, w=36%	1.215	1.189	Sat. at p'=15 kPa, I.C. at 20 kPa, C.I.U.	MaTRIX
SP3	Consolidometer, Sr≠0	1.246	1.135	Sat. at p'=15 kPa, I.C. at 20 kPa, C.I.U.	MaTRIX
SP5	proctor standard, w=32%	1.377	0.931	Sat. at p'=20 kPa, I.C. at 100 kPa, C.I.U.	MaTRIX
SP6	proctor standard, w=30%	1.380	0.928	Sat. at p'=20 kPa, I.C. at 150 kPa, C.I.U.	MaTRIX
SP7	proctor standard, w=30%	1.399	0.902	Sat. at p'=20 kPa, I.C. at 150 kPa, C.I.U.	MaTRIX
SP8	Consolidometer	1.214	1.191	Sat. at p'=20 kPa, I.C. at 100 kPa, C.I.U.	MaTRIX
SP9	Consolidometer	1.220	1.180	Sat. at p'=20 kPa, I.C. at 100 kPa, C.I.U.	MaTRIX
SP10	proctor standard, w=42%	1.157	1.299	Sat. at p'=20 kPa, I.C. at 100 kPa, C.I.U.	MaTRIX
SP11	proctor standard, w=42%	1.159	1.294	Sat. at p'=20 kPa, I.C. at 100 kPa, C.I.U.	MaTRIX
SP12	Consolidometer	1.103	1.411	Sat. at p'=20 kPa, I.C. at 100 kPa, C.I.U.	MaTRIX
SP13	proctor standard, w=32%	1.166	1.282	Sat. at p'=20 kPa, I.C. at 100 kPa, C.I.U.	MaTRIX
SP14	proctor standard, w=32%	1.031	1.581	Sat. at p'=20 kPa, I.C. at 300 kPa, C.I.U.	MaTRIX

AIRP1	Air pluviation	0.830	2.203	Sat. at p'=15 kPa, I.C. at 50 kPa, C.I.U.	MaTRIX
AIRP2	Air pluviation	0.913	1.912	Sat. at p'=15 kPa, I.C. at 100 kPa, C.I.U.	MaTRIX
AIRP3	Air pluviation	0.878	2.030	Sat. at p'=15 kPa, I.C. at 30 kPa, C.I.U.	MaTRIX
AIRP4	Air pluviation	0.915	1.907	Sat. at p'=50 kPa, I.C. at 100 kPa C.I.U.	MaTRIX
AIRP6	Air pluviation	0.889	1.993	Sat. at p'=15 kPa, I.C. at 30 kPa C.I.U.	MaTRIX
AIRP7	Air pluviation	0.866	2.072	Sat. at p'=15 kPa, I.C. at 100 kPa C.I.U.	MaTRIX
AIRP8	Air pluviation	0.899	1.960	Sat. at p'=15 kPa, D.S.L.C.	MaTRIX
AIRP9	Air pluviation	0.905	1.940	Sat. at p'=15 kPa, I.C. at 35 kPa C.I.U.	MaTRIX
AIRP10	Air pluviation	0.890	1.988	Sat. at p'=15 kPa, I.C. at 75 kPa C.I.U.	MaTRIX
NAT02	Natural sample	1.157	1.299	Sat. at p'=15 kPa, I.C. at 20 kPa C.I.U.	MaTRIX
NAT03	Natural sample	1.085	1.451	Sat. at p'=15 kPa, I.C. at 20 kPa C.I.U.	MaTRIX
WETTP01	Wet tamping, w=36%	0.888	1.994	Sat. at p'=10 kPa, I.C. at 20 kPa C.I.U.	MaTRIX
WETTP03	Wet tamping, w=36%	0.895	1.972	Sat. at p'=10 kPa, I.C. at 20 kPa C.I.U.	MaTRIX
WETTP04	Wet tamping, w=36%	0.873	2.048	Sat. at p'=10 kPa, I.C. at 50 kPa C.I.U.	MaTRIX
WETTP05	Wet tamping, w=36%	0.867	2.068	Sat. at p'=10 kPa, I.C. at 15 kPa C.I.U.	MaTRIX
WETTP06	Wet tamping, w=30%	0.952	1.795	Sat. at p'=15 kPa, I.C. at 50 kPa C.I.U.	MaTRIX
WETTP07	Wet tamping, w=30%	0.885	2.005	Sat. at p'=12 kPa, I.C. at 40 kPa C.I.U.	MaTRIX
WETTP08	Wet tamping, w=30%	0.889	1.991	Sat. at p'=15 kPa, I.C. at 100 kPa C.I.U.	MaTRIX

spl01	Consolidometer	1.190	1.236	comp. 200 kPa, unload 30kPa, reload 400kPa, C.I.D	Bishop
spl02	Consolidometer	1.174	1.266	Compression at 400 kPa, C.I.U.	Bishop
spl03	Consolidometer	1.181	1.252	Compression at 100 kPa, C.I.U.	Bishop
spl04	Consolidometer	1.160	1.292	Compression at 400 kPa	Bishop
spl05	Consolidometer	1.173	1.268	Compression at 100 kPa, constant p' shear	Bishop
spl06	Consolidometer	1.170	1.273	Compression at 200 kPa, C.I.U.	Bishop
spl07	Consolidometer	1.199	1.218	Compression at 200 kPa, C.I.D.	Bishop
spl08	Consolidometer	1.164	1.286	Compression at 200 kPa, constant p' shear	Bishop
spl09	Consolidometer	1.163	1.287	Compression at 100 kPa, C.I.D.	Bishop
spl11	Consolidometer	1.165	1.283	Compression at 400 kPa, constant p' shear	Bishop
spl12	Consolidometer	1.156	1.302	Compression at 200 kPa, cycles	Bishop
spl13	Consolidometer	1.167	1.280	Compression at 200 kPa, cycles	Bishop
spl14	Consolidometer	1.174	1.265	Compression at 200 kPa, cycles	Bishop
spl15	Consolidometer	1.186	1.244	Compression at 200 kPa, cycles	Bishop
spl16	Consolidometer	1.200	1.216	Compression at 200 kPa, cycles	Bishop
spl17	Consolidometer	1.250	1.127	Compression at 200 kPa, cycles	Bishop
spl18	Consolidometer	1.225	1.171	Compression at 200 kPa, cycles	Bishop

spl19	Consolidometer	1.234	1.155	Compression at 200 kPa, cycles	Bishop
spl23	Water sedimentation	0,863	2,082	Compression at 200 kPa, cycles	Bishop
spl24	Water sedimentation	0,807	2,297	Compression at 200 kPa, cycles	Bishop

Table 4-1 Triaxial tests performed on San Pantaleone pozzolana

4.2 Behaviour of the material under isotropic stress conditions

All data are plotted in the semi logarithmic scale, so that they can be fitted with the classical equation:

$$v = N - \lambda \cdot \ln(p')$$

Equation 4-1

In which N is the specific reference volume, obtained at a medium effective confining stress of $p'=1$ kPa, and λ is the compressibility index of the material.

In Figure 4-1 the data relative to an unloading-reloading curve are plotted, in terms of specific volume-mean effective stress. Data can be fitted through the well known equation:

$$v = v_k - k \cdot \ln(p')$$

Equation 4-2

In which k is the compressibility index for the expansion curve, and v_k represents the specific volume at $p'=1$ kPa, on the same line.

For the test reported, it was found that the compressibility for the first load line is about 4.5 times larger than the one relative to the load-unload stage ($k = 0.00740$).

The compressibility of the material can be analyzed through the graph in Figure 4-2 and in Figure 4-3, related to tests performed at a medium confining stress of 400 kPa.

In Figure 4-2 are plotted data in terms of volumetric strain and axial strain, versus the mean effective confining stress. As you can see, the strain measured under isotropic loads shows up as lightly anisotropic, since the stress strain response is stiffer in the vertical then in the horizontal direction.

In Figure 4-3 data are plotted on the specific volume-mean effective stress plane.

Table 4-2 are reported the parameter N and λ , evaluated for each of the tests performed. Looking at the data reported, it is possible to locate a unique Isotropic compression line (ICL) for specimens prepared with consolidometer and with proctor, that is, for denser specimens. The average values for N and λ , in case of dense specimens are 1.232 and 0.0343.

For looser specimens, prepared with wet tamping and air pluviation method, it is possible to locate a different I.C.L., characterized by the parameters $N=3.2153$ and $\lambda=0.0921$.

In terms of compressibility, the material tested has a behaviour similar to granular materials, for which it is not possible to define a unique I.C.L., since its place in the $v-p'$ plane is extremely variable with the relative density of the material, with the water content and with the reconstitution technique adopted for the preparation of the specimen.

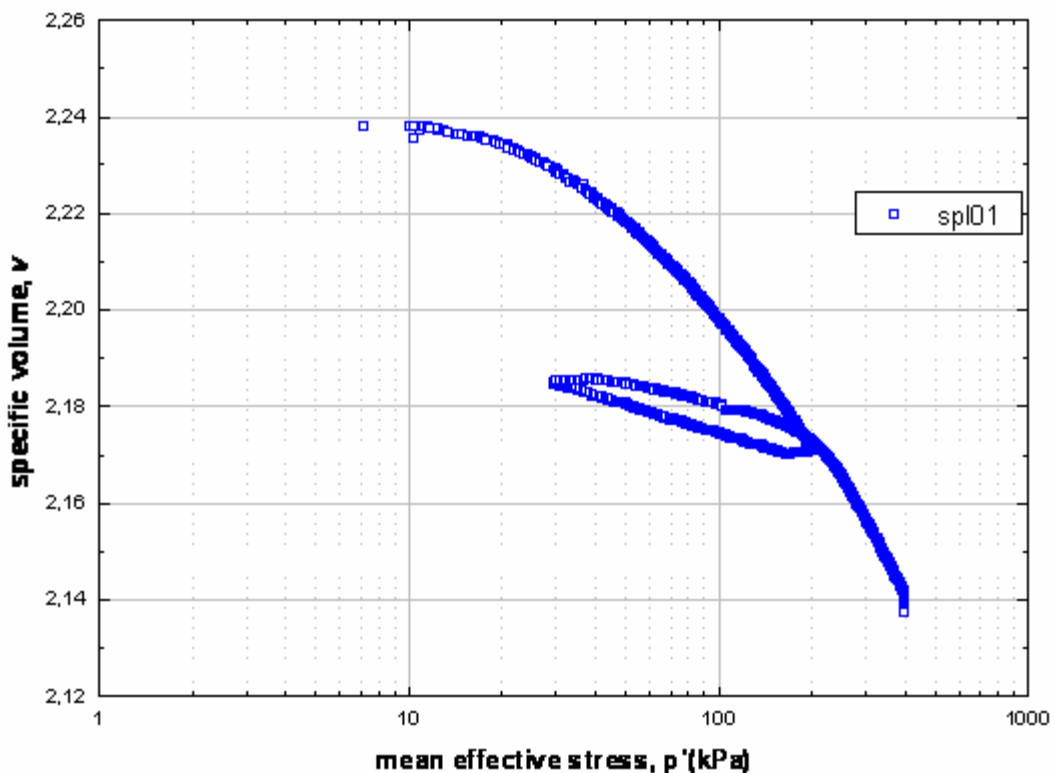


Figure 4-1: Isotropic compression curve and load-reload curve for specimen 01, prepared in consolidometer.

Test id.	Reconstitution technique	Initial porosity, e_0	λ	N	Triaxial Apparatus
SP5	proctor standard, w=32%	0.919	0.0334	2.056	MaTRIX
SP6	proctor standard, w=30%	0.927	0.0144	1.978	MaTRIX
SP10	proctor standard, w=42%	1.285	0.0403	2.433	MaTRIX
SP11	proctor standard, w=42%	1.293	0.0452	2.453	MaTRIX
SP13	proctor standard, w=32%	1.282	0.0160	2.338	MaTRIX
SP14	proctor standard, w=32%	1.581	0.0420	2.762	MaTRIX
	Average Proctor value	1.214	0.0319	2.337	
SP9	Consolidometer	1.180	0.0412	2.332	MaTRIX
SP12	Consolidometer	1.403	0.0377	2.526	MaTRIX
spl01	Consolidometer	1.236	0.0456	2.329	Bishop
spl02	Consolidometer	1.266	0.0444	2.332	Bishop
spl03	Consolidometer	1.252	0.0288	2.221	Bishop
spl04	Consolidometer	1.292	0.0405	2.323	Bishop
spl05	Consolidometer	1.268	0.0252	2.193	Bishop
spl06	Consolidometer	1.273	0.0359	2.284	Bishop
spl07	Consolidometer	1.218	0.0309	2.226	Bishop
spl08	Consolidometer	1.286	0.0405	2.292	Bishop
spl09	Consolidometer	1.287	0.0257	1.785	Bishop
spl11	Consolidometer	1.283	0.0451	2.306	Bishop
spl12	Consolidometer	1.302	0.0366	2.277	Bishop
spl13	Consolidometer	1.280	0.0413	2.302	Bishop
spl14	Consolidometer	1.265	0.0388	2.311	Bishop
spl15	Consolidometer	1.244	0.0374	2.275	Bishop
spl16	Consolidometer	1.216	0.0395	2.274	Bishop
spl17	Consolidometer	1.127	0.0329	2.194	Bishop
spl18	Consolidometer	1.171	0.0326	2.211	Bishop
spl19	Consolidometer	1.155	0.0344	2.257	Bishop
	Average consolidometer value	1.250	0.0368	2.262	
Average value for medium density spec.		1.232	0.0343	2.300	

Test id.	Reconstitution technique	Initial porosity, e_0	λ	N	Triaxial Apparatus
spl23	water sedimentation	1,866	0,0819	2,864	Bishop
spl24	water sedimentation	1,985	0,0853	2,960	Bishop
	Average water sedim. value	1,926	0,0836	2,9120	
AIRP2	Air pluviation	1.889	0.0906	3.144	MaTRIX
AIRP4	Air pluviation	1.898	0.0552	3.072	MaTRIX
AIRP7	Air pluviation	2.018	0.1010	3.335	MaTRIX
	Average Air pl. value	1.935	0.0823	3.184	
WETTP07	Wet tamping, w=30%	2.005	0.0757	3.065	
WETTP08	Wet tamping, w=30%	1.903	0.1020	3.247	MaTRIX
	Average wet tamp. value	1.954	0.0885	3.156	
Average value for low density spec.		1.993	0.0801	2.926	

Table 4-2: Compressibility parameters evaluated through isotropic compression tests.

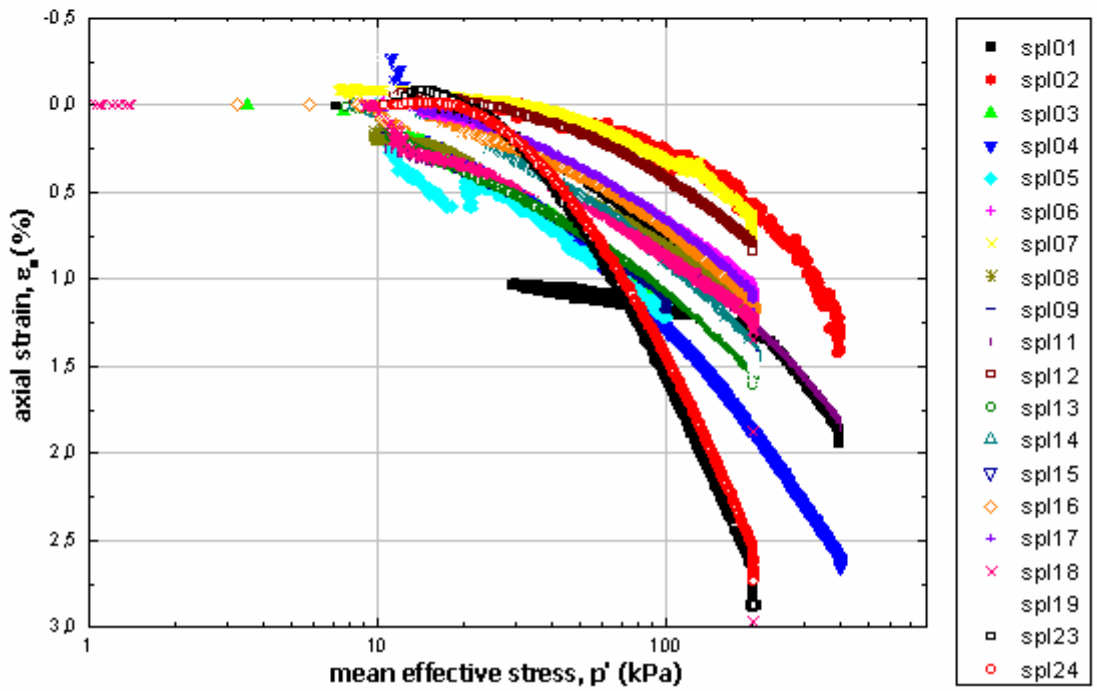
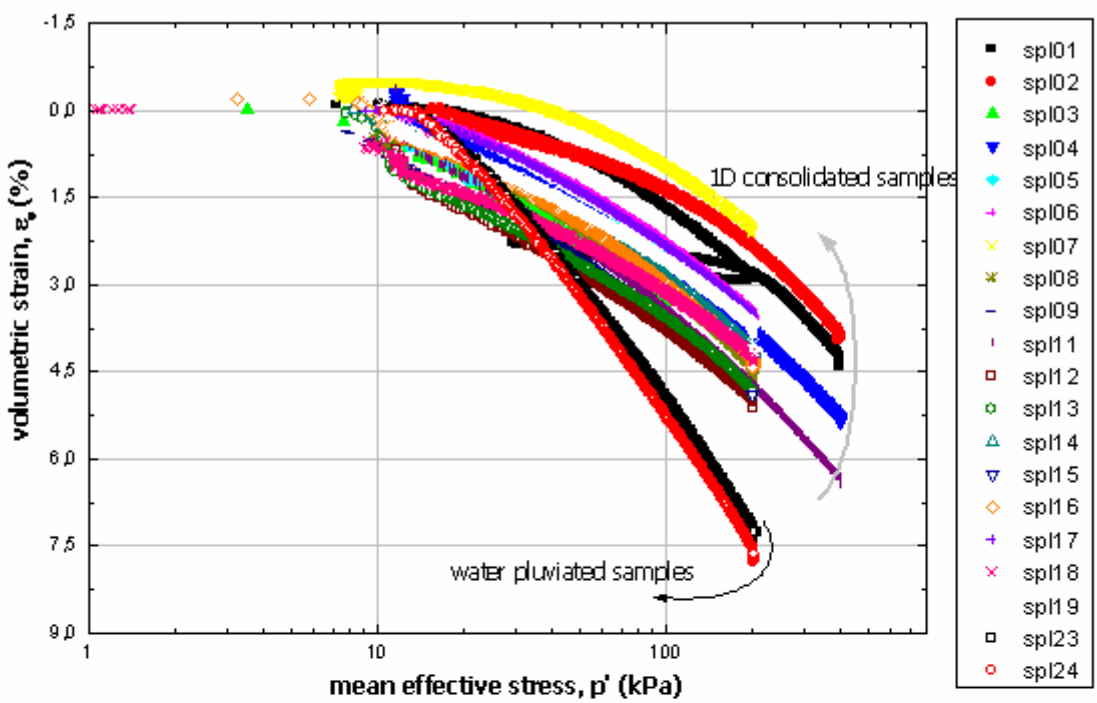


Figure 4-2: Isotropic compression tests for specimen prepared with 1D consolidation from slurry or with water sedimentation : (a) volumetric strain and (b) axial strain versus mean effective stress.

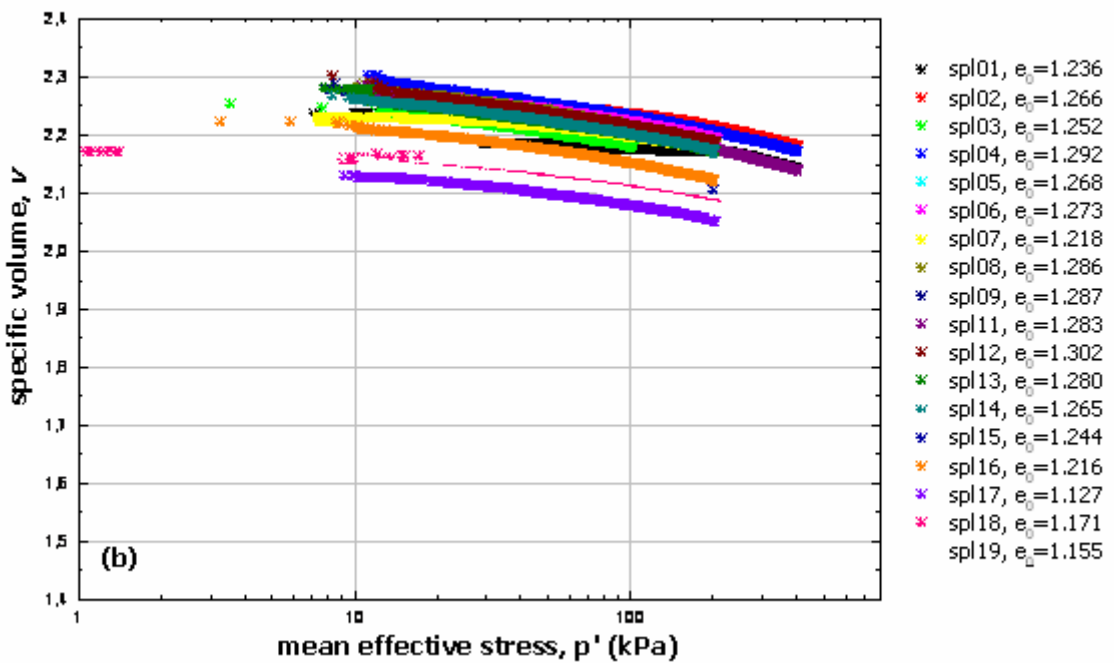


Figure 4-3: Isotropic compression curves in terms of specific volume $v=1+e$ versus mean effective stress, for specimens prepared in consolidometer or with water pluviation method.

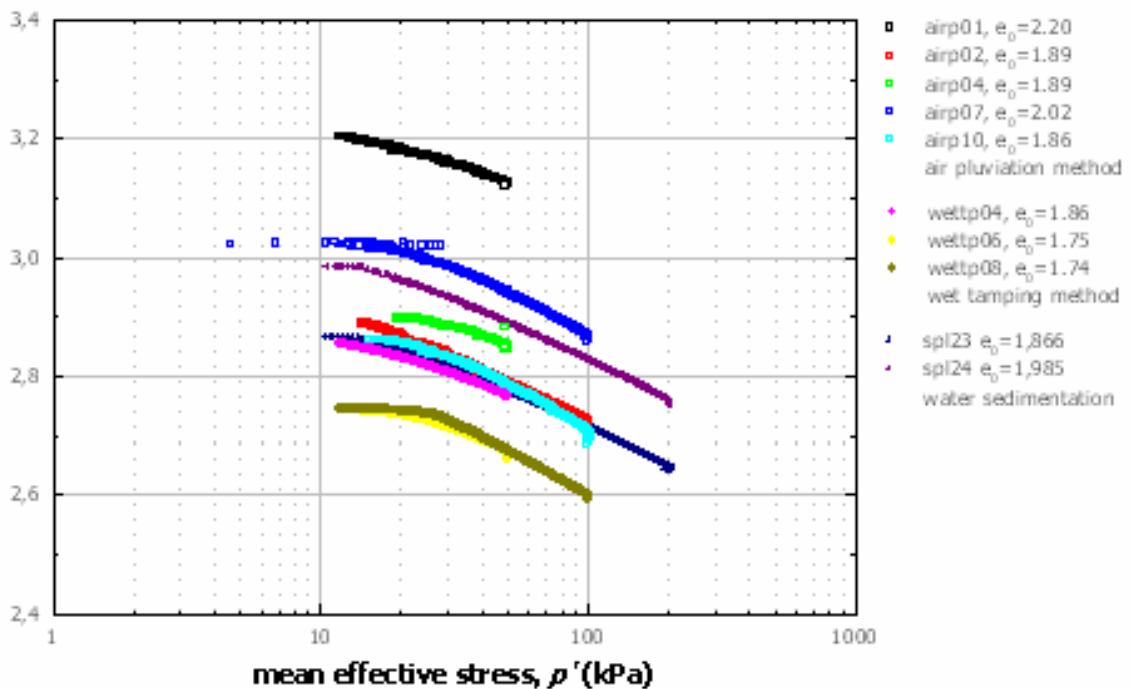


Figure 4-4: compression curves in terms of specific volume $v=1+e$ versus mean effective stress, for loose specimens.

4.3 Shear tests

4.3.1 Behaviour of specimen reconstituted in the consolidometer

The behaviour of specimens reconstituted in consolidometer during the shear stage has been analyzed.

The abbreviations spl02, spl03, spl06 refer to conventional isotropic compression undrained shear (CIU) triaxial tests. The abbreviations spl01, spl07, spl09 refer to conventional isotropic compression drained shear (CID) triaxial tests. Finally, the abbreviations spl05, spl08, spl09 refer to p' constant triaxial tests.

All the tests were executed starting from confining pressure of 100, 200 or 400 kPa.

In Figure 4-5 are plotted the stress-strain curves of the tests performed, while in Figure 4-7 are plotted the pore pressure increment-axial strain curves for undrained tests and the volume strain-axial strain curves for drained tests. The material undergoes at first a contraction stage, and when approaching the critical stage shows an expanding behaviour.

In

Figure 4-6 are plotted synthetically the results obtained in drained and undrained tests. In particular, in

Figure 4-6a the results are plotted in terms of $\eta = q/p'$ by the axial strain and in Figure 4-6b are reported the effective stress paths.

All the curves plotted in the $\eta:\varepsilon_a$ chart group in a narrow band; the undrained tests curves plotted in the $q:p'$ chart shows the typical behaviour of dense sand.

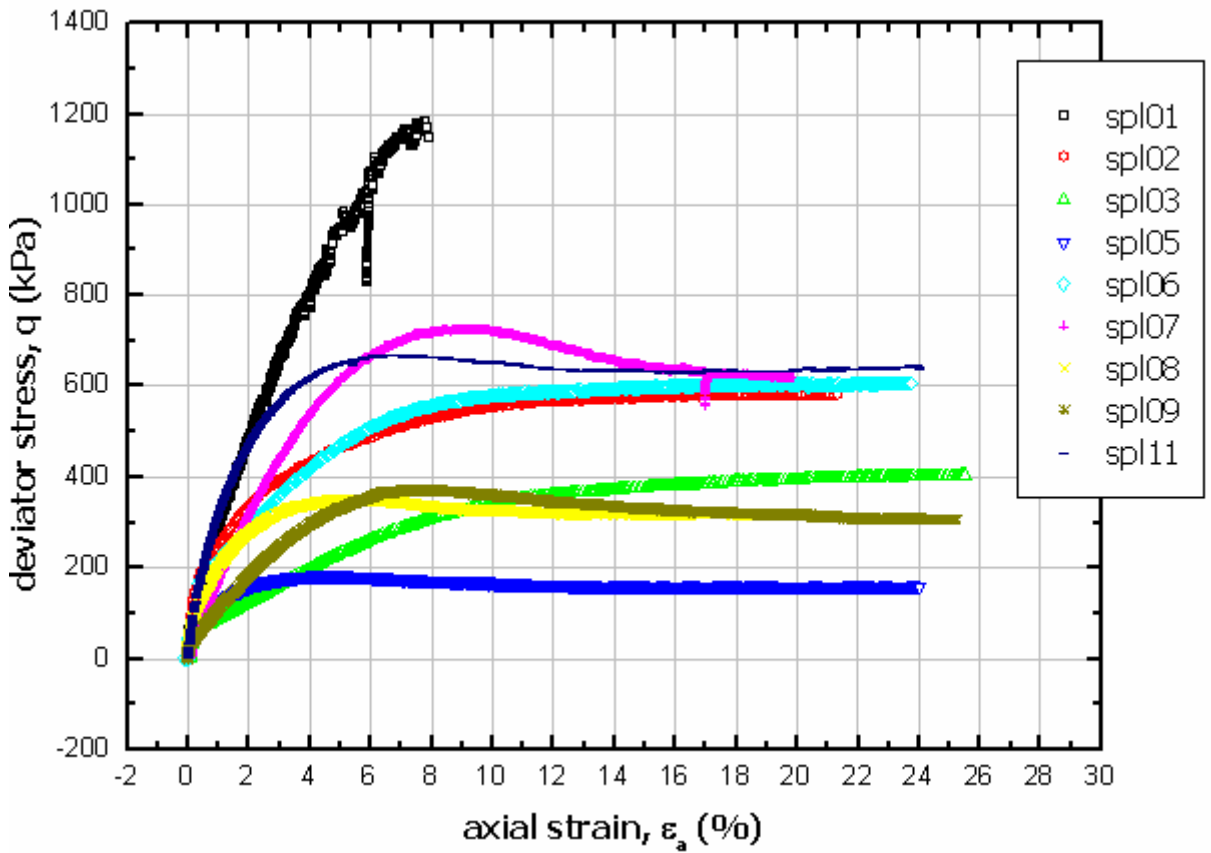


Figure 4-5: Stress-strain curve for specimen reconstituted in consolidometer.

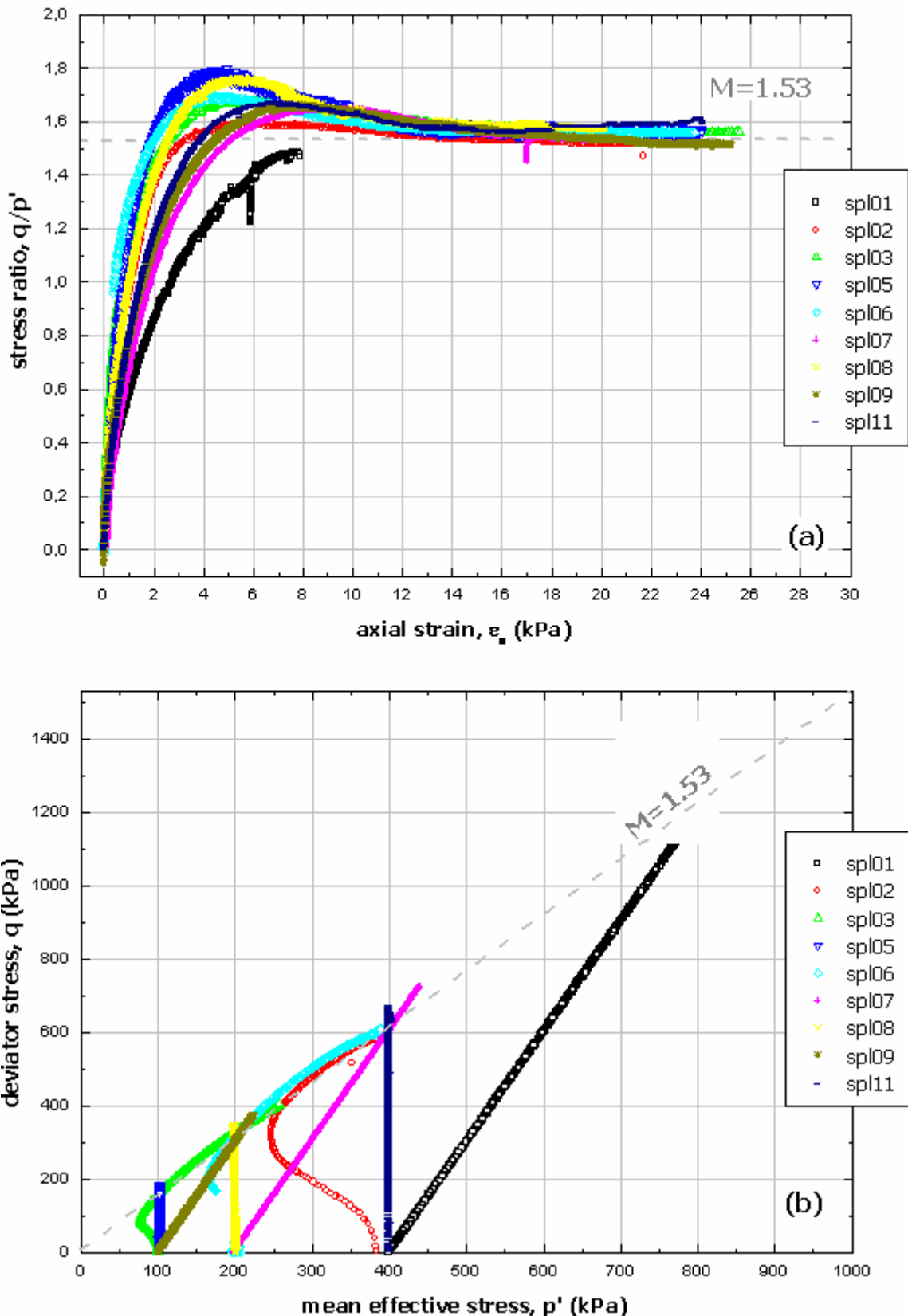
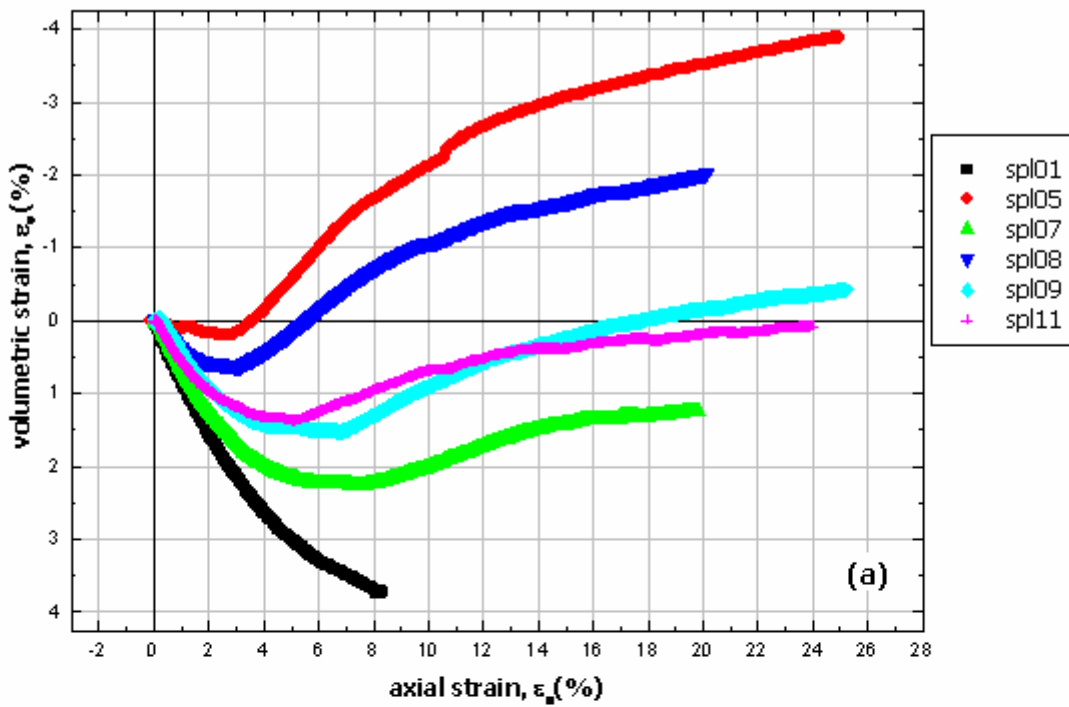
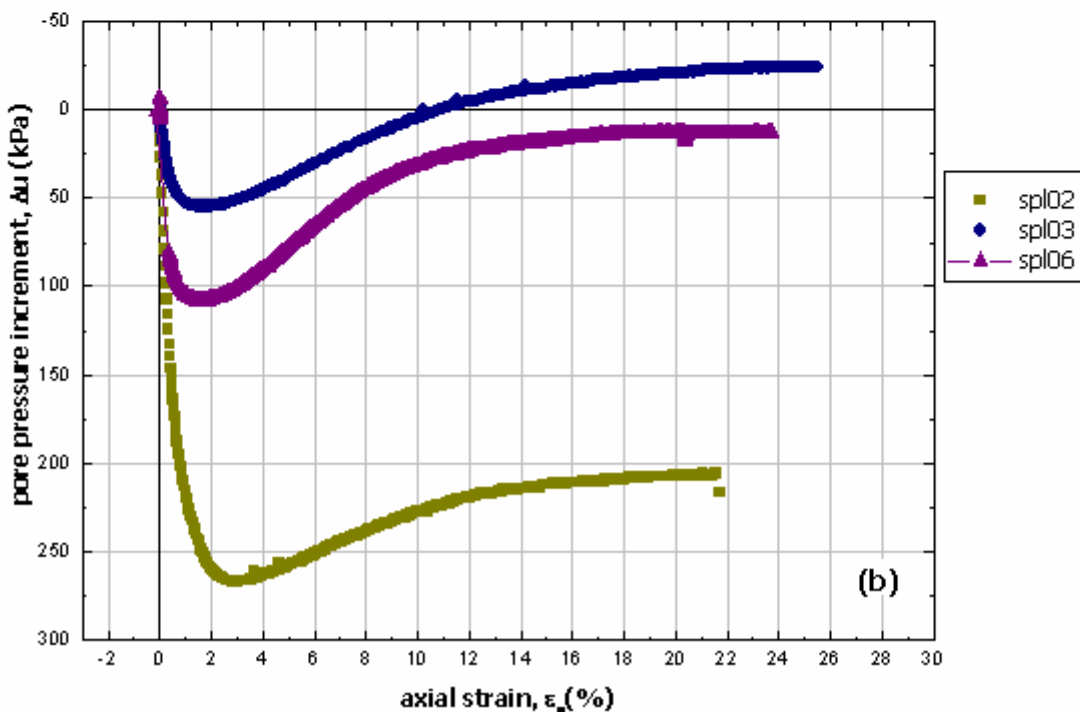


Figure 4-6 : $M=q/p'$ versus axial strain (a); $\eta=q/p'$ versus mean effective (b) for specimen reconstituted in consolidometer.



(a)



(b)

Figure 4-7: axial strain-volume strain plot (a) and pore pressure increment-axial strain plot (b); for specimen reconstituted in consolidometer.

4.3.2 Behaviour of specimen prepared with Proctor

The behaviour of specimens reconstituted with Proctor standard during the shear stage has been analyzed.

The multi-step shape of the stress-strain curve is due to sharp loading rate variations.

All the tests were executed starting from confining pressure of 100, 150 or 300 kPa.

In Figure 4-8a are plotted the stress-strain curves of the tests performed, while in Figure 4-8b are plotted the pore pressure increment-axial strain curves for undrained tests. The material undergoes at first a contraction stage, and when approaching the critical stage shows a dilating behaviour.

In the following figures are plotted synthetically the results obtained in the undrained tests. In particular, in Figure 4-9a the results are plotted in terms of $\eta = q/p'$ by the axial strain and in Figure 4-9b are reported the effective stress paths.

All the curves plotted in the $\eta:\varepsilon_a$ chart group in a narrow band; the undrained tests curves plotted in the $q:p'$ chart shows the typical behaviour of dense sand.

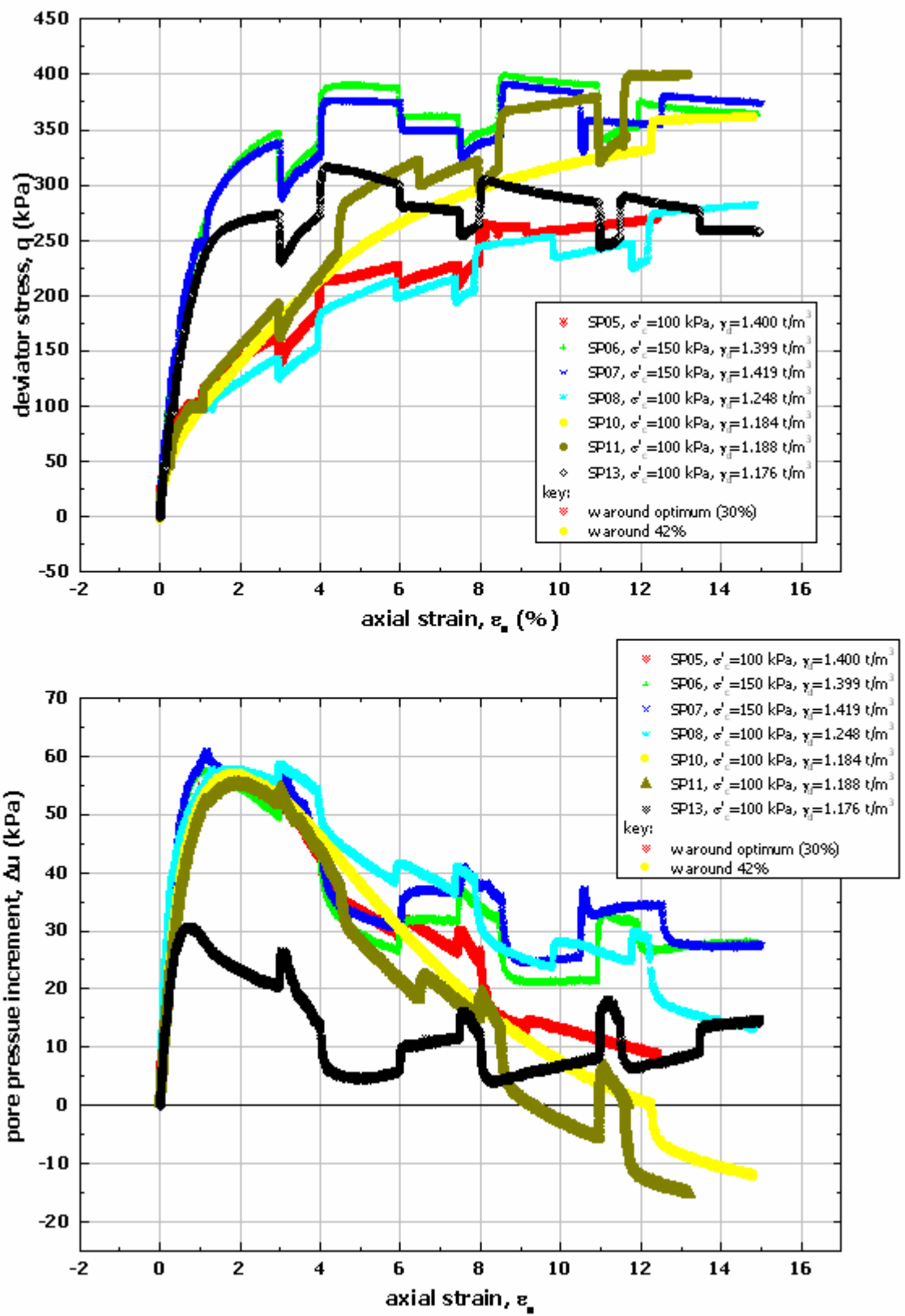


Figure 4-8 Deviator stress- axial strain curve (a) and pore pressure increment- axial strain curve (b); for specimen reconstituted with proctor standard procedure.

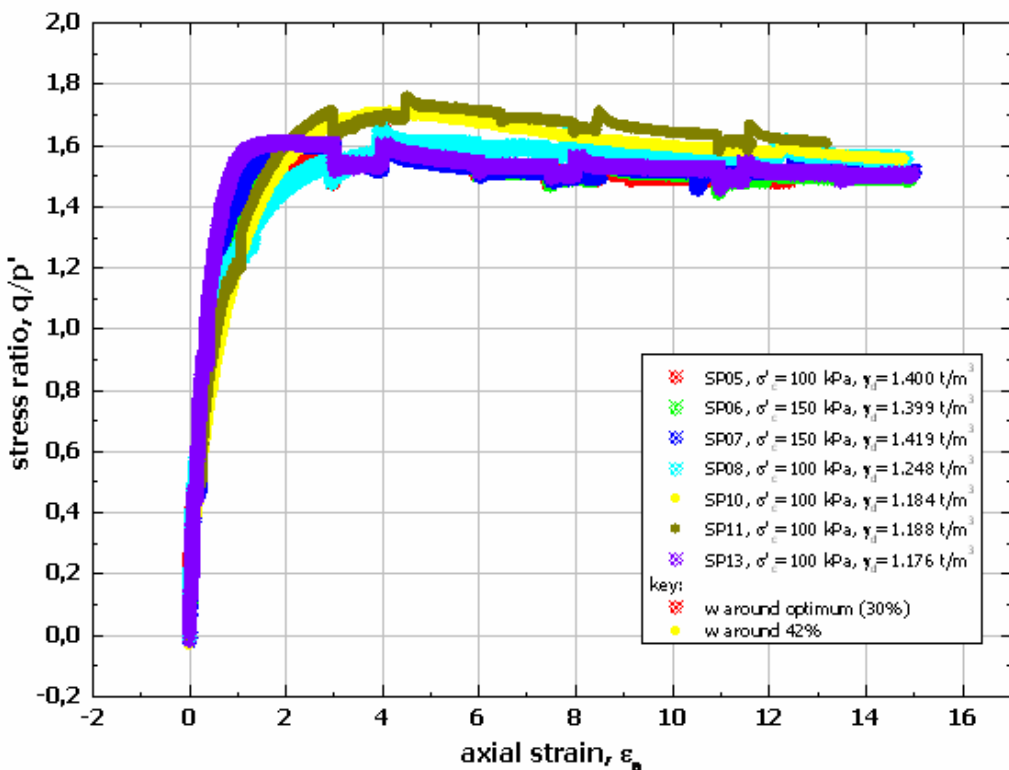
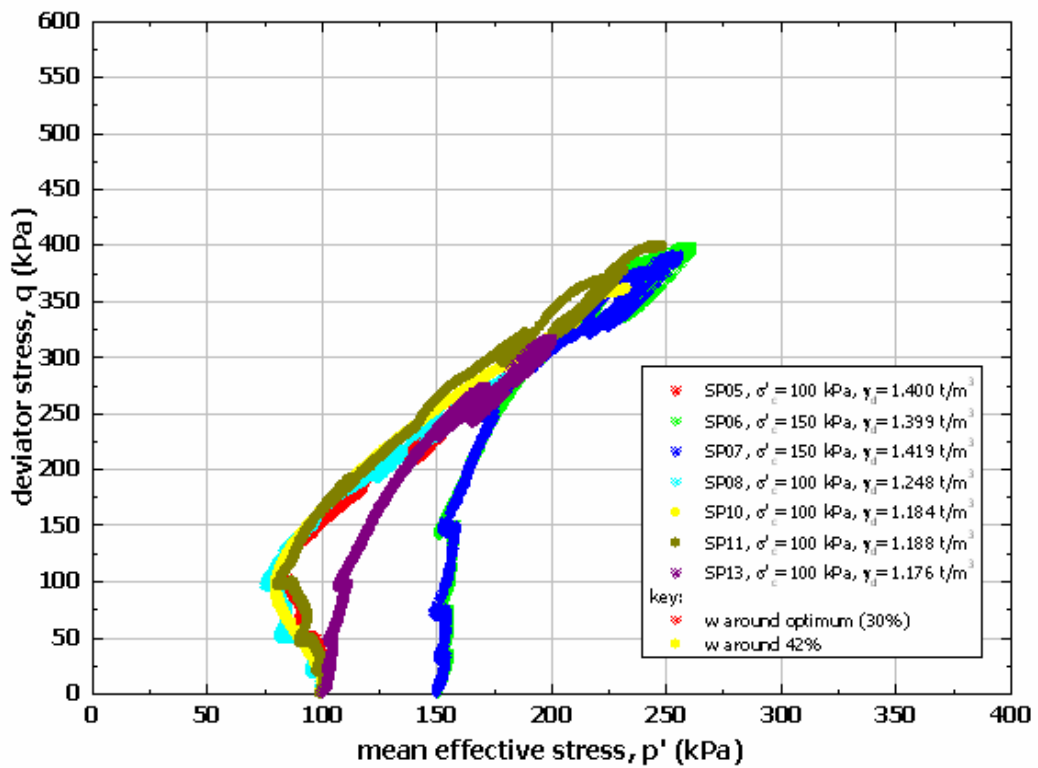


Figure 4-9 Deviator stress – mean effective stress curve (a) and stress ratio - axial strain curve (b); for specimen reconstituted with proctor standard procedure.

4.4 Undrained shear tests over specimen reconstituted with different techniques: flow liquefaction susceptibility

Static liquefaction can be explained with the steady state theory, that was deduced on the basis of experimental data obtained through undrained triaxial tests.

Depending on the conditions assumed by the specimen at the end of consolidation, in terms of mean effective stress and porosity, in the shear tests it can express one of the following behaviour (Figure 4-10):

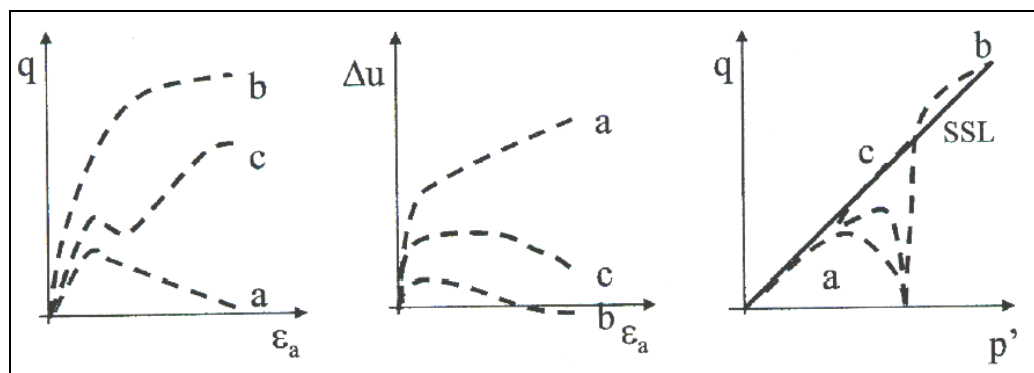


Figure 4-10: Typical behaviour of granular soils in consolidated undrained triaxial tests CIU: a) unstable behaviour, b) stable behaviour, c) intermediate behaviour.

- a) (high porosity): unstable behaviour. The specimen develops first a monotonic increment of shear stress until peak strength is reached; then, a rapid strength reduction takes place, stabilizing at high deformations, around a value lower than the peak value. This behaviour can be justified with the natural tendency of loose soil to contraction, that in undrained conditions leads to pore pressure increase, reducing confining stress and thus shear strength.
- b) (low porosity): stable behaviour. The specimen develops a monotonic increment of shear stress until peak strength is reached. Peak strength is coincident with final strength. Pore pressure rises up in the first stage of the shear test, but then decrease down to negative values thanks to the specimen dilating behaviour.

c) (intermediate porosity): intermediate behaviour. Shear stress rises up till the peak value is reached. Following, there could be a strength reduction, followed by a new strength increment (phase transformation point) until, at high strain, the ultimate value is reached. Peak strength can be coincident with the ultimate strength. Pore pressure stay positive, following the change in the specimen behaviour.

Looking at the effective stress path $p'-q$ (Figure 4-11 - Figure 4-12- Figure 4-13), for loose specimen (initial void ratio in the range $0,928 \div 1,581$) consolidated at confining stress in the range $0 \div 100$ kPa, at which natural specimen, specimen prepared with air pluviation and wet tamping were tested, san Pantaleone pozzolana shows up a contractive behaviour, typical of loose sands.

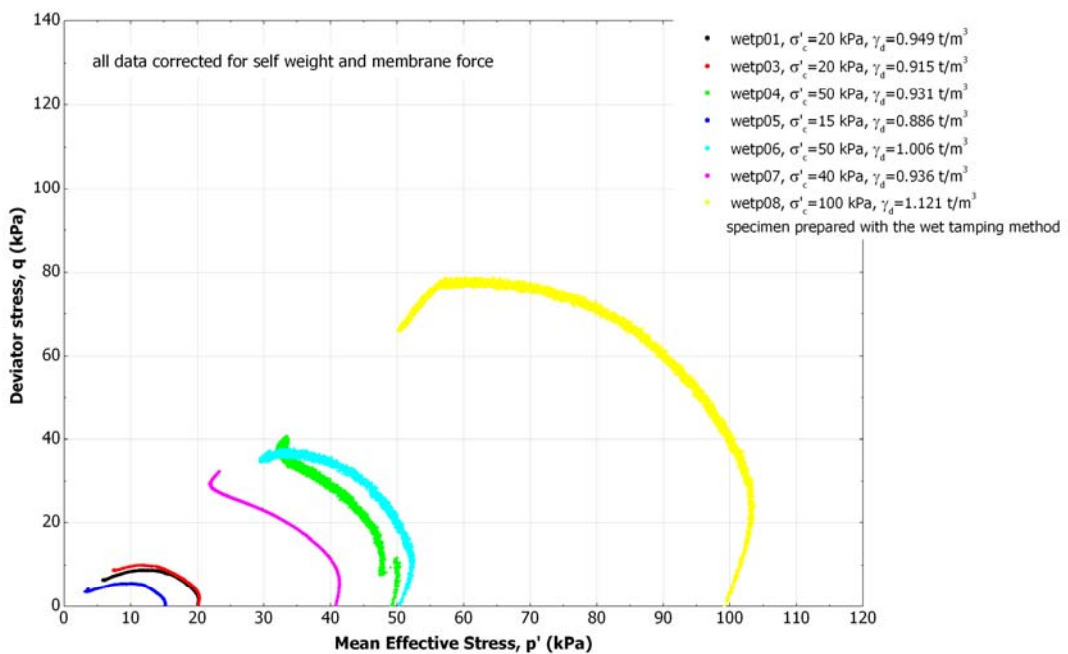


Figure 4-11 Effective stress path for specimen reconstituted with the wet tamping method.

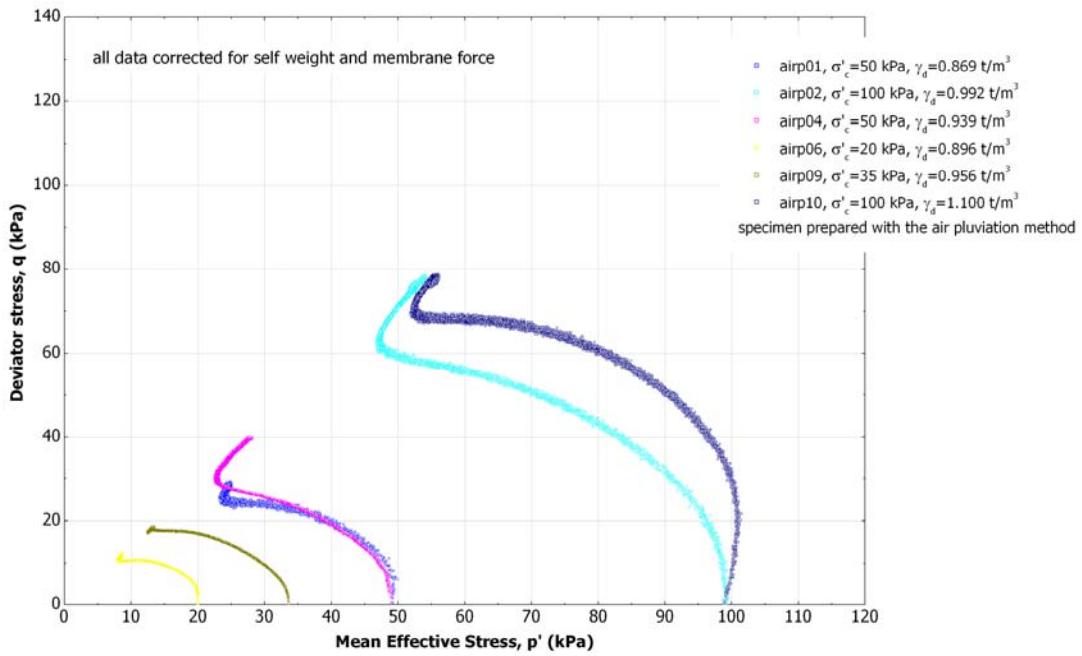


Figure 4-12 Effective stress path for specimen reconstituted with the air pluviation method.

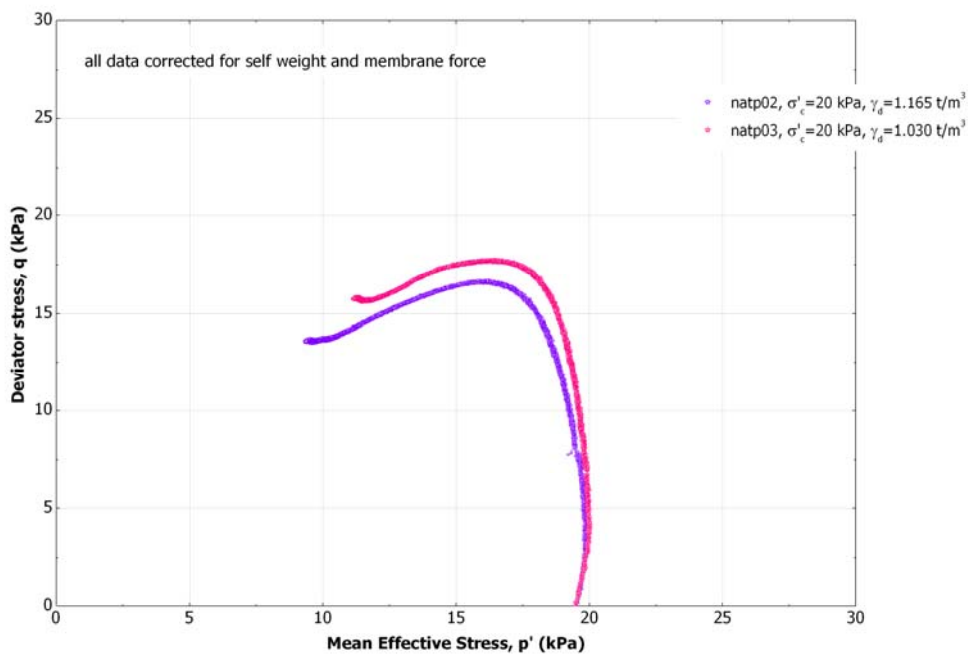


Figure 4-13 Effective stress path for natural specimens.

Remoulded specimens, prepared in proctor standard or in consolidometer (at an initial void ratio in the range $0,928 \div 1,581$), and consolidated to a mean effective stress up to 400 kPa, show a dilating behaviour (Figure 4-14), similar to dense sand behaviour.

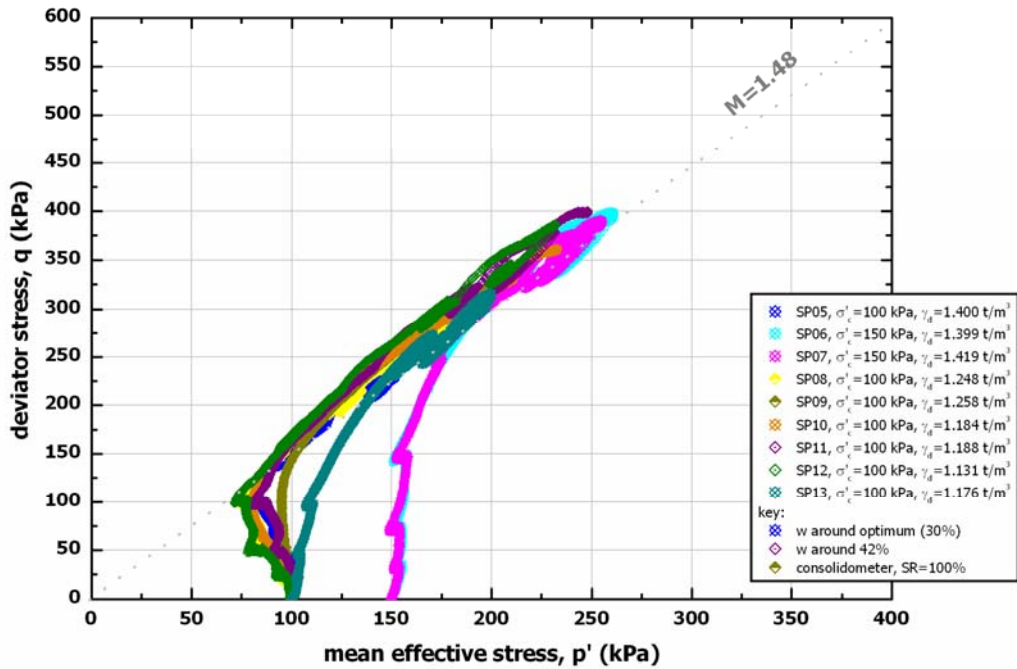


Figure 4-14 Effective stress path for specimens reconstituted with the proctor standard method.

For the study of the undrained shear behaviour of San Pantaleone pozzolana, diagram in ε_a - q , ε_a - Δu and ε_a - q/p' plane are useful: see Figure 4-15 to Figure 4-8. In all the graph reported in this section to describe the undrained shear behaviour of our pozzolana the axial deformation was measured using LVDT. In fact at this stage axial deformations exceed gap sensor measuring range.

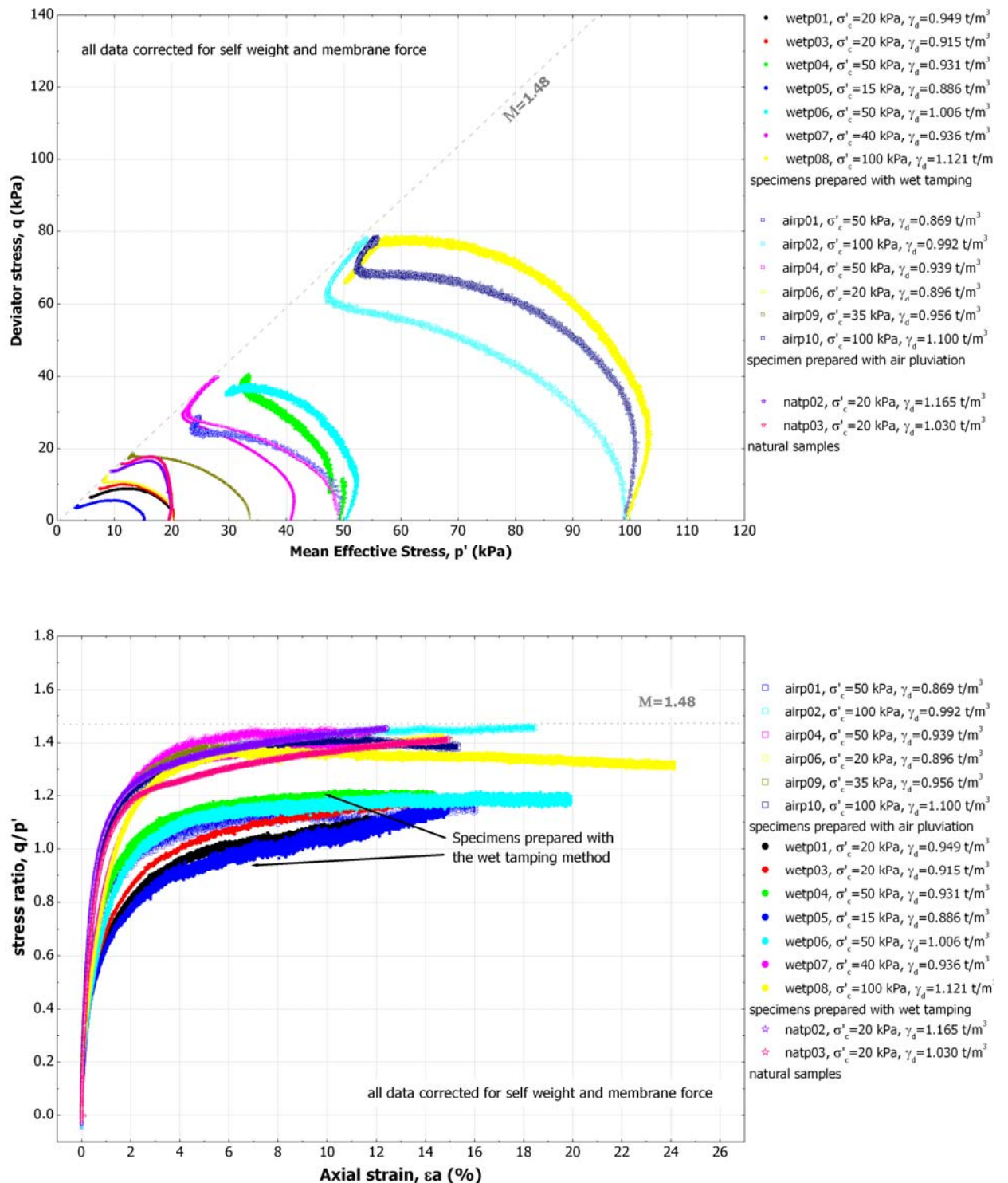


Figure 4-15 $\eta=q/p'$ graphs in function of the axial strain (a); effective stress path (b); for loose specimens, natural and reconstituted with different techniques.

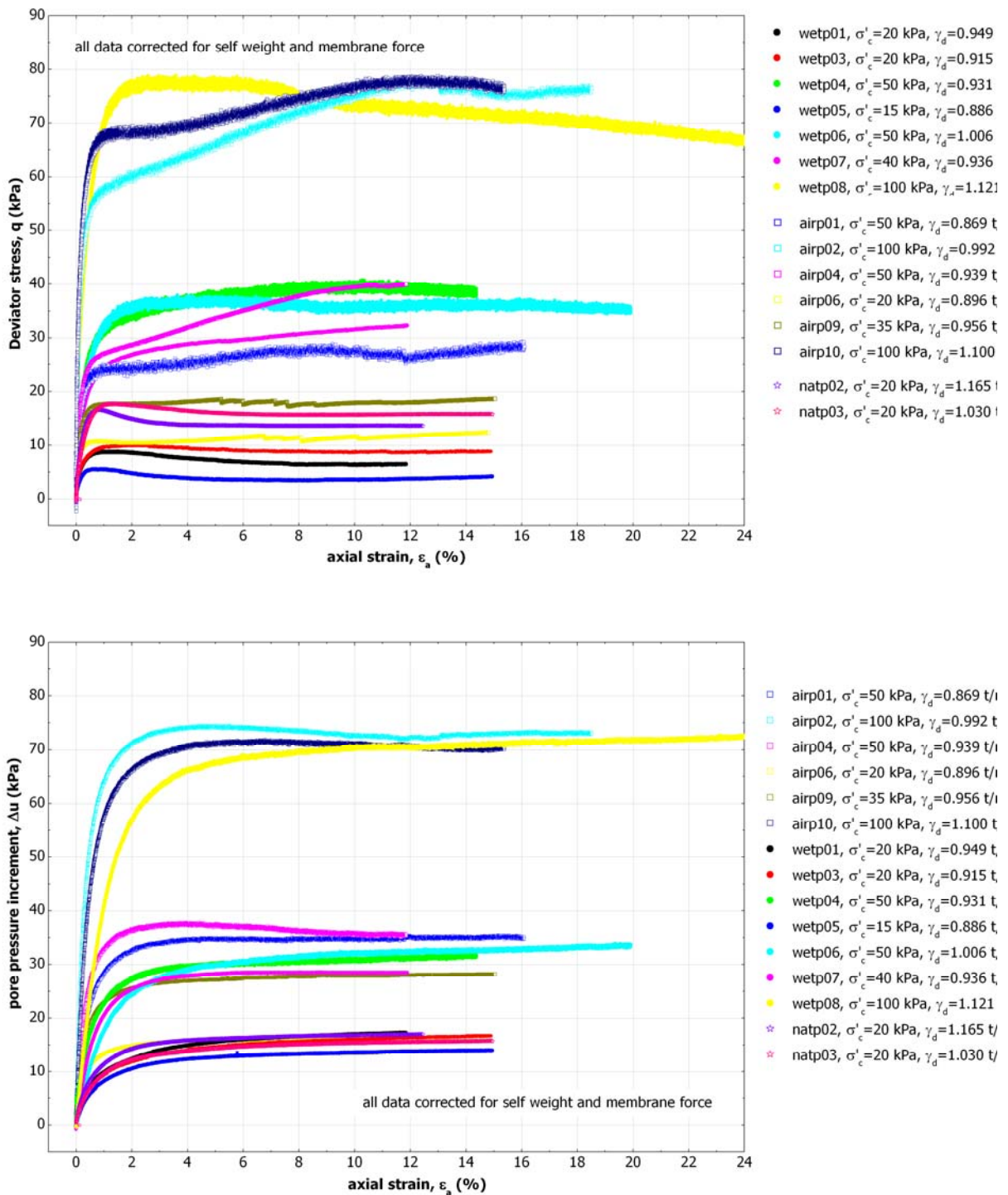


Figure 4-16 Deviator stress – axial strain (a) and pore pressure increment - axial strain (b); for loose specimens, natural and reconstituted with different techniques.

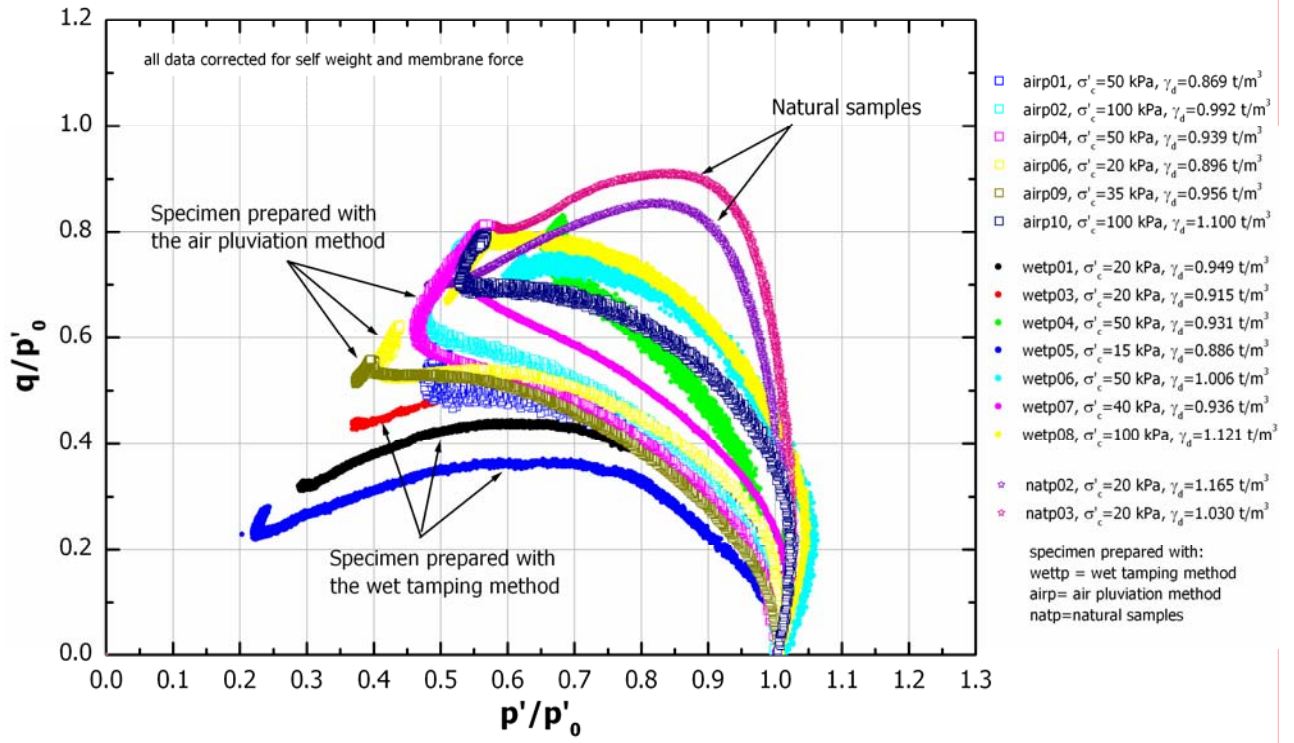


Figure 4-17 Effective stress paths adimensionalized according to the confining stress, for loose specimen, prepared with different reconstitution techniques.

4.5 Undrained shear tests over specimen reconstituted with different techniques: critical state behaviour

In this paragraph, data obtained in triaxial tests executed on specimen prepared with different reconstitution technique are shown.

In Figure 4-18 data relative to critical state are plotted in a q-p' chart. Data are separated per reconstitution technique. Since data scattering seems not to be due to the reconstitution technique but to experimental errors (deriving from difficulties in sampling specimens and in collecting specimen material after failure in low density specimen), all data have been interpolated with only one line (see Figure 4-19). Thus, the q vs p' interpolation line slope results 1,53. Using Equation 4-3: it is possible to evaluate the friction angle for San Pantaleone pozzolana: the material analyzed exhibits a friction angle of 37.6°.

$$\sin \phi' = \frac{3M}{6+M} \quad \text{Equation 4-3}$$

In Figure 4-20 data relative to critical state are plotted in a v-p' semi-log chart, grouping data relative to the same reconstitution technique. Also in this case, a unique interpolation line has been chosen (Equation 4-4).

$$v = \Gamma - \lambda \cdot \ln(p') \quad \text{Equation 4-4}$$

In coherence with the critical state theory, the parameters that define the critical state line do not depend on the load history previously experienced by the specimen. However, the slope of the critical state line in the v-p' semi log plane should be the same as the isotropic compression line for very loose soils. For San Pantaleone pozzolana this aspect of the theory seems not to be respected (see Figure 4-22)

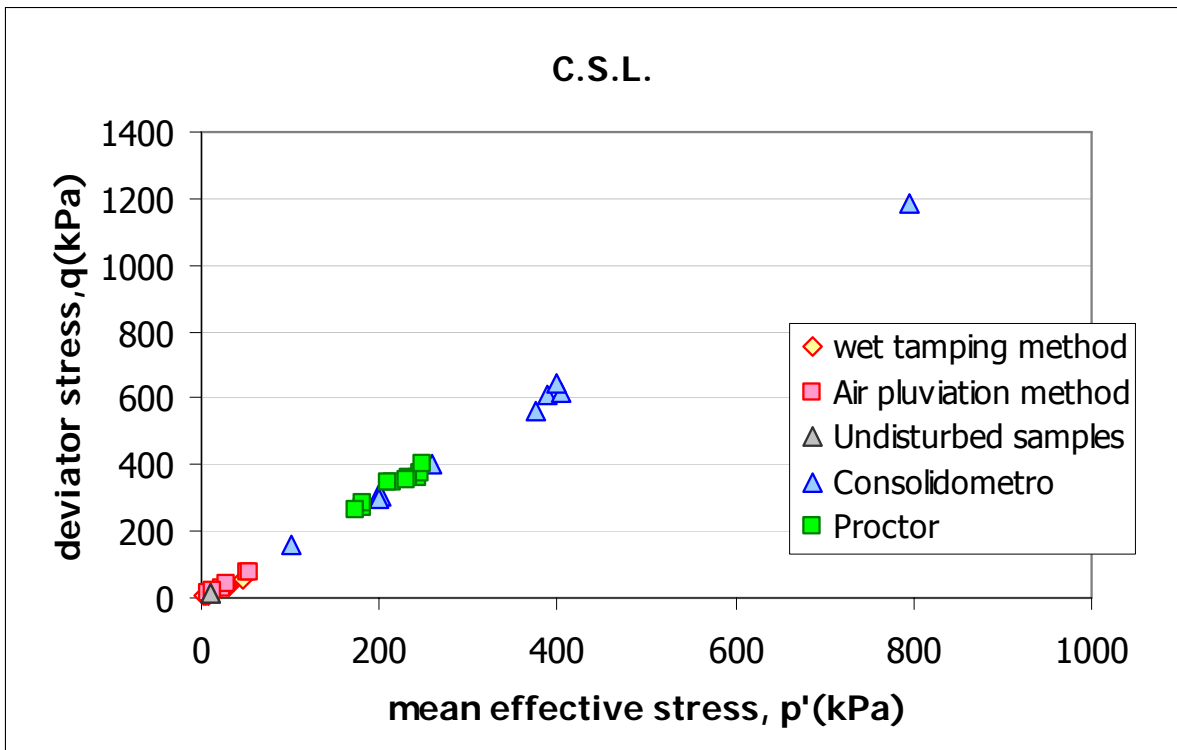


Figure 4-18: Values at failure in the $q-p'$ plane for specimens prepared with different reconstitution techniques and for undisturbed specimens.

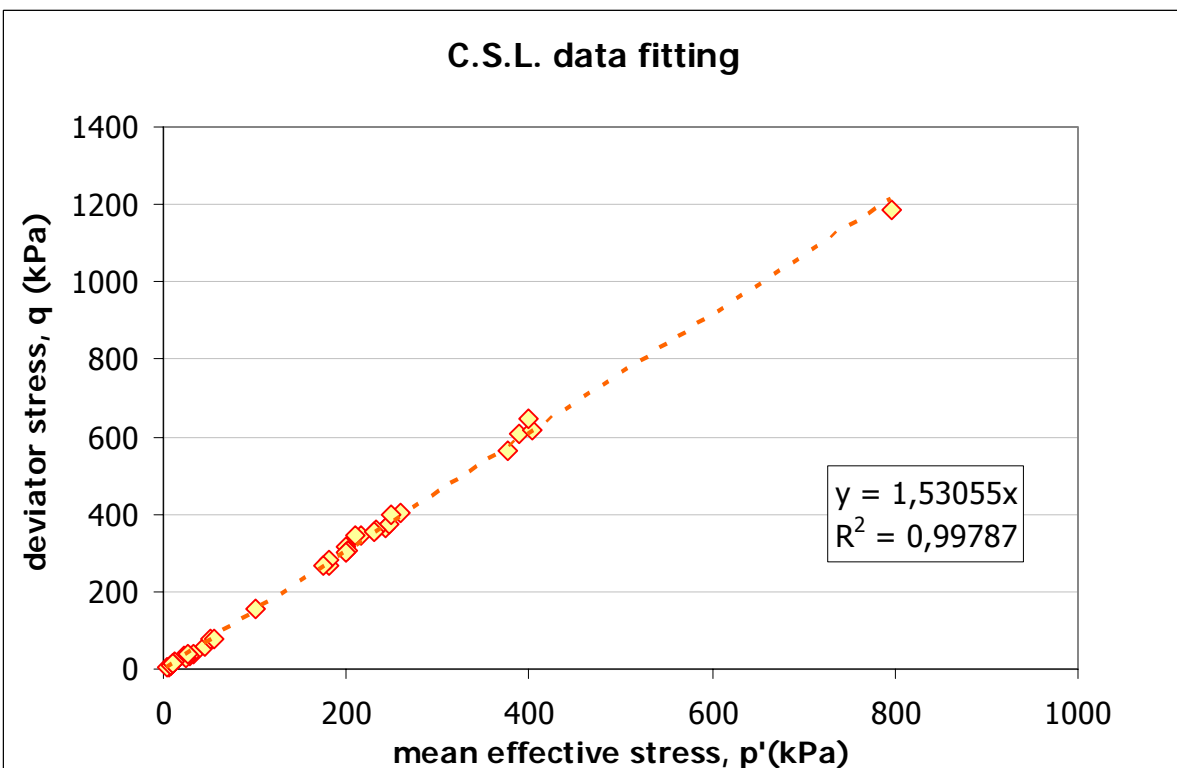


Figure 4-19: Interpolation of all data at failure to obtain critical state parameter M.

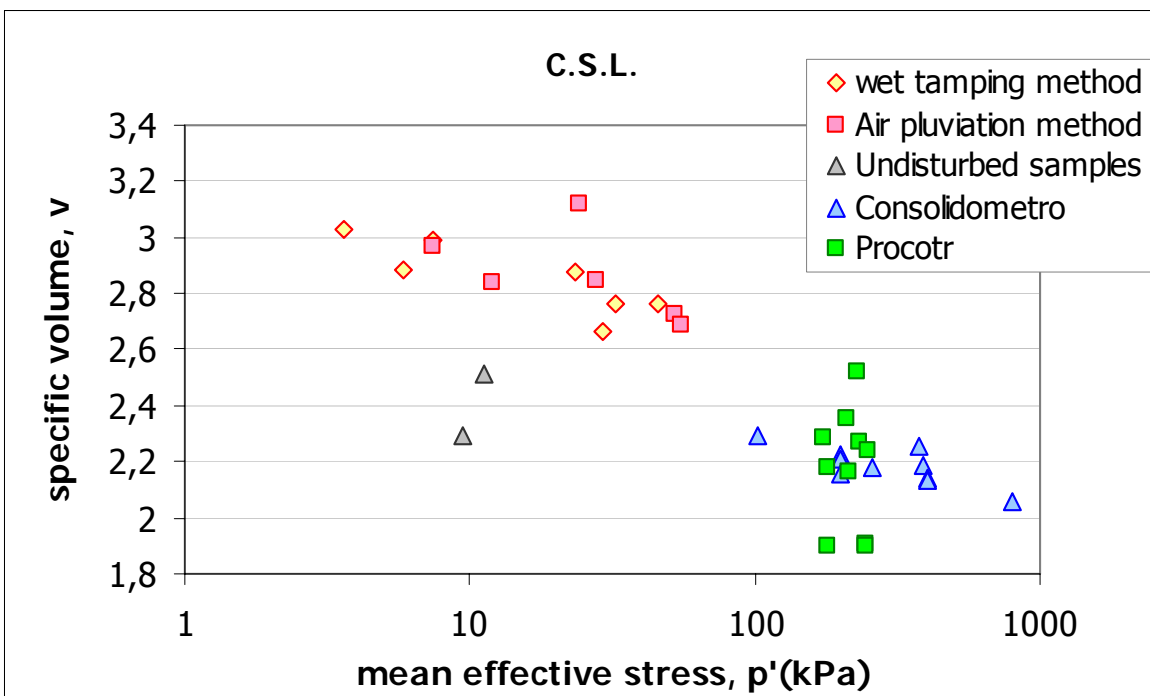


Figure 4-20 Values at failure in the v-p' plane for specimens prepared with different reconstitution techniques and for undisturbed specimens.

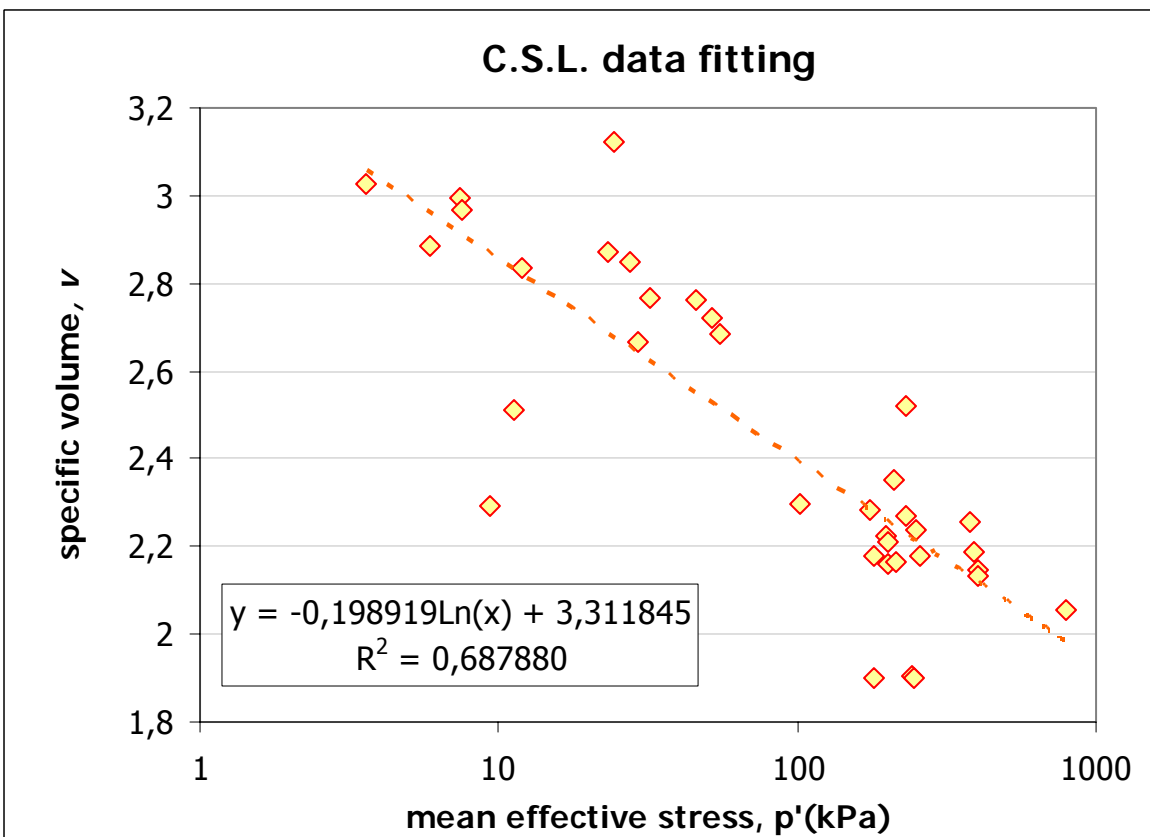


Figure 4-21 Interpolation of all data at failure to obtain critical state parameter k and λ .

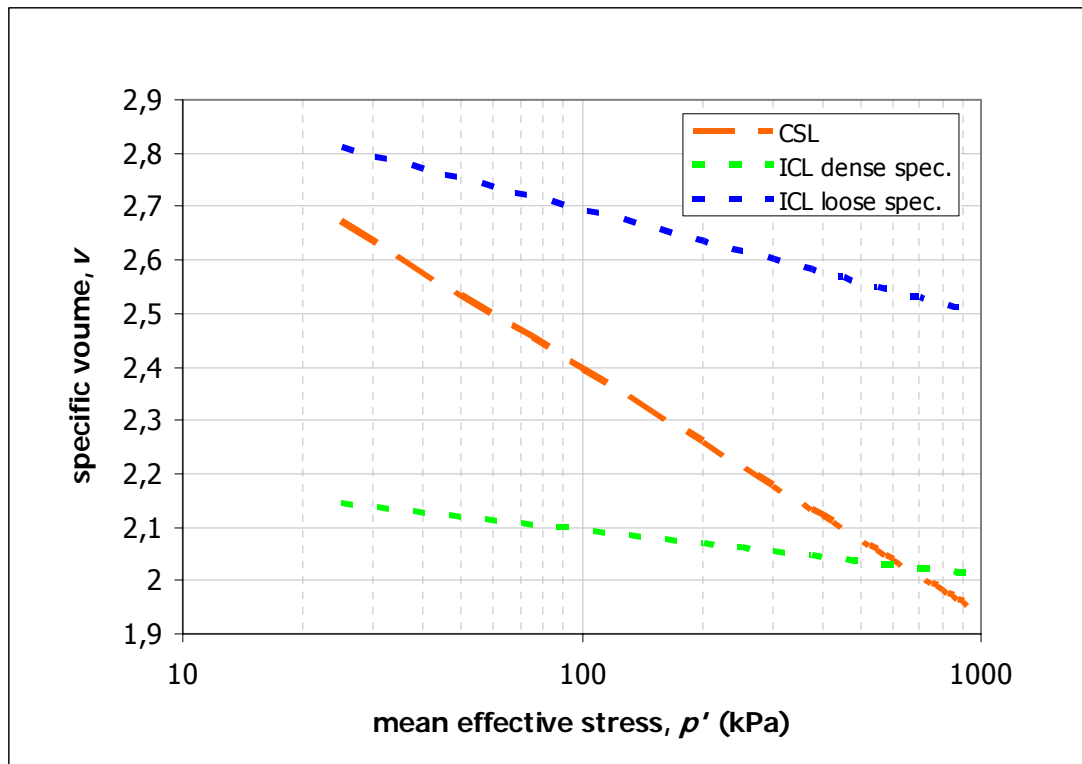


Figure 4-22 Isotropic compression line (ICL) for loose specimens, ICL for dense specimen and critical state line (CSL) for both loose and dense specimens.

REFERENCES

- Grasso, A. (2006): **Comportamento meccanico della pozzolana di S. Pantaleone mediante prove di laboratorio monotone e cicliche**, Bachelor thesis. (in Italian).
- Henkel, D. J. & Gilbert, G. C. (1952): **The effect of rubber on the measured triaxial compression strength of clay samples**, Geotéchnique, Vol. 3, pp. 20-29.
- Koseki, J., Itakura, D., Kawakami, S., Sato, T. (2001): **Cyclic torsional shear tests on liquefaction resistance of sands under low confining stresses**, Proceedings of the Fourth International Conference on Recent Advances in Geotechnical Earthquake Engineering and Soil Dynamics, San Diego, California, March 26-31, 2001.
- Lampitiello, S. (2003): **Resistenza non drenata e suscettibilità alla liquefazione di ceneri vulcaniche della Regione Campania**, Phd Thesis. (in Italian).
- Parlato, A. & Santucci de Magistris, F. (2006): **Comportamento meccanico di una pozzolana a medie e basse pressioni di confinamento**. Incontro annuale dei ricercatori di geotecnica, IARG2006 (in Italian).
- Riemer, M. (2004): **Emerging Trends in Cyclic Triaxial Testing**, International Workshop on the Uncertainties in Nonlinear Soil Properties and their Impact on Modeling Dynamic Soil Response, PEER Headquarters, UC Berkeley, March 18-19, 2004
- Tatsuoka, F., Fukushima, S. (1984): **Strength & deformation characteristics of saturated sand at extremely low pressures**, Soils & Foundations, 24 (4), 30-48.
- Vaid, Y. P. & Negussey, D. (1984): **A critical Assessment of membrane penetration in the triaxial test**, Geotchnical Testing Journal, 7(2), pp. 70-76.

Chapter 5

Stiffness and cyclic behaviour

5.1 Introduction

Until 20 years ago, it was of common knowledge within the international geotechnical community that soil has a different behaviour in static (i.e. small strain rate) and in dynamic (high loading frequency) load tests. In particular, the widespread opinion was that the dynamic stiffness of the soil (obtained in geophysical tests) was different from the static stiffness (obtained in cyclic or monotonic laboratory tests).

A revolution took place in the eighties, with the especial contribution of Burland(1988), Jardine (1984) and Tatsuoka (1992).

Thanks to significant technical improvement (see charter 1), it has been understood that the discrepancies observed in the past were not due to the physical nature of the soil, but to experimental errors related to instrumentation deformability or to bedding errors.

This aspect has a huge practical importance: nowadays it is of common knowledge that in the study of soil dynamics, it is possible to use mechanical parameters obtained in static monotonic tests as well as in cyclic dynamic tests.

5.2 Soil Stiffness

A soil subjected to cyclic loading might exhibit a hysteresis loop of the type shown in figure 5.1. This hysteresis loop can be described in two ways: first, by the actual path of the loop itself, and second by parameters that describe its general shape. In general terms, two important characteristics of shape of a hysteresis loop are its inclination and its breadth. The inclination of the loop depends on the stiffness of the soil, which can be described at any point during the loading process by the tangent shear modulus, E_{tan} .

Obviously, E_{tan} varies throughout a cycle of loading but its average value over the entire loop can be approximated by the peak to peak Young modulus

$$E_{pp} = \frac{q_{pp}}{\varepsilon_{pp}} \quad \text{Equation 5-1}$$

where q_{pp} and ε_{pp} are the deviator stress and the axial strain amplitude, respectively. Thus E_{pp} describes the general inclination of the hysteresis loop. The breadth of the hysteresis loop is related to the area, which as a measuring of energy dissipation can conveniently be described by the damping ratio:

$$D = \frac{W_D}{4\pi W_s} = \frac{1}{2\pi} \frac{A_{loop}}{E_{sec} \varepsilon_c^2} \quad \text{Equation 5-2}$$

where W_D is the dissipated energy, W_s the maximum strain energy, and A_{loop} the area of the hysteresis loop. The parameters E_{pp} and D are often referred to as equivalent linear material parameters.

In monotonic loading tests, the average Young modulus for a certain axial strain level ε_a is often referred to as the secant Young Modulus E_s . In an isotropic elastic medium, it would be $E_{sec}=E_{tan}=E_{pp}$.

In the following, we will refer to E_{pp} when talking about the stiffness evaluated in cyclic tests, and to E_{sec} when talking about the stiffness evaluated in monotonic triaxial tests.

Soil stiffness has been measured in all the triaxial tests executed for this PhD Thesis. For specimen set up in the MaTRIX apparatus, peak to peak Young modulus was evaluated in small strain cyclic tests, executed both over specimen in otherwise isotropic conditions and over specimen in anisotropic stress conditions, in the midst of otherwise conventional undrained triaxial tests.

Moreover, secant Young modulus was measured during monotonic shear tests. In triaxial tests performed in MaTRIX cells, it has been possible to calculate small strain stiffness of San Pantaleone soil. The stiffness was evaluated using both gap sensor and LDT transducers. The results obtained are reported in Appendix I. For homogeneity and comparability reason, all the data illustrated in this chapter, derive from axial strains measured using gap sensor. In fact, it is not possible to use LDT on weak specimen: the measuring strange of the instrument is narrow, and the starting of plastic, irreversible strain in the strain gauge would cause breakage. In Figure 5-2 the results of a typical triaxial test are represented in terms of soil stiffness. The secant Young modulus (in green, measure in the monotonic shear stage) is compared with the peak to peak Young modulus (in orange, measured in small strain cyclic tests). When Bishop triaxial machine has been used, soil stiffness has been evaluated from external axial strain measures (LVDT). These results are not comparable with the stiffness obtained through gap sensor. However, Bishop cells were used to study the behaviour of soil specimen undergoing large strain loading cycles, and consequently the cyclic strength of san Pantaleone sand (see par. 5-18).

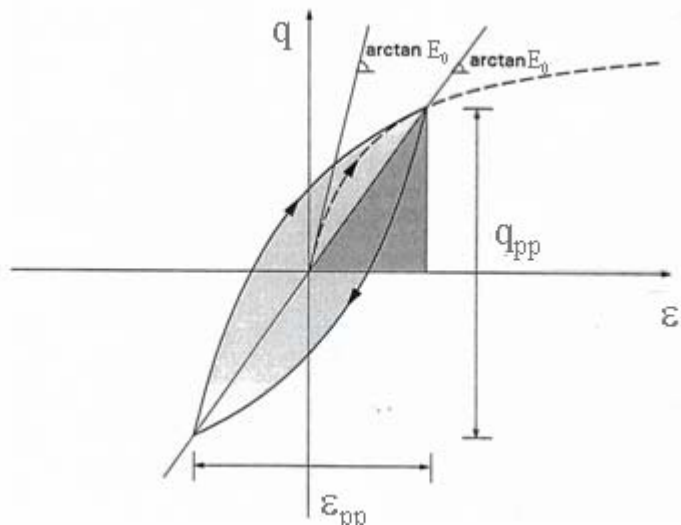


Figure 5-1 Peak to peak Young modulus, E_{pp} , and tangent Young modulus, E_{tan}

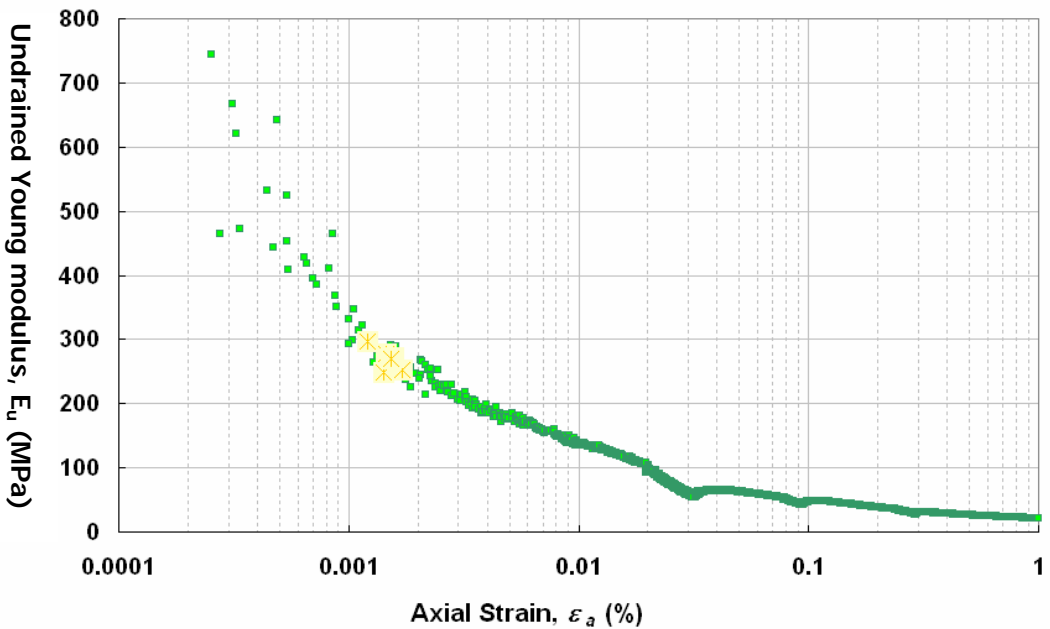


Figure 5-2 Comparison between Secant Young modulus (in green) and peak to peak Young modulus (in orange), measured in the course of the same triaxial test.

5.3 Young modulus

The Young modulus of an element of soil varies with cyclic load amplitude. It has been proven in laboratory that the Young modulus decreases as the strain amplitude increases, whilst the damping ratio increases as the strain amplitude increases.

As the axial deformation increases, it is possible to characterize three distinct behaviours.

At first, the soil specimen behaves linearly. The soil stiffness assumes its highest value E_0 , and then it slowly decreases as the deformation increases. Even though soil non linearity might manifest even at very small deformations, it is generally assumed that $E(\epsilon)$ is constant and equal to E_0 if the axial strain is lower than a conventional linear threshold ϵ_l . The linear threshold can range between 0.00001% and 0.01%, depending on the grading curve and on the micro-structural nature of the tested soil. For axial strain lower than the elastic threshold, damping ratio is on the contrary at his minimum (D_0), and stays quite unchanged.

At such small strains, the soil behaviour is not dependent on the strain level, and load-unload cycles have very narrow width.

Granular soils are not very sensitive to load frequency, and have a low tendency to dissipate energy, so that D_0 can almost be neglected.

Cohesive soils are instead very sensitive to load frequency, also at low strain levels. It has been proved (see for instance D'Onofrio et al. 1999) that both G_0 and D_0 increase with load frequency after a certain threshold frequency level.

For axial strain beyond the linear threshold, the soil shows a heavily non linear-dissipative behaviour: Young modulus decreases and correspondently the damping ratio increases. q - ε cycles shape modifies as the cycles amplitude increases: the typical hysteresis loop shape is gradually reached.

However, the material keeps a stable behaviour, that does not depend on the load history. Moreover there is no coupling between shear strain and volumetric strain: this means that an axial loading cycles will not lead do ε_v developing in drained test nor to ΔU developing in undrained tests.

As axial strain increases, it is possible to identify another threshold, called "volumetric threshold", ε_v , beyond which the soil undergoes irreversible micro-structural changes. This strain level is always ten to one hundred times larger than the linear threshold.

Beyond ε_v , cyclic loading effects shows up in terms of coupling between shear strain and volumetric strain: after a q - ε cycle volumetric strain for drained tests and pore pressure increment for undrained tests start developing.

The soil specimen condition changes in terms of density and/or effective confining stress, thus affecting soil mechanical behaviour.

Typically, a degradation of the mechanical behaviour of the specimen can be observed, highlighted by a progressive strain increment under constant load amplitude cycles, or by a progressive strength reduction under constant strain amplitude cycles. Equivalent parameters start changing with the number of cycles performed, N_c : usually the soil stiffness decreases with N_c and the damping ratio increases.

These alteration of soil behaviour can be expressed through two degradation indexes, δE and δD , defined as:

$$\delta_G = \frac{G(N_c)}{G(1)}; \quad \delta_D = \frac{D(N_c)}{D(1)} \quad \text{Equation 5-3}$$

Where $G(1)$ and $D(1)$ are the equivalent parameters measured on the first load cycle.

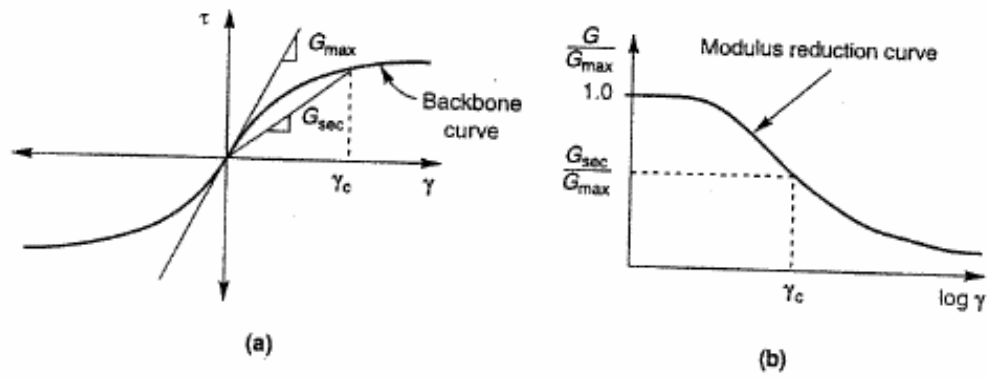


Figure 5-3 Backbone curve showing typical variation of E_{sec} with shear strain

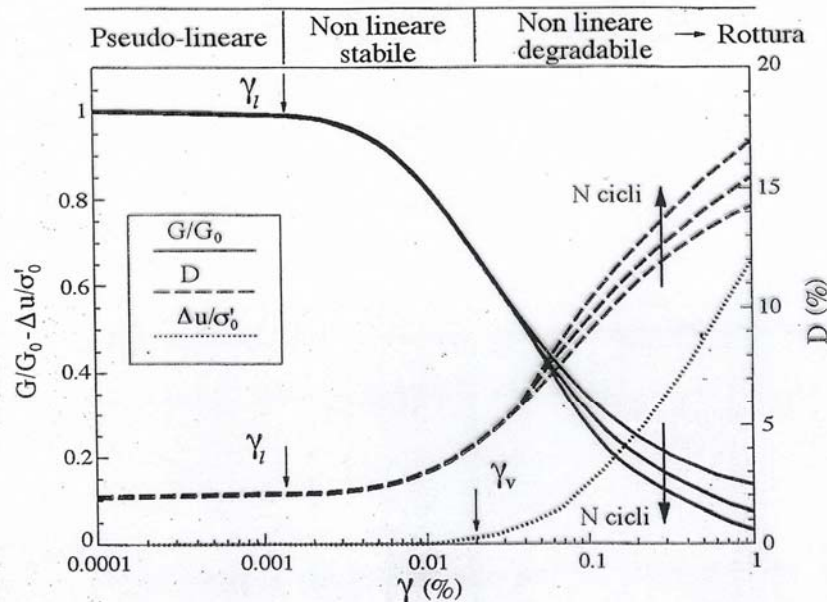


Figure 5-4 Three distinct soil behaviours on the ongoing of axial strain.

Laboratory tests have shown that soil stiffness is influenced by void ratio, mean principal effective stress, plasticity index, overconsolidation ratio, and number of cyclic loadings.

The locus of points corresponding to the tips of hysteresis loops of various cyclic strain amplitudes is called a backbone curve (or skeleton) curve (Figure 5-3); its slope at the origin (near zero cyclic strain amplitude) represents the largest value of the Young modulus, E_{max} . At greater cyclic strain amplitudes, the modulus ratio E_{sec}/E_{max} drops to values lower than 1. Characterization of the stiffness of an element of soil therefore requires consideration of both E_{max} and the manner in which the modulus ratio E/E_{max} varies with cyclic strain amplitude and other parameters. The variation of the modulus ratio with shear strain is described graphically by a modulus reduction curve; either one can be determined from the other.

5.4 Experimental results

5.4.1 Small strain stiffness

In geotechnical literature, many semi-empirical equations have been proposed to describe the relation between stiffness or damping ratio and the confining stress, the porosity and the load history experienced by the specimen.

Typically, the equation proposed derive from Equation 5-4, firstly proposed by Hardin (1978) for specimen subjected to small shear cycles under otherwise isotropic stress condition.

$$\frac{G_0}{p_a} = Sf(e) \left(\frac{p'}{p_a} \right) OCR^k \quad \text{Equation 5-4}$$

A more general expression (Equation 5-5) has been proposed by Hardin and Blandsford(1984):

$$E_{ij} = S_{vh} F(e) p_a^{1-2n} (\sigma'_v \sigma'_h)^n OCR^k \quad \text{Equation 5-5}$$

This equation, for the vertical Young's modulus becomes:

$$E_v = S_v F(e) p_a^{1-2n} (\sigma'_v)^n OCR^k \quad \text{Equation 5-6}$$

where:

S_v is a constant depending on the soil microscopic structure

$F(e)$ is a function of the void ratio

OCR overconsolidation ratio

σ'_v is the vertical effective stress

σ'_h is the horizontal effective stress

p_a is the atmospheric pressure, in the same unit as σ'_m

Equation 5-6 can be used to analyze the small strain stiffness of San Pantaleone pozzolana. Since we hypotized that compacted, air pluviated and natural specimen behaviour is not dependent on OCR, it will be considered OCR=1. In fact, as indicated in Chapter 4, it is not easy or tational to define an overconsolidation ration for artificially prepared specimens.

The influence of the confining stress on the small strain stiffness of San Pantaleone pozzolana is clear from the experimental test results. In Figure 5-5 the stiffness increment with the variation of confining stress is evident. Moreover, two different

trends have been singled out: loose specimens trend, plotted in blue referring to specimens having $\gamma_{d0} = 1.03 \div 1.40 \text{ t/m}^3$ and dense specimen ($\gamma_{d0} = 0.80 \div 1.15^1 \text{ t/m}^3$) trend, plotted in green. All data refer to cyclic tests performed at an amplitude variable in the range of $\varepsilon_a 0,001\% \div 0,05\%$

A copious data scattering in the stiffness measurement is also visible.

This scattering could derive from experimental errors, but could also be due to different internal structure or to different the specimen density.

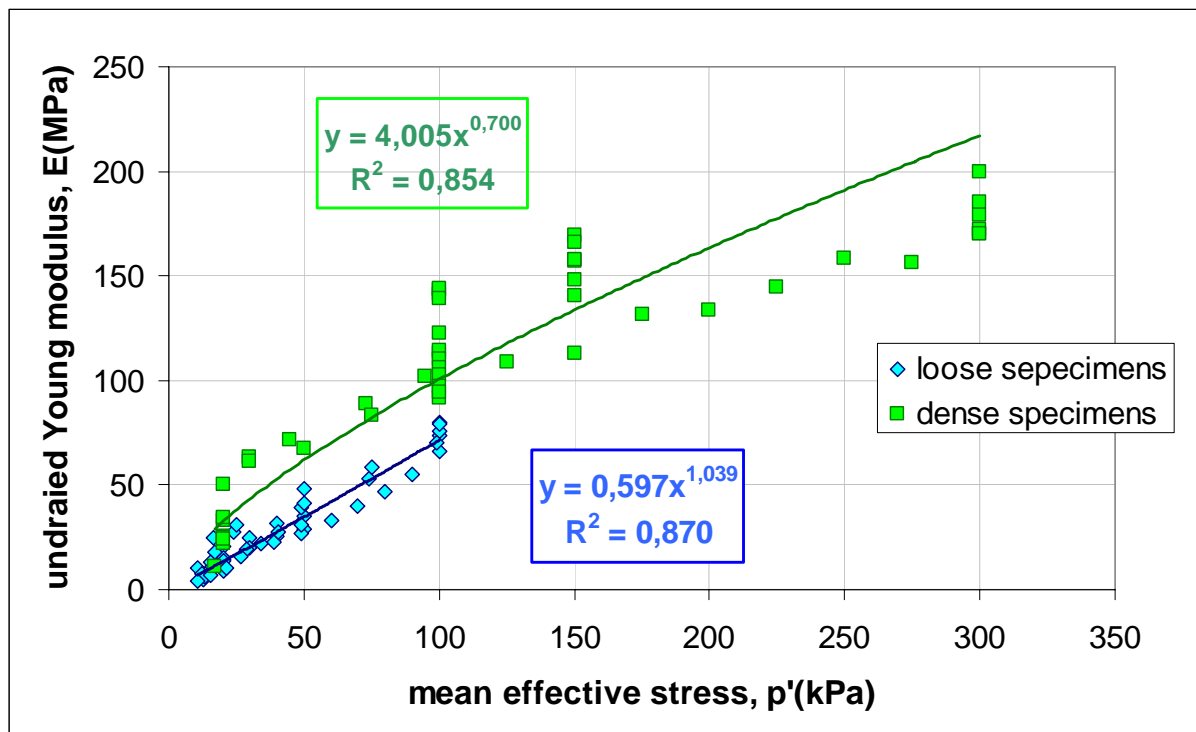


Figure 5-5 Undrained young modulus vs mean effective stress, for loose and dense specimens.

Specimen density is strictly related to specimen porosity (e). In Figure 5-6 and in Figure 5-7 stiffness data have been adimensionalized using two different expression for the porosity function $f(e)$: Equation 5-7, that was proposed by Hardin & Black (1968), and Equation 5-8 was proposed by Jamiolkowski et al. (1991)

$$f(e) = \frac{(2.973 - e)^2}{1 + e} \quad \text{Equation 5-7}$$

$$f(e) = \frac{1}{e^{1.3}} \quad \text{Equation 5-8}$$

None of the equation proposed seems to reduce effectively the scattering of the plotted data. However, if Equation 5-7 seems to increase the data scattering,

¹ $\gamma_d = 1.57 \text{ t/m}^3$ is for natural sample Nat02.

5.4.2 Influence of the load frequency

In Figure 5-8 the influence of load frequency on the measured stiffness is represented. In the range of frequency investigated in the course of this thesis no significant variation in the young modulus has been identified.

However, it is worth underlying that for technical reason the investigated frequency range is narrow, maybe not sufficient to obtain substantial stiffness variation.

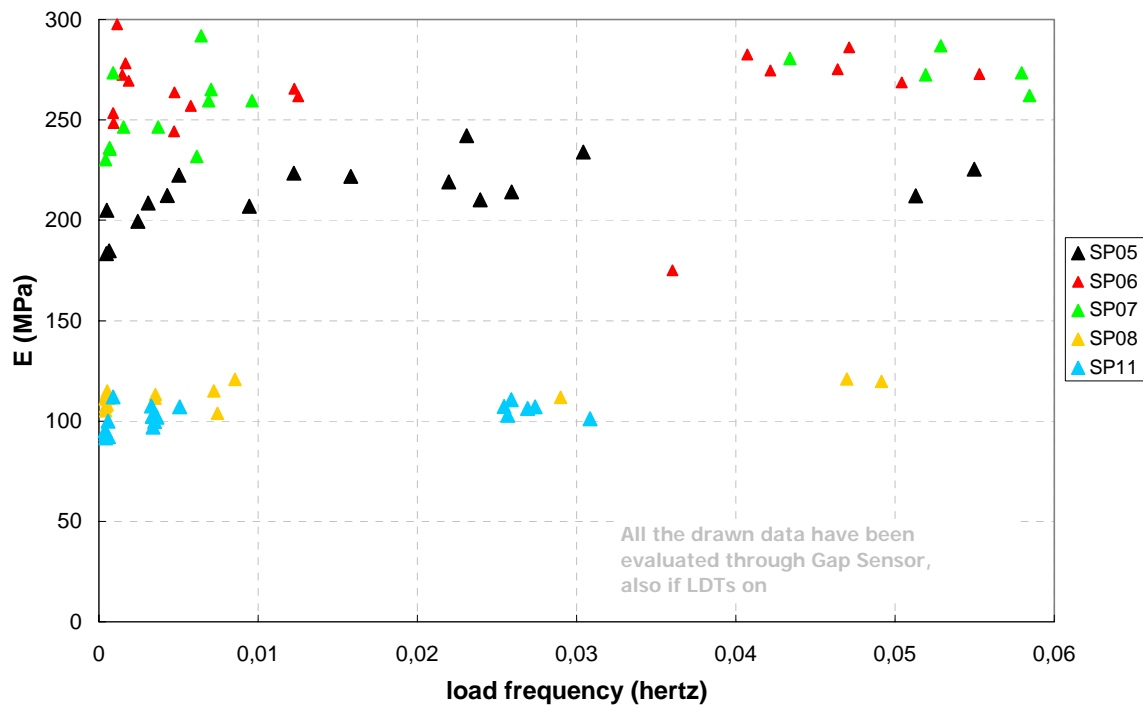


Figure 5-8 load frequency influence over undrained Young modulus.

5.4.3 Young modulus evaluated during shear: influence of the mean deviator stress

In some triaxial tests, executed over proctor compacted specimens, small strain stiffness has been measured in the course of the shear stage. Once a certain deviator stress was reached, after a short creep period, small strain cycles were performed symmetrically around the deviator stress reached.

The results are plotted in Figure 5-9: no clear trend can be identified.

Data scattering could be due both to experimental difficulty, and to the pore pressure increment (leading to p' changes) brought about by the shear stage.

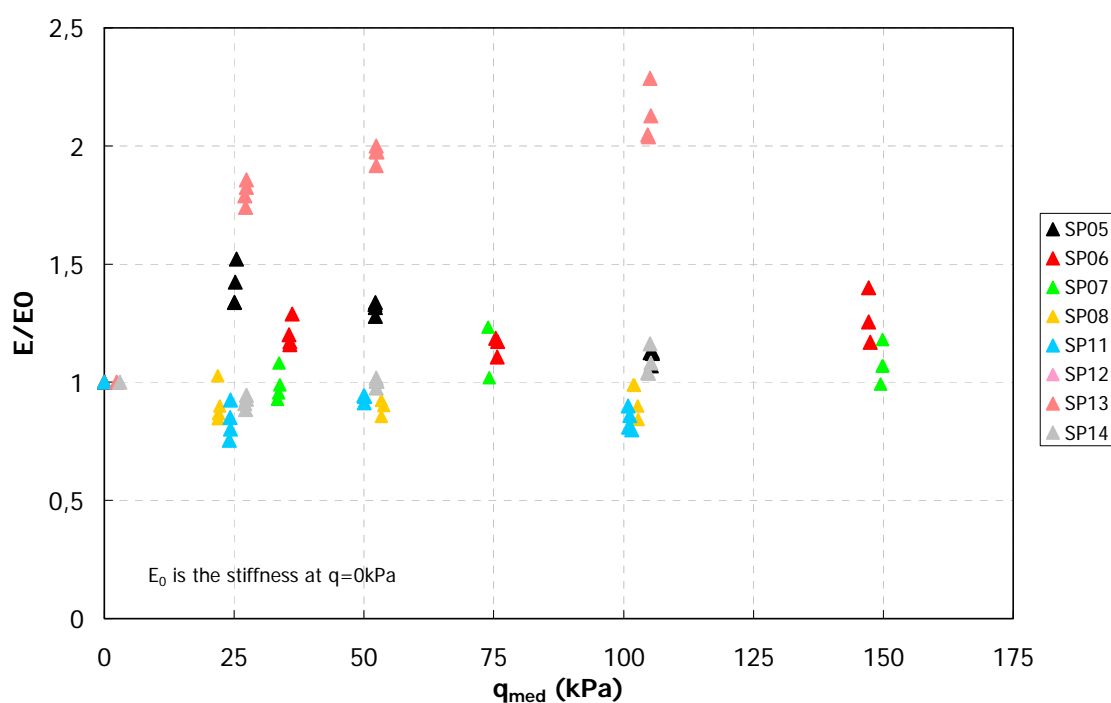


Figure 5-9 Young modulus measured in different deviator stress condition.

5.4.4 Influence of cyclic load amplitude

In Figure 5-10 and Figure 5-11 are reported the results of a series of cyclic load tests performed at increasing load amplitude.

The young modulus decay with increasing load amplitude is evident. Moreover, the trespassing of volumetric threshold is recognizable by young modulus degradation and cyclic shape alteration with number of cycles.

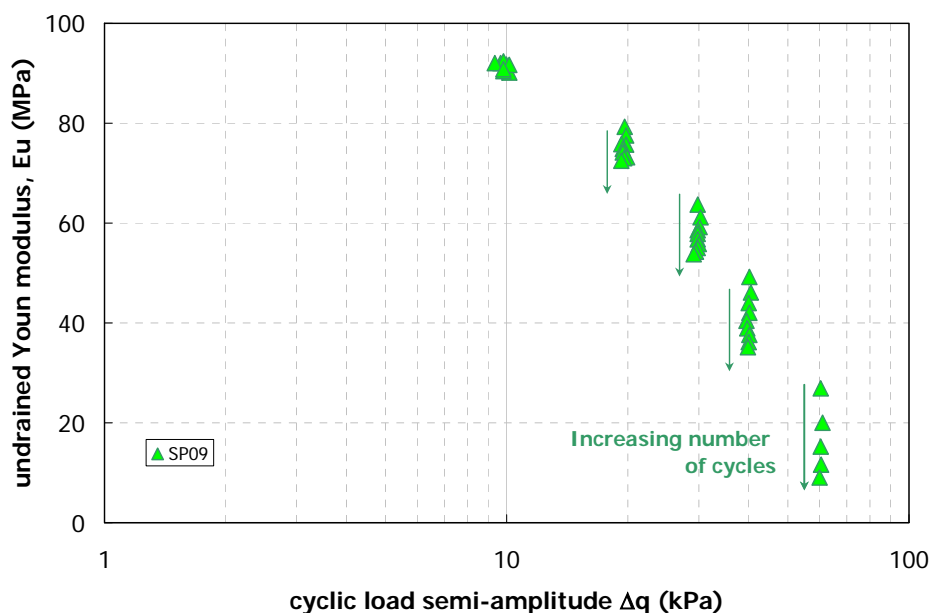


Figure 5-10 Variation of undrained Young modulus with cyclic load amplitude.

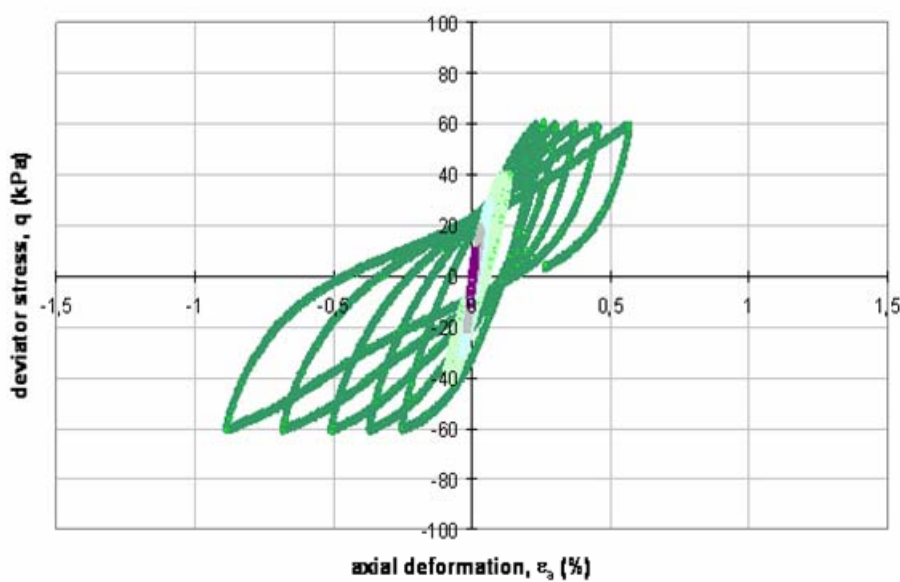


Figure 5-11 Cyclic loading shape changing with increasing cyclic load amplitude.

5.4.5 Pore pressure development

In Figure 5-12 is showed the pore pressure increment, divided by the effective confining stress p'_0 , in relation with axial strain.

Only the aliquot of pore pressure due to distortional strain, and referred to as Δu_q , has been plotted in Figure 5-13 to Figure 5-18.

In fact, in the course of an undrained triaxial test, part of the pore pressure increment is due to total stress increment. In the hypothesis of isotropic elastic soil, this aliquot is totally adsorbed by water. The other aliquot is responsible for the effective stress path slope and can be expressed through Skempton coefficient α .

Δu_p represents the pore pressure increment that would develop in a constant p' triaxial test.

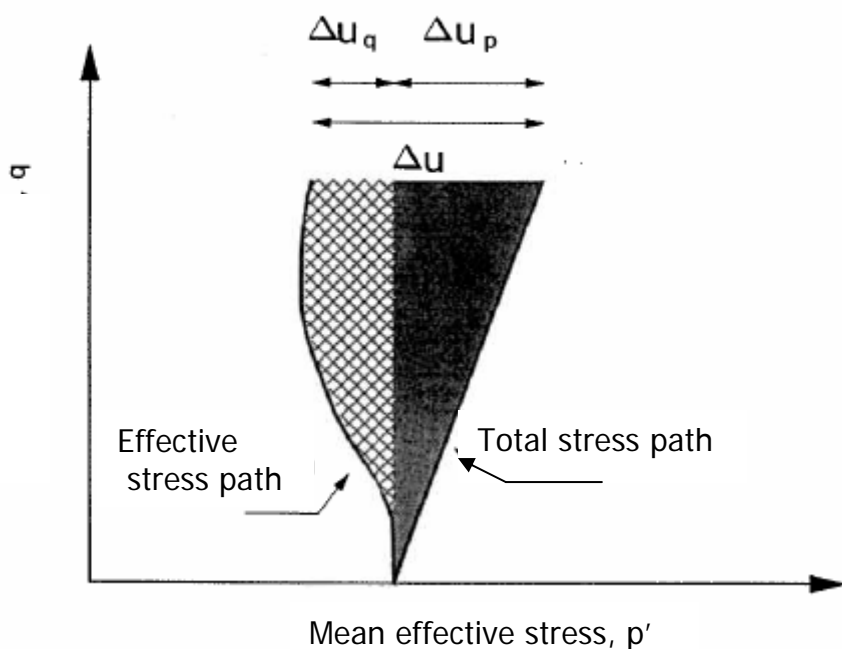


Figure 5-12 Two different aliquot composing pore pressure increment.

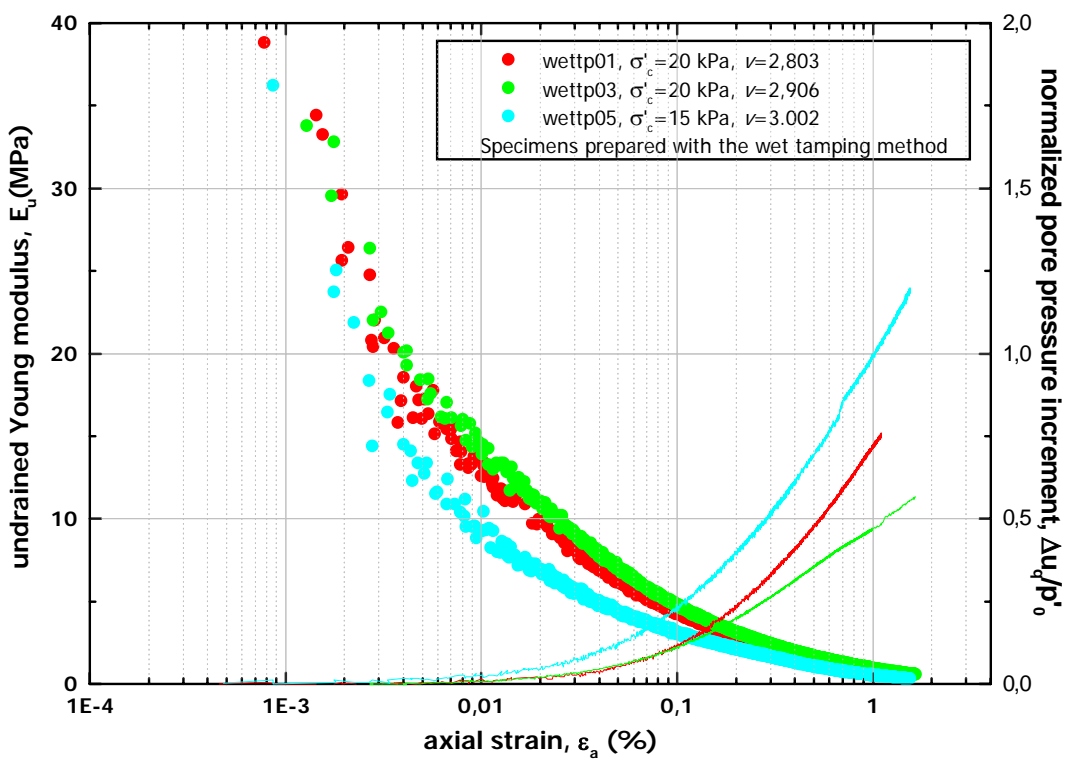


Figure 5-13 Secant young modulus-axial strain and pore pressure increment-axial strain semi-log plot for specimens prepared with the wet tamping method.

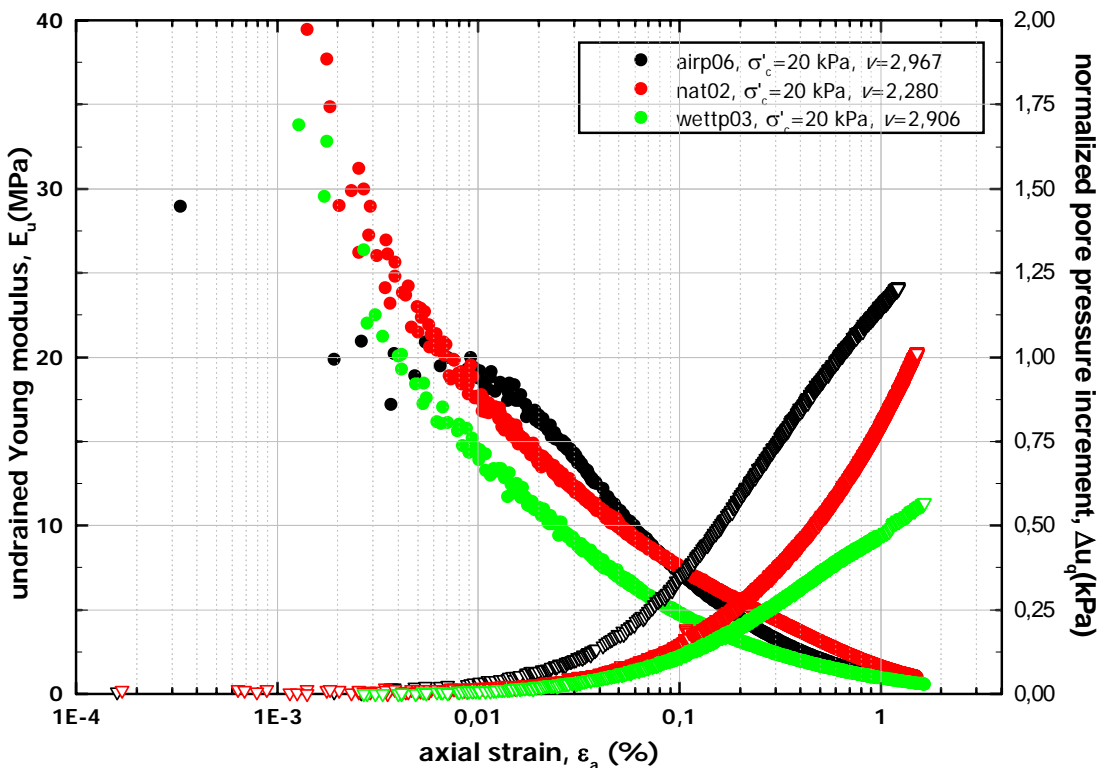


Figure 5-14: Secant young modulus-axial strain and pore pressure increment-axial strain semi-log plot for specimen prepared with three different methods.

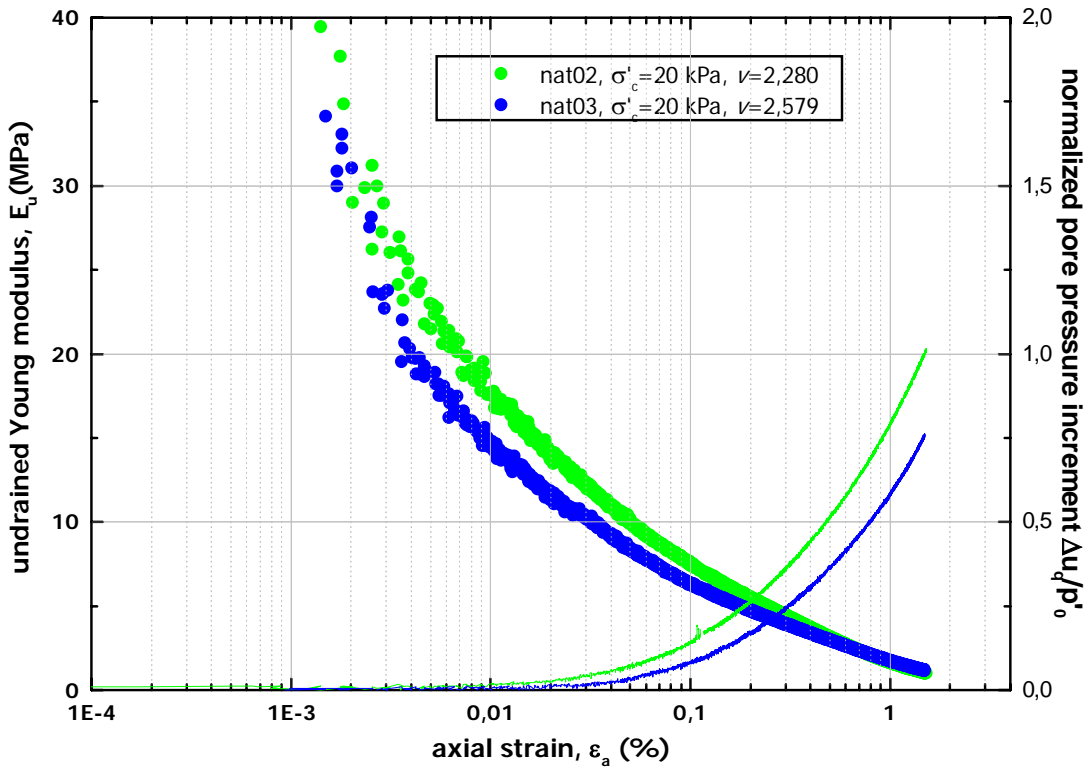


Figure 5-15: Secant young modulus-axial strain and pore pressure increment-axial strain semi-log plot for natural specimens.

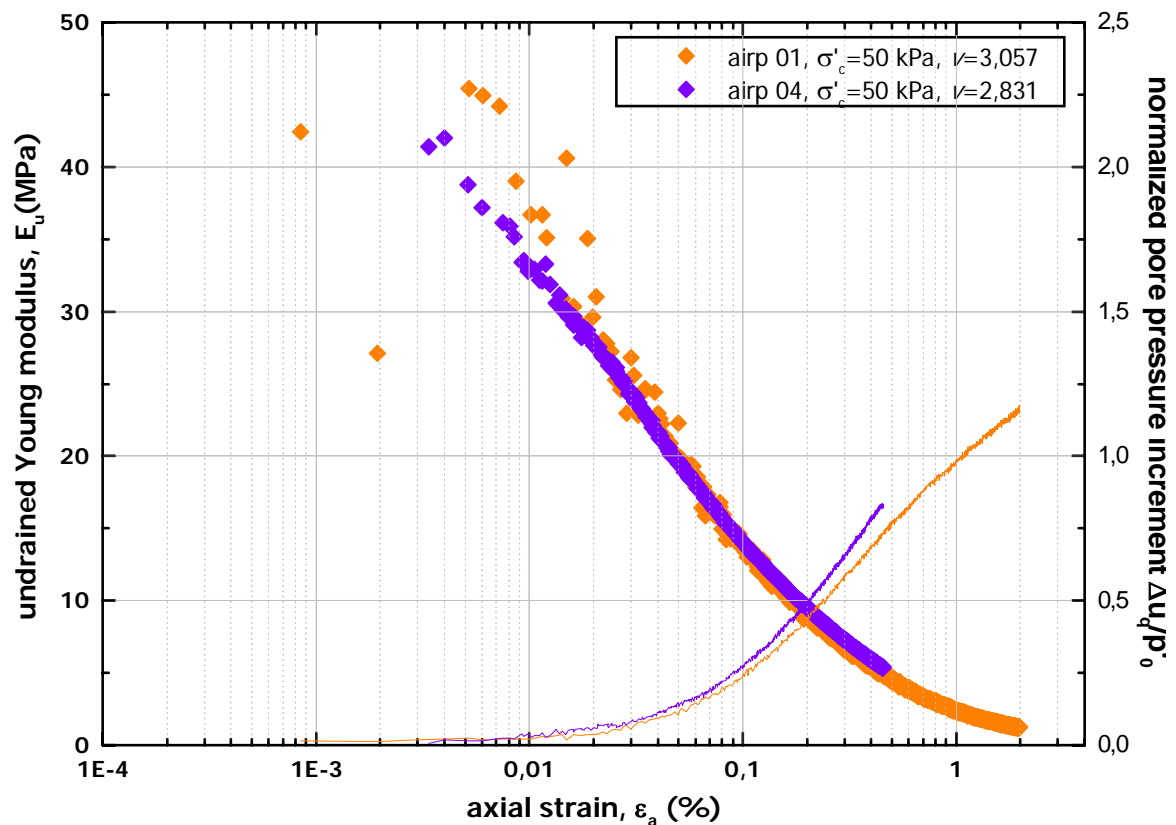


Figure 5-16: Secant young modulus-axial strain and pore pressure increment-axial strain semi-log plot for specimen prepared with the air pluviation method

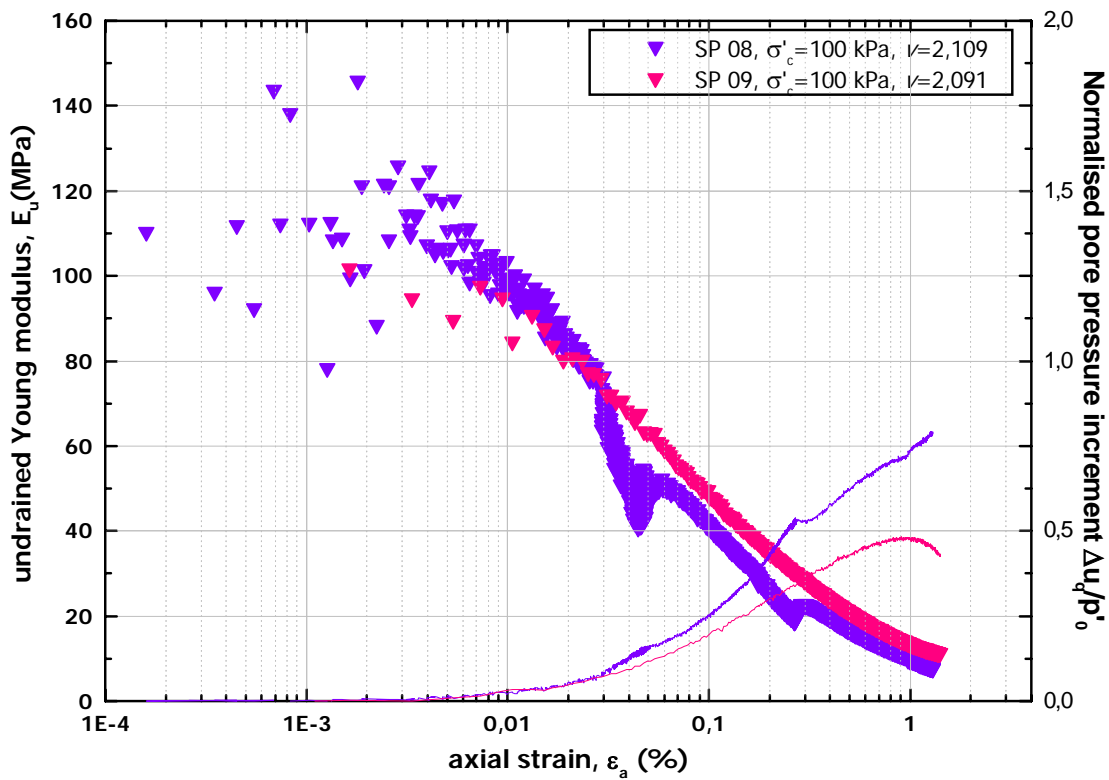


Figure 5-17: Secant young modulus-axial strain and pore pressure increment-axial strain semi-log plot for specimen prepared with the consolidometer.

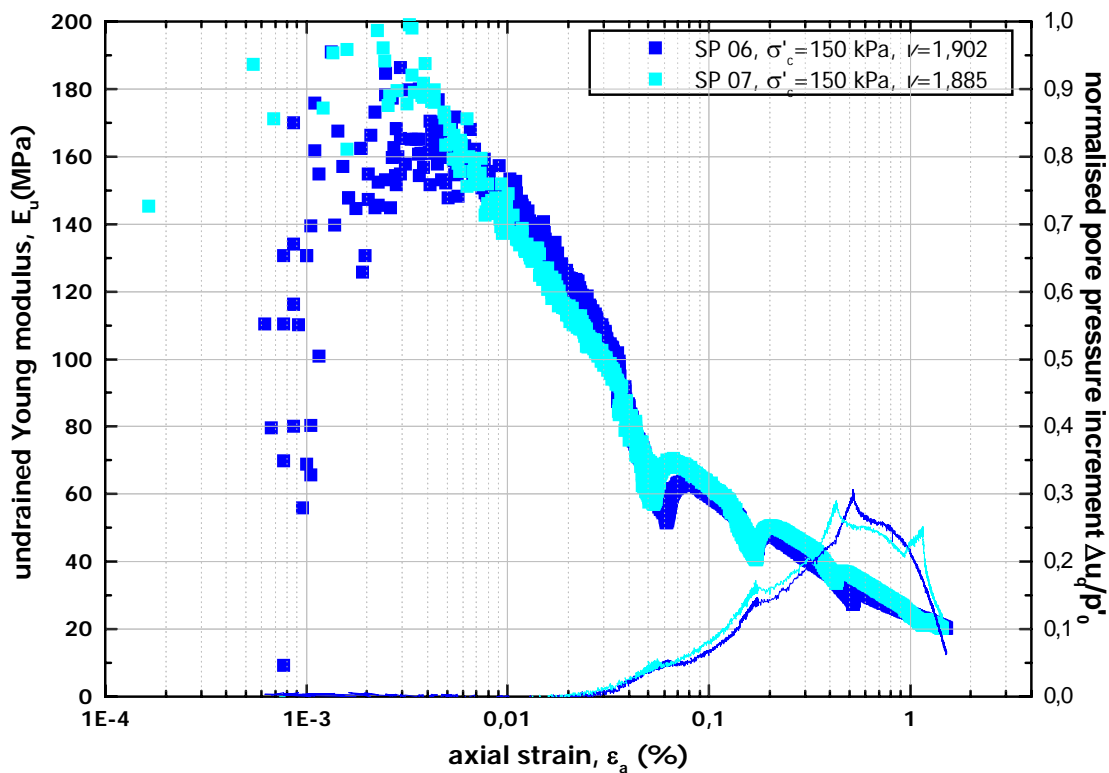


Figure 5-18: Secant young modulus-axial strain and pore pressure increment-axial strain semi-log plot for specimen prepared with proctor compaction method.

5.5 Cyclic strength of San Pantaleone Pozzolana.

As discussed beforehand, soil behaviour at high strain level is subjected to mechanical degradation leading to irreversible strains growth in drained tests, or to pore pressure increment in undrained tests.

Granular soil behaviour at failure is strongly influenced by soil density.

Loose sand has a contractive behaviour, and after a number of undrained loading cycles can develop a pore pressure increment equal to the mean effective stress, thus resulting in a sudden loss of shear strength: this phenomenon is called "flow liquefaction".

Dense sand, on the contrary, shows a more stable behaviour: under shear cycles it tends to dilate, recovering the initial strength when the seismic action is over. In these soils the sudden shear strain increment typical of liquefaction does not take place.

The cyclic strength of a granular soil can be represented through the relation between stress ratio at failure ($CSR = q/\sigma'_c$) and number of cyclic loadings at failure N_c . On a practical point of view, liquefaction triggering can be defined referring either to tensional or deformational specimen condition.

When referring to specimen effective stress condition, liquefaction triggering can be identified with the condition:

$$r_u = \frac{\Delta u}{\sigma'_0} = 1 \quad \text{Equation 5-9}$$

Alternatively, liquefaction triggering can be assumed when a defined strain threshold is reached.

The criterion adopted herein is based on the definition of a threshold value for axial deformations, since in all the executed tests the excess pore water pressure ratio $r_u = \Delta u/\sigma'_0$ never clearly reaches the unit value. The failure has been conventionally established at a threshold deformation equal to $\varepsilon_a = 2.5\%$.

$$R_{\max} = \frac{0.9}{C_k} \cdot \frac{(1+2k_0)}{3} \cdot \left(\frac{\tau_l}{\sigma_c} \right)_{N_c=20} \quad \text{Equation 5-10}$$

In Figure 5-20, are reported the cyclic strength curves relevant for San Pantaleone specimens prepared with the 1D consolidation technique. On the vertical axis of the diagram cyclic stress ratio CSR is reported; on the horizontal axis there are the number of cycles necessary to trigger liquefaction. In the figure the two green squares are due to two tests on 1-D consolidated specimens (Test SPL17 and Test SPL19) subjected to cyclic loading of an amplitude of 60 and 75 kPa that were stopped after 138 and 150 cycles respectively without reaching the conventional failure condition. Therefore the strength curve for 1-D consolidated specimen should be located above the points.

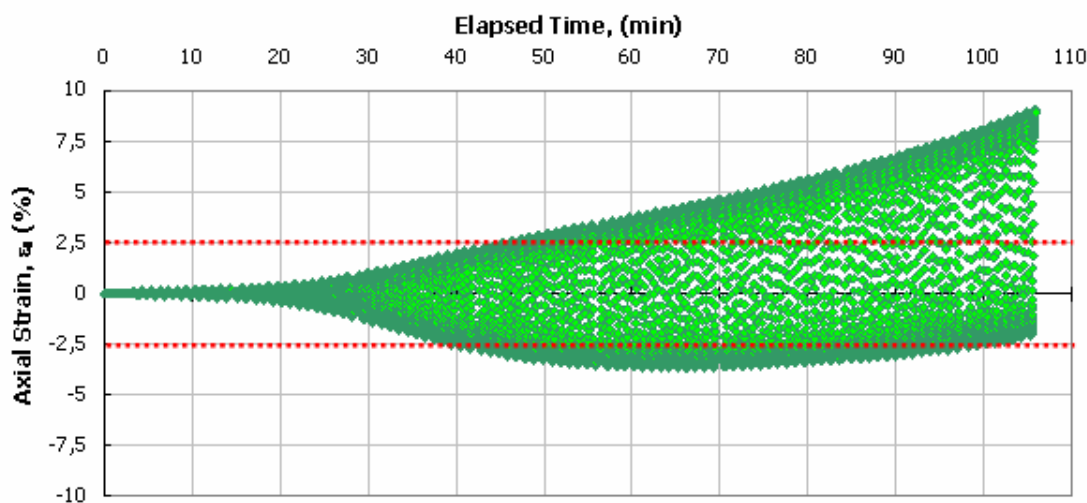


Figure 5-19 Strain threshold at $\epsilon_a=2,5\%$.

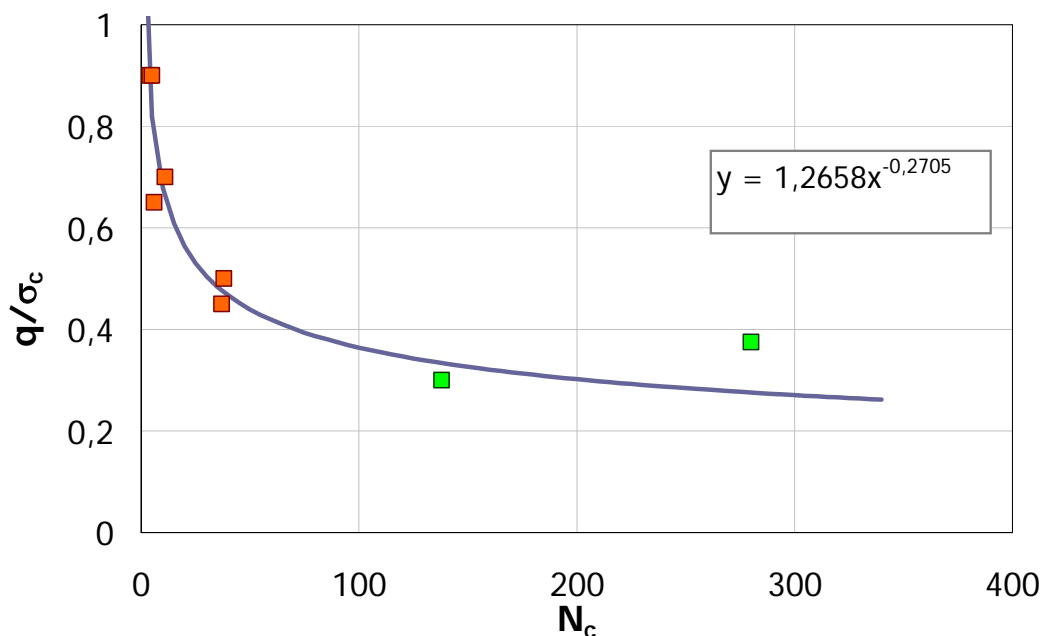


Figure 5-20 Cyclic strength curves for 1-D consolidated specimen of San Pantaleone pozzolana soil. Red squares are for liquefied specimen, green squares for specimens that did not experience liquefaction.

References

- A.G.I. (2005) Aspetti geotecnici della progettazione in zona sismica, Linee guida. Patron editore, Bologna.
- Burland, J. B. (1989): **Small is beautiful - The stiffness of soil at small strains**, Canadian Geotechnical Journal, Vol. 26, No. 4, pp.499-516.
- Hardin B.O. & Black W.L. (1968): **Vibration modulus of normally consolidated clay**, Journal of Geotechnical Engineering, ASCE, 89(1): 33-65.
- Hardin B.O. (1978): **The nature of stress-strain behaviour for soils**, Proc. Of the Geotechnical Div. Spec. Conf. on Earthquake Engineering and Soil Dynamics, Pasadena CA ASCE 3-90.
- Hardin B.O. & Blandford G.E. (1989): **Elasticity of particulate materials**, ASCE J. Geotechnical Engineering, Vol. 115 No.6, 788-805.
- Jardine R.J., Symes M.J. and Burland J.B. (1984): **The measurement of soil stiffness in the triaxial apparatus**, Geotechnique Vol. 34, No. 3 323-340
- Jamiolkowski, M., Leroueil, S., and Iopresti, D.C.F.(1991): **Theme lecture- Design parameters from theory to practice**, Proceedings, Geo-Coast '91, Yokohama, Japan, pp. 1-41.

Conclusions

In the course of this Phd thesis, the mechanical behaviour of a Neapolitan pyroclastic soil, under monotonic and cyclic loading condition, has been studied. The soil was prepared, using different reconstitution techniques, in loose and dense samples, and was tested at very low to medium confining stress.

The following conclusions can be argued from the experimental campaign performed:

- the specimen reconstitution technique is influent on specimens pre-failure behaviour, but has no effect on the critical state behaviour, nor on small strain stiffness.
- The soil behaviour at very low confining stresses can be explained with the same models used at higher confining stresses. This is true in terms of stiffness and of mechanical behaviour at the critical state.
- San Pantaleone sand compressibility has been evaluated: a different behaviour in the $v-p'$ plane has been found for loose and dense samples.
- The influence of confining stress on soil stiffness is clear, and the same equation can be utilized to interpolate the confining stress - stiffness experimental points from very low to medium confining stresses.
- San Pantaleone Sand cyclic strength has been evaluated.

Appendix 1

Cyclic tests experimental results

v	σ'_c [kPa]	cyc n°	frequenza [hertz]	esa (%)	ε_a max [%]	Dev max [kPa]	ε_a min [%]	Dev min [kPa]	strain rate [%/min]	evaluated through GS			evaluated through LDT			
										E [MPa]	cor.Coeff.	D [%]	strain rate [%/min]	E [MPa]	cor.Coeff.	D [%]
SP01																
1,8924	20	1	0,024863	0,004738	0,00486	32,39	-0,00461	27,73	0,028274	47,49	0,93379	8,99				
1,8924	20	2	0,023386	0,004763	0,00466	31,41	-0,00486	26,89	0,026734	49,29	0,96819	4,10				
1,8924	20	3	0,025558	0,004590	0,00447	31,41	-0,00471	26,60	0,028153	53,35	0,94568	8,19				
1,8924	20	4	0,024903	0,004639	0,00476	30,84	-0,00451	26,89	0,027727	50,82	0,95009	4,85				
1,8924	20	5	0,024254	0,004689	0,00481	31,55	-0,00456	26,32	0,027293	49,75	0,947	5,28				
SP02																
2,1994	17	1	0,015909	0,004636	0,00483	-0,35	-0,00444	-1,79	0,017702	10,37	0,46913	9,63				
2,1994	17	2	0,016178	0,004612	0,00498	0,09	-0,00425	-1,50	0,017906	14,30	0,57465	13,13				
2,1994	17	3	0,015557	0,004636	0,00537	-0,20	-0,00390	-1,21	0,017311	11,09	0,51182	6,32				
2,1994	17	4	0,016281	0,004832	0,00576	0,23	-0,00390	-1,50	0,018879	12,78	0,49013	8,32				
2,1994	17	5	0,015496	0,004636	0,00561	-0,64	-0,00366	-1,50	0,017242	6,28	0,36227	16,11				
2,2016	20	1	0,020346	0,003275	0,00347	0,66	-0,00308	-1,06	0,015993	18,46	0,52845	85,27				
2,2016	20	2	0,020629	0,003226	0,00332	0,09	-0,00313	-2,06	0,015973	21,39	0,57946	15,57				
2,2016	20	3	0,019293	0,003299	0,00352	0,23	-0,00308	-1,20	0,015278	23,38	0,63099	23,71				
2,2016	20	4	0,019411	0,003251	0,00342	0,09	-0,00308	-1,35	0,015143	22,23	0,61332	37,36				
2,2016	20	5	0,019572	0,003275	0,00328	0,52	-0,00328	-1,63	0,015385	24,47	0,62702	48,52				
2,2016	20	6	0,019447	0,003471	0,00362	0,09	-0,00332	-1,20	0,016198	20,78	0,60275	46,83				
SP03																
1,9749	20	1	0,022916	0,002520	0,00223	0,79	-0,00281	-1,37	0,013861	43,50	0,74281	-0,18				
1,9749	20	2	0,024369	0,002442	0,00210	0,63	-0,00278	-0,60	0,014281	27,24	0,5364	9,54				
1,9749	20	3	0,022577	0,002504	0,00210	0,94	-0,00291	-1,06	0,013569	39,71	0,72119	-0,82				
1,9749	20	4	0,023546	0,002426	0,00198	0,79	-0,00288	-0,29	0,013709	22,61	0,49271	0,32				
1,9748	20	1	0,014654	0,004135	0,00314	1,10	-0,00513	-1,68	0,014543	33,90	0,77579	0,72				
1,9748	20	2	0,014650	0,004072	0,00292	1,25	-0,00522	-1,37	0,014316	38,85	0,82988	2,46				
1,9748	20	3	0,014632	0,004182	0,00314	1,41	-0,00522	-1,99	0,014685	32,46	0,774	1,07				
1,9748	20	4	0,014898	0,004057	0,00305	1,25	-0,00507	-1,06	0,014504	34,82	0,80375	4,21				
1,9748	20	5	0,014573	0,004151	0,00311	0,79	-0,00519	-1,53	0,014517	33,01	0,75243	3,86				
1,9748	20	1	0,000525	0,004075	0,00528	-0,14	-0,00288	-0,75	0,000513	20,59	0,65699	11,95				
1,9748	20	2	0,000501	0,004011	0,00480	0,17	-0,00322	-1,99	0,000482	25,42	0,68505	10,46				
1,9748	20	3	0,000568	0,003994	0,00458	-0,29	-0,00341	-1,84	0,000545	25,92	0,73831	8,60				
1,9748	20	4	0,000544	0,003946	0,00420	-0,14	-0,00369	-2,45	0,000516	29,67	0,74826	6,87				
1,9748	20	5	0,000550	0,003960	0,00395	-0,14	-0,00397	-2,61	0,000523	27,30	0,73804	10,43				
1,9749	20	1	0,009174	0,008092	0,00702	1,87	-0,00916	-2,30	0,017817	22,73	0,85361	9,78				
1,9749	20	2	0,008472	0,008221	0,00740	3,10	-0,00904	-2,30	0,016715	25,81	0,91704	6,60				
1,9749	20	3	0,008202	0,008253	0,00747	2,02	-0,00904	-3,38	0,016245	25,96	0,90377					
1,9749	20	4	0,008320	0,008300	0,00750	1,71	-0,00910	-2,45	0,016573	24,57	0,89953	5,44				
1,9749	20	5	0,008082	0,008268	0,00747	2,33	-0,00907	-2,30	0,016037	26,61	0,92018					
1,9745	20	1	0,000262	0,008205	0,00944	0,94	-0,00697	-3,38	0,000517	23,82	0,90738	11,57				
1,9745	20	2	0,000261	0,008169	0,00890	0,79	-0,00744	-3,53	0,000512	24,16	0,88543	9,82				
1,9745	20	3	0,000288	0,008149	0,00839	0,48	-0,00791	-3,69	0,000563	23,47	0,89651	9,66				
SP05																
1,8995	100	1	0,021966	0,002463	0,00526	4,27	0,00033	-3,26	0,012985	150,71	0,98335	1,89	0,008913	219,11	0,968070	1,06
1,8995	100	2	0,025924	0,002200	0,00435	3,66	-0,00005	-3,26	0,013688	140,06	0,96123		0,008907	214,18	0,961245	2,59
1,8995	100	3	0,023110	0,002487	0,00502	4,12	0,00005	-3,57	0,013794	143,71	0,96477	3,83	0,008328	242,16	0,959073	0,51
1,8995	100	4	0,023960	0,002511	0,00526	3,50	0,00024	-3,11	0,014439	130,84	0,94037	2,49	0,009163	210,13	0,926608	1,13
1,8995	100	1	0,062584	0,001526	0,00169	4,48	-0,00137	-3,30	0,022926	147,99	0,94255		0,016364	212,14	0,953044	1,73
1,8995	100	2	0,054981	0,001705	0,00188	5,10	-0,00153	-3,46	0,022495	137,73	0,94508	2,93	0,013601	225,35	0,952264	2,06
1,8995	100	3	0,051310	0,001622	0,00157	4,17	-0,00167	-3,61	0,019970	144,51	0,96179	2,89	0,014261	212,09	0,945042	1,12
1,9002	100	1	0,015828	0,002367	0,00091	3,96	-0,00383	-3,26	0,008992	144,40	0,96167	1,00	0,005857	221,88	0,953631	2,10

v	σ'_c [kPa]	cyc n°	evaluated through GS							evaluated through LDT						
			frequenza [hertz]	esa (%)	ε_a max [%]	Dev max [kPa]	ε_a min [%]	Dev min [kPa]	strain rate [%/min]	E [MPa]	cor.Coef.	D [%]	strain rate [%/min]	E [MPa]	cor.Coef.	D [%]
1,9002	100	2	0,030433	0,002343	0,00100	4,43	-0,00368	-3,26	0,017116	145,07	0,95027	4,21	0,010044	234,03	0,963152	0,70
1,9002	100	3	0,009460	0,002821	0,00148	4,73	-0,00416	-3,42	0,006406	137,49	0,96173	-0,30	0,004312	207,07	0,952440	1,48
1,9002	100	4	0,012238	0,002511	0,00124	4,43	-0,00378	-3,42	0,007375	149,22	0,94419		0,004979	223,42	0,932007	1,22
1,8999	100	1	0,004297	0,002535	0,00191	3,96	-0,00316	-2,95	0,002614	135,76	0,95395	-1,84	0,001642	212,44	0,956089	2,88
1,8999	100	2	0,003152	0,002415	0,00187	4,12	-0,00296	-3,11	0,001827	141,69	0,98201	64,13	0,000722	436,98	0,978002	-0,28
1,8999	100	3	0,003103	0,002463	0,00167	3,66	-0,00325	-3,11	0,001834	129,40	0,95816	13,83	0,000944	208,61	0,952143	0,83
1,8999	100	4	0,005033	0,001889	0,00158	4,12	-0,00220	-2,95	0,002282	150,88	0,95525		0,001411	222,38	0,958412	3,35
1,8998	100	1	0,002441	0,002415	0,00273	3,66	-0,00210	-3,11	0,001415	126,04	0,96351	2,22	0,000931	199,42	0,954406	3,20
1,8998	100	2	0,000646	0,002439	0,00292	4,27	-0,00196	-2,80	0,000378	112,41	0,93545	3,85	0,000229	184,83	0,925567	3,54
1,8998	100	3	0,000492	0,002295	0,00325	4,12	-0,00134	-3,26	0,000271	139,69	0,93378	3,28	0,000231	205,07	0,916355	5,15
1,8998	100	4	0,000465	0,002032	0,00373	3,96	-0,00033	-2,96	0,000227	112,36	0,91521	6,59	0,000147	183,47	0,926038	8,43
SP06																
1,9044	150	1	0,046338	0,002060	0,00208	4,45	-0,00204	-3,26	0,022908	172,25	0,94934	2,12	0,013446	300,65	0,936801	0,68
1,9044	150	2	0,046410	0,002060	0,00194	4,00	-0,00218	-2,80	0,022944	172,91	0,95399	-1,79	0,015034	275,21	0,941680	2,38
1,9044	150	3	0,055311	0,001965	0,00204	3,55	-0,00189	-2,95	0,026088	158,04	0,93496	2,77	0,014843	272,78	0,904339	2,61
1,9044	150	4	0,047117	0,002060	0,00208	4,00	-0,00204	-2,95	0,023294	176,00	0,97394	0,43	0,014395	286,03	0,960927	0,98
1,9044	150	5	0,040717	0,002320	0,002415	4,75	-0,00223	-3,56	0,022675	168,74	0,96717	1,51	0,013660	282,61	0,931386	0,57
1,9045	150	1	0,050436	0,001267	0,00432	4,25	0,00179	-3,34	0,015336	154,72	0,96377	3,25	0,009143	268,75	0,951815	1,31
1,9045	150	2	0,042172	0,001391	0,00441	4,25	0,00163	-3,49	0,014075	162,54	0,95745	2,45	0,008474	274,69	0,933905	0,79
1,9045	150	3	0,036034	0,001291	0,004279	3,94	0,001696	-3,49	0,011169	103,22	0,66333	3,61	0,006502	175,04	0,652821	1,18
1,9043	150	1	0,012269	0,001161	0,00061	3,94	-0,00172	-2,72	0,003419	163,50	0,96232	-7,84	0,002255	265,58	0,946335	2,29
1,9043	150	2	0,005787	0,002202	0,00114	4,00	-0,00327	-3,26	0,003058	158,65	0,95039	1,06	0,001825	256,97	0,954001	0,40
1,9043	150	3	0,012532	0,001918	0,00052	4,15	-0,00331	-3,11	0,005768	158,45	0,97533	-0,55	0,003227	261,80	0,957300	
1,9043	150	4	0,004758	0,002036	0,00095	4,15	-0,00312	-3,11	0,002325	171,43	0,96386	-0,49	0,001616	263,76	0,931973	1,18
1,9043	150	5	0,004730	0,002225	0,001089	4,15	-0,00336	-2,96	0,002526	137,89	0,86377		0,001500	244,27	0,879283	-2,05
1,9041	150	1	0,001156	0,000983	0,00120	3,48	-0,00076	-3,49	0,000273	187,47	0,90205		0,000179	297,56	0,880228	
1,9041	150	2	0,000937	0,001141	0,00142	4,41	-0,00086	-3,03	0,000257	139,48	0,89117	4,10	0,000160	248,44	0,878661	2,32
1,9041	150	3	0,001686	0,001155	0,00145	4,25	-0,00086	-3,18	0,000467	148,97	0,928	2,52	0,000237	278,23	0,951959	2,60
1,9041	150	4	0,000912	0,001232	0,00171	4,41	-0,00076	-2,87	0,000270	159,56	0,92799	-1,13	0,000168	253,39	0,890003	1,91
1,9041	150	5	0,001474	0,001049	0,00156	4,10	-0,00054	-3,03	0,000371	157,50	0,95064	4,46	0,000224	272,51	0,939954	0,70
1,9041	150	6	0,001868	0,001068	0,001526	3,94	-0,00061	-2,87	0,000479	148,96	0,94146	0,50	0,000243	269,40	0,948435	2,32
SP07																
1,8999	150	1	0,052872	0,002096	0,00248	3,12	-0,00171	-5,09	0,026593	162,89	0,96004	2,69	0,015743	286,89	0,953064	2,63
1,8999	150	2	0,043403	0,002453	0,00262	3,88	-0,00229	-5,24	0,025552	165,32	0,96492	2,21	0,015097	280,56	0,934299	-0,61
1,8999	150	3	0,058457	0,001500	0,00224	2,81	-0,00076	-5,39	0,021049	167,59	0,8579	-12,03				

v	σ'_c [kPa]	cyc n°	frequenza [hertz]	esa (%)	ϵ_a max [%]	Dev max [kPa]	ϵ_a min [%]	Dev min [kPa]	evaluated through GS				evaluated through LDT			
									strain rate [%/min]	E [MPa]	cor.Coef.	D [%]	strain rate [%/min]	E [MPa]	cor.Coef.	D [%]
SP08																
2,1797	100	1	0,068013	0,003180	0,00424	5,71	-0,00212	-2,76	0,051914	105,60	0,93457	1,23				
2,1797	100	2	0,049162	0,003446	0,00467	5,25	-0,00222	-2,91	0,040653	119,70	0,95526	1,51				
2,1797	100	3	0,029010	0,003204	0,00429	5,87	-0,00212	-2,76	0,022310	111,88	0,91516	0,84				
2,1797	100	4	0,107051	0,003012	0,00429	5,41	-0,00173	-2,76	0,077379	115,98	0,95561	2,07				
2,1795	100	1	0,003516	0,002361	0,00390	4,94	-0,00082	-2,14	0,001992	111,46	0,91299	-1,44				
2,1795	100	2	0,003549	0,003156	0,00400	4,64	-0,00231	-2,76	0,002689	113,31	0,92815	0,04				
2,1795	100	3	0,007233	0,002988	0,00429	5,10	-0,00169	-2,45	0,005186	114,92	0,92804	1,34				
2,1795	100	4	0,007442	0,002795	0,00414	5,25	-0,00145	-2,45	0,004992	103,94	0,91591	2,35				
2,1795	100	5	0,046964	0,002361	0,00347	4,64	-0,00125	-2,14	0,026615	121,00	0,97018	-0,23				
2,1795	100	6	0,008561	0,002650	0,00347	4,79	-0,00183	-2,30	0,005446	120,66	0,96524					
2,1794	100	1	0,000428	0,002764	0,00457	4,84	-0,00096	-2,01	0,000284	105,12	0,86361	4,04				
2,1794	100	2	0,000533	0,002404	0,00437	4,68	-0,00043	-2,63	0,000307	115,04	0,93078	5,27				
2,1794	100	3	0,000616	0,002259	0,00586	5,15	0,00135	-2,16	0,000334	111,16	0,93544	7,75				
2,1794	100	4	0,000477	0,002860	0,00721	4,84	0,00149	-2,16	0,000328	113,44	0,92688	4,44				
2,1794	100	5	0,000396	0,003077	0,00692	5,00	0,00077	-2,32	0,000292	110,95	0,92638	2,88				
2,1794	100	6	0,000436	0,003221	0,00711	5,00	0,00067	-2,16	0,000337	107,25	0,92768	0,95				
2,1794	100	7	0,000534	0,002788	0,00659	4,84	0,00101	-1,85	0,000357	108,01	0,90985	3,15				
SP09																
2,1795	100	1	0,011329	0,010367	0,01179	10,15	-0,00894	-10,76	0,028187	90,11	0,99388	4,08				
2,1795	100	2	0,011094	0,010391	0,01208	9,66	-0,00870	-10,92	0,027666	91,99	0,9936	3,04				
2,1795	100	3	0,011348	0,010343	0,01237	9,99	-0,00831	-10,76	0,028168	91,77	0,9945	3,02				
2,1795	100	4	0,010924	0,010608	0,01295	9,82	-0,00826	-10,92	0,027814	92,38	0,99455	2,92				
2,1795	100	5	0,011188	0,010415	0,01310	9,82	-0,00773	-10,76	0,027965	90,44	0,99401	3,06				
2,1795	100	6	0,011500	0,010173	0,01261	9,33	-0,00773	-10,76	0,028079	92,05	0,99496	2,85				
2,1795	100	7	0,011039	0,010439	0,01310	10,15	-0,00778	-10,76	0,027657	91,68	0,99383	2,81				
2,1795	100	8	0,010864	0,010681	0,01387	9,82	-0,00749	-10,27	0,027849	90,81	0,99454	2,59				
2,1800	100	1	0,004443	0,024962	0,02977	19,62	-0,02015	-20,73	0,026619	79,27	0,99572	6,98				
2,1800	100	2	0,004328	0,025131	0,03035	19,78	-0,01991	-21,06	0,026101	77,50	0,99735	6,16				
2,1800	100	3	0,004186	0,026097	0,03209	19,78	-0,02010	-21,06	0,026219	75,75	0,99794	5,71				
2,1800	100	4	0,004133	0,025928	0,03219	19,29	-0,01967	-20,73	0,025717	75,78	0,99777	5,80				
2,1800	100	5	0,004175	0,026049	0,03223	19,46	-0,01986	-21,06	0,026103	74,84	0,99768	5,81				
2,1800	100	6	0,004158	0,026218	0,03306	19,46	-0,01938	-20,57	0,026162	74,10	0,99759	5,61				
2,1800	100	7	0,004049	0,026967	0,03470	19,95	-0,01923	-21,39	0,026206	73,16	0,99782	5,26				
2,1800	100	8	0,004014	0,027185	0,03528	19,62	-0,01909	-20,89	0,026187	72,97	0,99759	5,16				
2,1800	100	9	0,004040	0,027064	0,03504	19,29	-0,01909	-21,06	0,026241	72,45	0,9979	5,10				
2,1871	100	1	0,001979	0,046873	0,05678	29,84	-0,03697	-30,81	0,022265	63,73	0,99502	8,97				
2,1871	100	2	0,001852	0,048564	0,06011	30,33	-0,03702	-31,30	0,021590	61,15	0,99707	7,96				
2,1871	100	3	0,001885	0,049096	0,06243	30,17	-0,03576	-30,48	0,022209	59,19	0,99707	7,73				
2,1871	100	4	0,001855	0,049869	0,06480	29,84	-0,03494	-30,64	0,022202	58,59	0,99724	7,71				
2,1871	100	5	0,001792	0,051246	0,06669	29,84	-0,03581	-31,14	0,022036	57,80	0,99746	7,27				
2,1871	100	6	0,001792	0,051923	0,06920	29,84	-0,03465	-								

v	σ'_c [kPa]	cyc n°	evaluated through GS								evaluated through LDT					
			frequenza [hertz]	esa (%)	ϵ_a max [%]	Dev max [kPa]	ϵ_a min [%]	Dev min [kPa]	strain rate [%/min]	E [MPa]	cor.Coef.	D [%]	strain rate [%/min]	E [MPa]	cor.Coef.	D [%]
2,1858	100	5	0,001091	0,096573	0,11588	39,48	-0,07727	-40,83	0,025291	40,45	0,99561	10,03				
2,1858	100	6	0,001058	0,100826	0,11844	39,65	-0,08321	-41,32	0,025597	38,94	0,9955	9,95				
2,1858	100	7	0,001034	0,103749	0,12385	40,14	-0,08365	-41,32	0,025758	37,61	0,99541	9,97				
2,1858	100	8	0,001001	0,108147	0,12632	39,97	-0,08998	-41,16	0,025991	36,17	0,99521	9,83				
2,1858	100	9	0,000989	0,110684	0,12839	39,81	-0,09297	-41,49	0,026266	35,15	0,99498	9,90				
2,1833	100	1	0,000511	0,241542	0,23050	60,37	-0,25258	-61,44	0,029599	26,88	0,97683	16,06				
2,1833	100	2	0,000403	0,313302	0,25935	61,01	-0,36725	-61,68	0,030278	20,01	0,98438	15,93				
2,1833	100	3	0,000319	0,402312	0,29980	60,33	-0,50483	-61,60	0,030807	15,20	0,98408	16,23				
2,1833	100	4	0,000246	0,526889	0,37093	60,45	-0,68285	-61,38	0,031149	11,62	0,9846	15,81				
2,1833	100	5	0,000196	0,665817	0,45119	59,91	-0,88044	-61,17	0,031307	9,03	0,98083	15,68				
SP11																
2,2440	100	1	0,030843	0,003227	0,00206	2,17	-0,00440	-5,78	0,023888	101,07	0,95245	0,90				
2,2440	100	2	0,025901	0,003418	0,00258	2,33	-0,00426	-6,11	0,021250	110,72	0,95798	0,68				
2,2440	100	3	0,026924	0,003395	0,00296	2,50	-0,00383	-6,43	0,021934	106,21	0,93963	2,54				
2,2440	100	4	0,025675	0,003586	0,00339	2,82	-0,00378	-5,78	0,022096	103,00	0,95765	0,99				
2,2440	100	5	0,025462	0,003562	0,00325	2,50	-0,00387	-5,94	0,021766	107,28	0,96415	2,06				
2,2440	100	6	0,027394	0,003610	0,00349	2,82	-0,00373	-5,62	0,023731	107,15	0,96334	0,63				
2,2433	100	1	0,003305	0,003155	0,00440	2,33	-0,00191	-5,62	0,002503	107,51	0,92674	3,18				
2,2433	100	2	0,003391	0,003131	0,00449	2,01	-0,00177	-5,94	0,002549	96,93	0,8787	2,67				
2,2433	100	3	0,005072	0,003036	0,00492	2,01	-0,00115	-5,62	0,003696	106,98	0,95941	3,67				
2,2433	100	4	0,003351	0,003299	0,00526	2,17	-0,00134	-5,78	0,002653	102,33	0,95155					
2,2433	100	5	0,003495	0,003179	0,00535	2,01	-0,00100	-5,62	0,002666	99,80	0,93578	3,20				
2,2433	100	6	0,003656	0,003155	0,00588	2,17	-0,00043	-5,30	0,002768	101,90	0,94642					
2,2433	100	1	0,000895	0,002462	0,00473	1,52	-0,00019	-5,94	0,000529	112,08	0,95421	9,48				
2,2433	100	2	0,000601	0,002749	0,00813	2,17	0,00263	-5,46	0,000397	92,17	0,9549	16,13				
2,2433	100	3	0,000425	0,002964	0,01080	1,85	0,00488	-5,46	0,000302	91,61	0,94393	11,53				
2,2433	100	4	0,000442	0,003107	0,01410	1,85	0,00789	-5,46	0,000330	93,54	0,9178	11,34				
2,2433	100	5	0,000409	0,002892	0,01573	2,01	0,00994	-5,62	0,000284	95,26	0,90184	10,25				
2,2433	100	6	0,000583	0,002510	0,01769	1,85	0,01267	-5,62	0,000351	99,99	0,94838					
AIRPO1																
3,1805	20	1	0,009957	0,005472	0,43426	2,49	0,42332	-3,27	0,013076	21,28	0,87346	64,81				
3,1799	20	2	0,007941	0,007625	0,45462	2,33	0,43937	-3,43	0,014530	20,24	0,88517	44,54				
3,1618	30	1	0,011184	0,006019	0,728367	2,17	0,71633	-3,77	0,016157	23,21	0,87389	59,48				
3,1612	30	2	0,010112	0,006566	0,741427	2,17	0,72829	-3,44	0,015937	24,79	0,88224	37,30				
3,1608	30	3	0,010591	0,006092	0,752371	2,66	0,74019	-3,94	0,015485	26,66	0,8864	28,09				
3,1418	40	1	0,014068	0,004195	0,989202	2,17	0,98081	-3,95	0,014164	32,76	0,90274	37,98				
3,1413	40	2	0,013631	0,004451	1,001022	2,17	0,99212	-3,95	0,014560	30,91	0,89537	25,28				
3,1266	50	1	0,016759	0,003611	1,212097	2,34	1,20487	-3,79	0,014526	34,58	0,87907	44,53				
3,1260	50	2	0,016862	0,003648	1,222676	2,18	1,21538	-3,29	0,014763	35,78	0,89666	22,83				
3,1255	50	3	0,013969	0,004524	1,233766	2,51	1,22472	-3,46	0,015167	34,12	0,88387	30,68				
3,1217	50	1	0,111843	0,005290	0,011455	3,21	0,00088	-4,00	0,141983	50,33	0,93459	7,82				
3,1217	50	2	0,107861	0,005472	0,011382	2,87	0,00044	-3,84	0,141656	47,91	0,92694	3,90				
3,1217	50	3	0,079532	0,006275	0,01393											

v	σ'_c [kPa]	cyc n°	frequenza [hertz]	esa (%)	ε_a max [%]	Dev max [kPa]	ε_a min [%]	Dev min [kPa]	evaluated through GS				evaluated through LDT			
									strain rate [%/min]	E [MPa]	cor.Cof.	D [%]	strain rate [%/min]	E [MPa]	cor.Cof.	D [%]
2,8343	30	4	0,008653	0,007649	0,786177	3,10	0,77088	-2,72	0,015885	22,92	0,8834	38,08				
2,8115	40	1	0,030501	0,001687	1,018476	2,61	1,01510	-2,73	0,012349	24,40	0,79003	243,09				
2,8106	40	2	0,039259	0,001334	1,034559	2,78	1,03189	-2,56	0,012566	24,94	0,76724	224,60				
2,8101	40	3	0,012204	0,006198	1,052759	2,94	1,04036	-2,73	0,018152	25,44	0,87823	29,80				
2,8093	40	4	0,010463	0,007061	1,064292	2,78	1,05017	-3,23	0,017730	26,93	0,82683	27,77				
2,7904	50	1	0,012804	0,005296	1,293689	3,12	1,283097	-2,57	0,016273	24,31	0,77485	137,41				
2,7901	50	2	0,013725	0,005610	1,302554	3,28	1,291335	-2,90	0,018477	30,72	0,91119	41,83				
2,7896	50	3	0,013059	0,006198	1,310556	3,45	1,298161	-3,57	0,019425	29,71	0,90463	29,12				
2,7893	50	4	0,014129	0,004982	1,318009	3,12	1,308045	-2,74	0,016892	30,03	0,8072					
2,7745	60	1	0,014136	0,004982	1,529361	3,12	1,519398	-2,74	0,016902	32,55	0,81345					
2,7742	60	2	0,015552	0,004903	1,537128	3,12	1,527321	-2,57	0,018302	34,15	0,85183					
2,7740	60	3	0,014131	0,005100	1,542463	3,29	1,532264	-3,08	0,017295	34,44	0,84257	26,35				
2,7737	60	4	0,013069	0,005492	1,549602	3,12	1,538619	-2,57	0,017225	31,22	0,81639	31,76				
2,7603	70	1	0,018640	0,003962	1,73428	2,63	1,726356	-2,75	0,017725	40,15	0,8753	32,43				
2,7600	70	2	0,016447	0,004158	1,741027	3,13	1,732711	-2,41	0,016412	40,62	0,84948	28,33				
2,7597	70	3	0,018061	0,004237	1,745891	3,13	1,737418	-2,41	0,018364	40,16	0,86362	21,77				
2,7597	70	4	0,013403	0,004472	1,749186	3,13	1,740243	-2,91	0,014384	39,30	0,87445	19,19				
2,7477	80	1	0,020078	0,003374	1,914487	2,97	1,90774	-3,09	0,016256	46,65	0,85907	27,03				
2,7475	80	2	0,017516	0,003570	1,919821	2,97	1,912682	-2,75	0,015006	49,66	0,87465	20,88				
2,7473	80	3	0,016474	0,004040	1,924528	2,80	1,916448	-2,75	0,015974	43,37	0,80205	24,43				
2,7472	80	4	0,017588	0,003452	1,928059	3,14	1,921155	-2,25	0,014571	47,41	0,88561	27,89				
2,7369	90	1	0,021106	0,002785	2,072726	2,47	2,067156	-2,42	0,014108	56,82	0,87432	17,77				
2,7368	90	2	0,021420	0,002550	2,075158	2,30	2,070059	-2,92	0,013107	57,27	0,79783					
2,7366	90	3	0,018178	0,003334	2,079316	2,97	2,072647	-2,92	0,014546	47,03	0,77955	20,94				
2,7364	90	4	0,016767	0,003491	2,081984	2,97	2,075001	-3,09	0,014049	57,92	0,8777	10,61				
2,7262	100	1	0,017768	0,002707	2,204292	3,14	2,198878	-2,76	0,011542	68,46	0,84801	16,58				
2,7260	100	2	0,018271	0,002589	2,207273	3,14	2,202095	-2,59	0,011352	67,10	0,8518	16,78				
2,7258	100	3	0,018913	0,002942	2,208999	2,81	2,203115	-2,93	0,013354	65,80	0,8625	11,38				
2,7257	100	4	0,027127	0,002040	2,209783	2,64	2,205703	-2,59	0,013281	64,00	0,84126	4,30				
2,7216	100	1	0,018300	0,002864	2,258973	3,15	2,253246	-2,76	0,012576	74,78	0,88168	9,79				
2,7216	100	2	0,018003	0,002824	2,259914	2,81	2,254266	-2,42	0,012203	69,74	0,81038	7,74				
2,7216	100	3	0,020799	0,002628	2,260229	2,81	2,254972	-2,76	0,013120	72,45	0,87743	6,15				
2,7216	100	4	0,019672	0,002550	2,26164	3,32	2,256541	-2,76	0,012037	78,05	0,83392	3,58				
2,7187	100	1	0,017963	0,003021	2,30628	3,15	2,300239	-2,59	0,013022	70,81	0,85496	10,55				
2,7189	100	2	0,015587	0,003099	2,30628	2,81	2,300082	-2,93	0,011593	73,77	0,82136	0,58				
2,7188	100	3	0,017587	0,002667	2,3073	3,32	2,301966	-2,59	0,011259	75,86	0,80196	2,78				
2,7188	100	4	0,018308	0,002707	2,306751	2,98	2,301338	-2,42	0,011893	81,32	0,87968	3,36				
2,7176	100	1	0,019033	0,003021	2,32048	2,81	2,314439	-2,26	0,013798	80,99	0,90878	2,92				
2,7176	100	2	0,019372	0,002550	2,320245	2,64	2,315146	-2,42	0,011854	67,40	0,8303	0,06				
2,7176	100	3	0,023310	0,002118	2,32048	2,30	2,316244	-2,59	0,011851	80,80	0,85447	4,32				
2,7176	100	4	0,020027	0,002432	2,321343	2,98	2,316479	-2,09	0,011689	89,30	0,89508	3,75				

SP13

v	σ'_c [kPa]	cyc n°	evaluated through GS							evaluated through LDT						
			frequenza [hertz]	esa (%)	ϵ_a max [%]	Dev max [kPa]	ϵ_a min [%]	Dev min [kPa]	strain rate [%/min]	E [MPa]	cor.Coeff.	D [%]	strain rate [%/min]	E [MPa]	cor.Coeff.	D [%]
2,2687	73	1	0,004475	0,002616	0,17530	1,94	0,17007	-5,21	0,002809	84,18	0,93526	21,19	0,001741	135,49	0,920791	12,54
2,2687	73	2	0,003749	0,003044	0,17886	1,94	0,17278	-5,21	0,002738	87,69	0,93207	15,24	0,001736	137,21	0,908171	7,73
2,2687	73	3	0,003913	0,002949	0,18081	2,40	0,17492	-5,21	0,002769	97,00	0,94951	9,77	0,001871	145,24	0,942241	5,27
2,2687	73	4	0,003376	0,003448	0,18329	2,56	0,17639	-5,52	0,002794	85,17	0,91805	10,81	0,001785	132,76	0,888315	5,94
2,2644	95	1	0,004501	0,002592	0,24368	2,41	0,23850	-5,06	0,002800	99,73	0,94412	16,84	0,001857	148,12	0,921982	11,04
2,2644	95	2	0,004148	0,003020	0,24606	2,41	0,24002	-5,06	0,003006	101,20	0,94766	6,60	0,001912	154,50	0,926501	4,90
2,2643	95	3	0,004033	0,002996	0,24758	2,41	0,24159	-4,75	0,002900	101,84	0,95608	8,05	0,001971	147,04	0,926081	5,97
2,2643	95	4	0,004229	0,002877	0,24853	2,41	0,24278	-5,22	0,002920	103,62	0,95092	6,71	0,001844	161,16	0,924781	4,67
Sp14																
2,5764	30	1	0,001272	0,005392	0,02993	3,78	0,01914	-3,95	0,003115	57,53	0,96335	13,47	0,001646	108,00	0,956613	10,61
2,5765	30	2	0,001370	0,004917	0,03012	2,54	0,02028	-3,80	0,002999	60,94	0,9571	6,44	0,001616	112,66	0,950456	4,42
2,5766	30	3	0,001268	0,004893	0,03216	3,78	0,02237	-3,34	0,002732	59,25	0,96442	6,64	0,001489	107,08	0,953515	3,42
2,5766	30	4	0,001274	0,005416	0,03197	3,47	0,02114	-4,42	0,003179	66,56	0,95776	6,00	0,001655	125,45	0,938867	3,18
2,5694	50	1	0,003204	0,004014	0,01943	3,63	0,01140	-4,11	0,003086	65,62	0,96288	18,99	0,001827	108,95	0,946528	17,50
2,5693	50	2	0,002940	0,004252	0,02233	3,16	0,01382	-3,49	0,003000	64,44	0,94784	9,26	0,001794	105,65	0,932821	5,97
2,5693	50	3	0,003189	0,004180	0,02375	3,01	0,01539	-3,65	0,003200	68,15	0,9547	7,50	0,001878	113,73	0,936418	5,35
2,5693	50	4	0,002620	0,004442	0,02503	3,47	0,01615	-4,11	0,002793	71,22	0,95852	6,81	0,001712	113,96	0,935883	4,81
2,5620	75	1	0,003649	0,003515	0,01401	3,62	0,00698	-4,26	0,003079	79,70	0,97217	13,65	0,002099	115,44	0,957868	10,04
2,5618	75	2	0,003813	0,002969	0,01520	3,31	0,00926	-3,95	0,002717	85,07	0,96376	11,34	0,001870	121,45	0,941714	5,09
2,5617	75	3	0,003358	0,003610	0,01810	3,62	0,01088	-4,26	0,002910	82,72	0,95718	7,85	0,002008	118,69	0,941294	4,87
2,5617	75	4	0,002868	0,004109	0,02043	3,93	0,01221	-4,57	0,002828	85,68	0,95636	4,85	0,001977	121,25	0,931676	3,20
2,5560	100	1	0,004864	0,002233	0,01321	3,62	0,00874	-4,26	0,002606	98,01	0,94512	10,85	0,001957	129,17	0,932415	10,29
2,5560	100	2	0,004382	0,002755	0,01601	3,16	0,01050	-3,95	0,002898	93,43	0,96384	9,33	0,002043	129,80	0,948718	6,39
2,5559	100	3	0,003606	0,003254	0,01786	3,78	0,01135	-3,80	0,002817	91,32	0,94701	5,47	0,001957	129,17	0,918731	3,44
2,5559	100	4	0,003571	0,003017	0,01853	3,47	0,01249	-4,26	0,002585	94,91	0,95531	5,86	0,001883	129,64	0,933174	2,75
2,5508	125	1	0,004150	0,002850	0,01610	3,78	0,01040	-4,11	0,002839	103,13	0,95818	14,39	0,002142	136,62	0,943248	
2,5508	125	2	0,004397	0,002470	0,01724	3,31	0,01230	-3,95	0,002607	116,35	0,95926	6,88	0,002006	148,11	0,944477	4,50
2,5508	125	3	0,004020	0,002779	0,01853	3,93	0,01297	-3,95	0,002681	112,78	0,9565	4,72	0,002077	145,03	0,950464	3,29
2,5507	125	4	0,003716	0,002755	0,01952	3,47	0,01401	-3,49	0,002457	103,74	0,94927	6,38	0,001870	130,80	0,893044	4,34
2,5466	150	1	0,004857	0,002351	0,01753	3,31	0,01283	-3,80	0,002741	108,11	0,91984	15,66	0,001988	148,70	0,908651	8,83
2,5466	150	2	0,004544	0,002375	0,01886	3,47	0,01411	-3,64	0,002591	116,10	0,94779	6,72	0,001979	151,50	0,930835	5,48
2,5465	150	3	0,004582	0,002494	0,01962	3,47	0,01463	-3,95	0,002743	117,95	0,95494	3,19	0,002011	162,21	0,941150	3,97
2,5465	150	4	0,003767	0,002589	0,02071	3,00	0,01553	-3,80	0,002340	110,08	0,94221	5,34	0,001726	146,33	0,909784	3,55
2,5420	175	1	0,005055	0,002138	0,00917	3,78	0,00489	-4,11	0,002593	131,95	0,96095		0,001995	169,87	0,943502	5,71
2,5421	175	2	0,004476	0,002352	0,01036	3,47	0,00565	-4,11	0,00252							

v	σ'_c [kPa]	cyc n°	evaluated through GS							evaluated through LDT						
			frequenza [hertz]	esa (%)	ϵ_a max [%]	Dev max [kPa]	ϵ_a min [%]	Dev min [kPa]	strain rate [%/min]	E [MPa]	cor.Coeff.	D [%]	strain rate [%/min]	E [MPa]	cor.Coeff.	D [%]
2,5264	275	2	0,005476	0,002043	0,00670	3,31	0,00261	-3,80	0,002684	136,80	0,91333	5,38	0,001861	206,33	0,913674	4,70
2,5264	275	3	0,005825	0,001995	0,00736	3,47	0,00337	-4,11	0,002789	156,71	0,94377	2,07	0,002027	219,66	0,937804	2,86
2,5263	275	4	0,005139	0,001995	0,00774	3,78	0,00375	-4,26	0,002460	167,04	0,92362	1,83	0,001822	239,43	0,933381	2,16
2,5222	300	1	0,008262	0,001208	0,00666	4,09	0,00425	-3,49	0,002395	177,38	0,96105	2,70	0,001896	224,53	0,942993	2,51
2,5222	300	2	0,007269	0,001326	0,00717	3,31	0,00452	-3,80	0,002313	166,60	0,94434	0,78	0,001849	215,50	0,913861	3,37
2,5221	300	3	0,007845	0,001263	0,00756	3,16	0,00503	-3,80	0,002378	178,19	0,9378	2,71	0,001867	229,33	0,906424	1,91
2,5221	300	4	0,010327	0,001189	0,00798	3,16	0,00561	-3,80	0,002946	167,02	0,95827	5,74	0,002164	221,39	0,952974	3,56
2,5213	300	1	0,005306	0,001710	0,00480	3,31	0,00138	-4,42	0,002178	182,77	0,9096	6,13	0,001658	246,11	0,899146	3,69
2,5213	300	2	0,005977	0,001781	0,00542	4,24	0,00185	-4,11	0,002555	169,31	0,94364	-3,06	0,001923	231,11	0,931379	2,38
2,5213	300	3	0,005887	0,001496	0,00584	3,16	0,00285	-3,64	0,002114	191,92	0,93614		0,001826	232,57	0,940602	1,53
2,5212	300	4	0,007420	0,001805	0,00627	3,31	0,00266	-3,95	0,003214	171,43	0,9378	1,16	0,002166	232,72	0,902371	-0,65
2,5208	300	1	0,006421	0,001710	0,00314	3,31	-0,00028	-4,11	0,002635	164,93	0,90827	3,79	0,001854	239,43	0,928225	2,50
2,5208	300	2	0,005997	0,001734	0,00304	3,78	-0,00043	-3,65	0,002496	192,03	0,94131	0,01	0,001936	245,26	0,923858	2,72
2,5209	300	3	0,005687	0,002138	0,00366	3,16	-0,00062	-3,95	0,002918	160,27	0,94047	2,75	0,001912	248,53	0,930831	2,96
2,5208	300	4	0,005437	0,001853	0,00328	3,16	-0,00043	-4,11	0,002418	162,38	0,90957	1,56	0,001919	224,20	0,913604	3,10
2,5201	300	1	0,009022	0,001220	0,00214	3,31	-0,00030	-3,34	0,002642	162,48	0,95722	3,67	0,001769	242,55	0,931253	2,12
2,5201	300	2	0,008268	0,001181	0,00194	3,00	-0,00043	-3,64	0,002344	184,30	0,90151		0,001844	228,22	0,875525	-0,90
2,5200	300	3	0,007831	0,001298	0,00227	3,16	-0,00033	-3,80	0,002439	172,27	0,91435	2,23	0,001825	229,92	0,891764	1,73
2,5197	300	1	0,006664	0,001663	0,00347	3,47	0,00014	-3,80	0,002659	168,82	0,93782	0,39	0,001754	253,74	0,935219	0,28
2,5198	300	2	0,005586	0,001829	0,00366	3,47	0,00000	-3,64	0,002452	180,14	0,94577	1,80	0,001739	258,09	0,920643	1,16
2,5199	300	3	0,005995	0,001615	0,00304	3,47	-0,00019	-3,95	0,002324	210,83	0,92856	0,06	0,001705	289,20	0,908348	-2,59
2,5200	300	4	0,006675	0,001781	0,00352	3,62	-0,00005	-3,65	0,002854	181,01	0,95153	-6,63	0,002102	259,14	0,949622	0,68
2,5196	300	1	0,009363	0,001099	0,00172	3,00	-0,00048	-3,64	0,002470	214,61	0,94779	1,73	0,002243	261,45	0,935579	-2,32
2,5196	300	2	0,010925	0,001297	0,00201	3,00	-0,00059	-3,80	0,003401	204,25	0,94854	1,64	0,002653	261,67	0,953495	-0,46
2,5196	300	3	0,016913	0,001249	0,00199	3,00	-0,00051	-3,64	0,005070	198,19	0,94767	-0,23	0,003576	268,20	0,971328	1,56
2,5197	300	4	0,009693	0,001367	0,00212	3,00	-0,00061	-3,64	0,003180	181,91	0,96032	-2,12	0,002473	244,69	0,930314	0,47
Airp03																
3,21410	20	1	0,003715	0,018429	0,28203	2,76	0,24517	-2,77	0,016433	9,32	0,99237	111,52				
3,21410	20	2	0,003708	0,018843	0,30496	2,79	0,26727	-2,76	0,016768	10,94	0,98946	27,96				
3,21410	20	3	0,003840	0,018093	0,31826	2,71	0,28208	-2,74	0,016672	11,66	0,99162	21,23				
3,21410	20	4	0,003664	0,018740	0,32996	2,77	0,29248	-2,80	0,016478	11,80	0,99342	17,57				
Airp04																
2,8975	17	1	0,004830	0,014487	0,03542	3,07	0,00644	-3,08	0,016794	16,51	0,01679	22,74				
2,8974	17	2	0,004731	0,015068	0,04343	3,11	0,01330	-3,07	0,017108	17,63	0,01711	12,83				
2,8974	17	3	0,004702	0,014894	0,04790	3,00	0,01812	-3,05	0,016807	18,05	0,01681	11,00				
2,8974	17	4	0,004830	0,014545	0,05255	3,04	0,02346	-3,00	0,016861	18,23	0,01686	11,57				
2,8855	29	1														

v	σ'_c [kPa]	cyc n°	frequenza [hertz]	esa (%)	ε_a max [%]	Dev max [kPa]	ε_a min [%]	Dev min [kPa]	evaluated through GS				evaluated through LDT			
									strain rate [%/min]	E [MPa]	cor.Coef.	D [%]	strain rate [%/min]	E [MPa]	cor.Coef.	D [%]
2,8486	49	3	0,008659	0,008594	0,81046	3,06	0,79327	-3,06	0,017859	30,81	0,99561	9,45				
2,8484	49	4	0,008804	0,008448	0,81365	3,06	0,79676	-3,08	0,017851	31,50	0,99545	9,22				
Airp06																
2,9919	10,5	1	0,002808	0,025121	0,03969	3,07	-0,01055	-3,00	0,016930	10,13	0,99216	17,35				
2,9910	10,5	2	0,002678	0,026646	0,04837	3,09	-0,00492	-2,97	0,017125	10,25	0,99567	11,22				
2,9903	10,5	3	0,002638	0,027056	0,05581	3,05	0,00170	-2,97	0,017128	10,24	0,99557	10,47				
2,9897	10,5	4	0,002580	0,027848	0,061499	3,04	0,00580	-3,00	0,017242	9,97	0,9958	9,99				
2,9645	20	1	0,004565	0,016738	0,017442	3,09	-0,01603	-3,02	0,018337	13,16	0,98693	36,46				
2,9639	20	2	0,004496	0,016767	0,030657	3,04	-0,00288	-2,99	0,018093	14,67	0,99192	18,29				
2,9634	20	3	0,004398	0,016973	0,04135	3,09	0,00740	-2,95	0,017914	14,87	0,99337	16,40				
2,9632	20	4	0,004354	0,017149	0,050331	3,04	0,01603	-2,94	0,017919	15,13	0,99382	14,94				
2,9628	20	5	0,004270	0,017390	0,058925	3,00	0,02415	-2,89	0,017822	15,38	0,99527	13,74				
Airp07																
3,0186	16,5	1	0,011051	0,004507	0,02611	2,02	0,03512	-3,06	0,011953	15,30	0,53344					
3,0179	16,5	2	0,012647	0,004369	0,06793	2,70	0,05919	-3,06	0,013262	28,29	0,85794	124,50				
3,0175	16,5	3	0,009742	0,006073	0,08447	2,53	0,07233	-3,22	0,014199	29,11	0,89055	49,04				
3,0175	16,5	4	0,007652	0,007475	0,09695	3,04	0,08200	-3,73	0,013727	27,26	0,82493	24,28				
2,9989	24,2	1	0,011094	0,005743	0,05386	2,52	0,04237	-2,88	0,015292	26,24	0,90908	112,88				
2,9981	24,2	2	0,011811	0,005441	0,064413	2,69	0,05353	-3,05	0,015423	28,93	0,92042	23,23				
2,9975	24,2	3	0,012291	0,005194	0,073316	2,86	0,06293	-3,05	0,015320	26,76	0,9215	37,11				
2,9434	49	1	0,015069	0,004204	0,033031	3,32	0,02462	-4,01	0,015205	37,53	0,94306	108,93				
2,9427	49	2	0,010691	0,006183	0,048804	3,49	0,03644	-4,01	0,015865	40,20	0,93447	37,21				
2,9422	49	3	0,011496	0,005633	0,055674	3,49	0,04441	-4,18	0,015543	39,24	0,94772	29,19				
2,9417	49	4	0,008229	0,007035	0,066336	3,16	0,05227	-4,51	0,013893	38,68	0,95233	22,04				
2,9010	74	1	0,015398	0,004205	0,016983	3,17	0,00857	-4,19	0,015538	54,70	0,96428	38,46				
2,9006	74	2	0,013923	0,005084	0,025501	3,67	0,01533	-3,86	0,016988	54,54	0,96529	19,14				
2,9003	74	3	0,013063	0,004534	0,030778	3,17	0,02171	-3,69	0,014215	50,81	0,92531	23,53				
2,9001	74	4	0,013069	0,005111	0,035889	3,17	0,02567	-3,69	0,016032	52,42	0,9595	14,98				
2,8695	99	1	0,015396	0,003847	0,011542	3,66	0,00385	-3,84	0,014216	66,00	0,96178	22,29				
2,8694	99	2	0,015959	0,003298	0,01396	2,83	0,00736	-4,34	0,012631	80,84	0,97232	11,31				
2,8691	99	3	0,014445	0,003682	0,018796	3,49	0,01143	-3,84	0,012766	66,79	0,89068	15,56				
2,8689	99	4	0,016438	0,003215	0,021379	3,33	0,01495	-3,34	0,012684	68,66	0,95316	24,19				
2,8648	99	1	0,015589	0,003765	0,009013	3,32	0,00148	-4,67	0,014085	79,61	0,96454	6,41				
2,8649	99	2	0,013652	0,003902	0,010607	3,16	0,00280	-4,01	0,012786	79,44	0,96642	2,97				
2,8648	99	3	0,013724	0,003463	0,010662	3,16	0,00374	-4,17	0,011405	86,00	0,92035	3,15				
2,8647	99	4	0,015687	0,003490	0,011651	3,16	0,00467	-4,34	0,013139	84,33	0,95498	4,23				
2,8607	99	1	0,016471	0,003243	0,007035	2,99	0,00055	-3,51	0,012818	86,28	0,96387	1,00				
2,8607	99	2	0,015061	0,003682	0,007914	3,32	0,00055	-3,84	0,013310	82,90	0,93334	4,47				
2,8606	99	3	0,016126	0,003215	0,008079	3,65	0,00165	-3,67	0,012444	94,62	0,95733	2,20				
2,8606	99	4	0,013818	0,003407	0,008848	4,32	0,00203	-3,67	0,011300	97,02	0,90895	3,38				
Airp08																
2,9622	16	1	0,003095	0,023024	0,05689	3,00	0,01084									

v	σ'_c [kPa]	cyc n°	evaluated through GS								evaluated through LDT					
			frequenza [hertz]	esa (%)	ϵ_a max [%]	Dev max [kPa]	ϵ_a min [%]	Dev min [kPa]	strain rate [%/min]	E [MPa]	cor.Coeff.	D [%]	strain rate [%/min]	E [MPa]	cor.Coeff.	D [%]
2,8578	26,5	1	0,007570	0,009134	0,089572	2,06	0,07131	-2,09	0,016594	13,88	0,98678	112,84				
2,8565	26,5	2	0,007091	0,009838	0,108251	2,11	0,08857	-2,02	0,016744	15,37	0,99008	32,82				
2,8560	26,5	3	0,007157	0,009721	0,11988	2,04	0,10044	-2,02	0,016698	15,98	0,99032	24,63				
2,8554	26,5	4	0,007243	0,009251	0,128514	2,02	0,11001	-2,02	0,016081	16,90	0,99106	21,90				
2,8367	34	1	0,009311	0,006549	0,050102	2,11	0,03700	-2,02	0,014635	19,56	0,98836	80,37				
2,8360	34	2	0,009022	0,006813	0,061908	2,11	0,04828	-2,07	0,014753	21,81	0,99019	28,53				
2,8354	34	3	0,008976	0,006843	0,070953	2,10	0,05727	-2,02	0,014741	23,81	0,99293	21,97				
2,8350	34	4	0,009009	0,006784	0,07806	2,11	0,06449	-2,04	0,014667	23,92	0,99178	20,26				
Airp10																
2,8419	25	1	0,011065	0,006307	0,05009	3,03	0,03748	-2,19	0,016749	23,71	0,89069	193,51				
2,8412	25	2	0,026843	0,001992	0,05377	2,86	0,04979	-2,54	0,012831	33,31	0,84961	88,07				
2,8407	25	3	0,018132	0,003018	0,06506	3,21	0,05902	-2,54	0,013132	32,59	0,87672	30,96				
2,8403	25	4	0,009350	0,007001	0,08504	3,73	0,07103	-2,71	0,015710	33,32	0,9007	39,26				
2,7844	50	1	0,012829	0,005643	0,020339	4,36	0,00905	-2,33	0,017374	35,20	0,86486	38,26				
2,7842	50	2	0,012543	0,005613	0,026012	4,19	0,01479	-2,85	0,016896	40,52	0,8827	22,27				
2,7841	50	3	0,014365	0,004889	0,030116	3,85	0,02034	-2,16	0,016854	43,79	0,84496	15,45				
2,7839	50	4	0,010796	0,006065	0,035065	4,02	0,02293	-2,68	0,015716	44,43	0,89867	13,91				
2,7412	75	1	0,017527	0,003802	0,011286	3,81	0,00368	-2,31	0,015993	56,04	0,91731	18,42				
2,7410	75	2	0,017493	0,003772	0,013639	3,13	0,00610	-2,14	0,015836	56,32	0,91621	9,89				
2,7408	75	3	0,017762	0,003681	0,015269	3,98	0,00791	-2,48	0,015694	64,93	0,89319	4,66				
2,7406	75	4	0,016062	0,004315	0,019373	4,15	0,01074	-1,97	0,016635	56,74	0,89822	10,78				
2,7048	100	1	0,013467	0,004466	0,01201	4,78	0,00308	-3,63	0,014435	72,32	13,4491	3,00				
2,7048	100	2	0,013531	0,004225	0,015088	4,78	0,00664	-3,13	0,013720	77,34	9,14669	2,94				
2,7047	100	3	0,011923	0,004828	0,017442	5,12	0,00779	-3,80	0,013816	75,95	7,30479	2,90				
2,7046	100	4	0,036069	0,004738	0,019916	4,95	0,01044	-3,97	0,041012	91,90	7,67491	2,92				
2,7003	100	1	0,015096	0,003953	0,007423	4,95	-0,00048	-2,96	0,014322	83,03	0,95209	9,58				
2,7001	100	2	0,011582	0,004647	0,009294	5,11	0,00000	-2,96	0,012917	75,63	0,90415	6,24				
2,6999	100	3	0,010547	0,004436	0,010743	4,78	0,00187	-3,46	0,011229	97,71	0,94695	2,84				
2,6999	100	4	0,011526	0,004496	0,011346	4,95	0,00235	-3,13	0,012437	89,02	0,93992	4,42				
2,6957	100	1	0,012622	0,004285	0,007363	5,11	-0,00121	-2,95	0,012980	83,03	0,94383	5,86				
2,6957	100	2	0,011394	0,004587	0,007967	4,77	-0,00121	-3,29	0,012543	85,41	0,93585	2,85				
2,6956	100	3	0,012078	0,004376	0,008449	4,77	-0,00030	-3,46	0,012684	91,16	0,93839	3,04				
2,6955	100	4	0,012473	0,004406	0,00857	4,61	-0,00024	-3,46	0,013189	84,32	0,91438	4,46				
2,6923	100	1	0,012539	0,003893	0,00688	4,77	-0,00090	-3,12	0,011715	92,95	0,92896	4,86				
2,6922	100	2	0,014050	0,004104	0,007725	4,60	-0,00048	-3,12	0,013838	93,44	0,96871	2,74				
2,6922	100	3	0,013444	0,004255	0,008208	4,43	-0,00030	-3,12	0,013729	89,18	0,93277	1,49				
2,6922	100	4	0,014646	0,003893	0,00851	4,94	0,00072	-2,95	0,013684	91,63	0,96343	3,43				
2,6904	100	1	0,014294	0,004134	0,005975	5,10	-0,00229	-3,12	0,014182	93,24	0,94909	2,67				
2,6903	100	2	0,015509	0,003983	0,005794	4,77	-0,00217	-3,45	0,014825	98,01	0,93221	3,78				
2,6903	100	3	0,022490	0,003923	0,006276	5,10	-0,00157	-3,12	0,021174	99,47	0,96749	2,65				
2,6904	100	4	0,015234	0,003470	0,005794	4,60	-0,00115	-3,12	0,012687	94,57	0,95246	1,39				
Nat02																
2,2940	15,7	1	0,0													

v	σ'_c [kPa]	cyc n°	frequenza [hertz]	esa (%)	ε_a max [%]	Dev max [kPa]	ε_a min [%]	Dev min [kPa]	evaluated through GS				evaluated through LDT			
									strain rate [%/min]	E [MPa]	cor.Coef.	D [%]	strain rate [%/min]	E [MPa]	cor.Coef.	D [%]
2,5170	12,5	2	0,003779	0,016306	0,03003	1,28	-0,00258	-1,44	0,014789	7,85	0,99593	5,98				
2,5173	12,5	3	0,003848	0,016073	0,03044	1,26	-0,00171	-1,43	0,014844	7,90	0,9961	5,29				
2,5175	12,5	4	0,003868	0,015996	0,03204	1,29	0,00005	-1,38	0,014849	7,92	0,99663	5,41				
2,5104	20	1	0,005662	0,010983	0,03215	1,21	0,01018	-1,37	0,014925	9,63	0,99484	16,04				
2,5106	20	2	0,005403	0,011293	0,03654	1,25	0,01395	-1,43	0,014644	10,69	0,99485	9,09				
2,5107	20	3	0,005571	0,010879	0,03861	1,25	0,01685	-1,33	0,014545	10,79	0,99639	7,27				
2,5108	20	4	0,005333	0,011086	0,04088	1,28	0,01871	-1,39	0,014188	11,08	0,9959	6,78				
Wettp01																
2,9185	12,7	1	0,002877	0,024579	0,188231	1,61	0,139073	-1,62	0,016972	4,27	0,98638	94,30				
2,9217	12,7	2	0,002222	0,031869	0,206767	1,61	0,14303	-1,61	0,016996	4,67	0,99156	10,42				
2,9249	12,7	3	0,002718	0,026096	0,200155	1,62	0,147962	-1,65	0,017026	5,40	0,99092	12,99				
2,8846	20	1	0,005432	0,012222	0,088452	1,57	0,064008	-1,62	0,015932	7,85	0,98456	91,10				
2,8832	20	2	0,005714	0,011897	0,109481	1,61	0,085688	-1,66	0,016315	9,04	0,98289	37,10				
2,8823	20	3	0,005528	0,011978	0,126337	1,60	0,102381	-1,60	0,015892	9,47	0,9865	30,05				
Wettp03																
2,9611	13,5	1	0,010032	0,006496	0,168022	0,87	0,155031	-0,73	0,015640	5,90	0,97594	283,15				
2,9591	13,5	2	0,009656	0,006821	0,188971	0,87	0,17533	-0,75	0,015806	6,74	0,9687	61,90				
2,9583	13,5	3	0,009712	0,006929	0,2077	0,79	0,193843	-0,73	0,016150	6,66	0,97609	55,02				
2,9306	21,3	1	0,019936	0,003167	0,058353	0,82	0,05202	-0,76	0,015151	10,01	0,96087	228,67				
2,9299	21,3	2	0,014623	0,004872	0,078165	0,86	0,068421	-0,76	0,017098	10,12	0,98098	60,13				
2,9294	21,3	3	0,016637	0,004845	0,092672	0,88	0,082983	-0,81	0,019345	10,32	0,98198	53,78				
Wettp05																
3,0522	10,5	1	0,009131	0,007171	0,054923	0,40	0,040582	-0,64	0,015714	3,98	0,96196	60,80				
3,0507	10,5	2	0,007769	0,008366	0,069956	0,51	0,053224	-0,68	0,015598	4,26	0,9571	30,96				
3,0500	10,5	3	0,008202	0,007941	0,080526	0,44	0,064644	-0,64	0,015631	4,41	0,96058	27,83				
3,0246	15,3	1	0,014189	0,004887	0,033411	0,52	0,023637	-0,67	0,016642	6,47	0,9661	52,99				
3,0245	15,3	2	0,013668	0,005020	0,040582	0,44	0,030543	-0,65	0,016466	6,67	0,96096	23,88				
3,0242	15,3	3	0,012422	0,005471	0,047859	0,52	0,036917	-0,67	0,016311	6,99	0,9592	17,72				
Wettp07																
2,8723	40,5	1	0,023094	0,002340	0,004206	0,93	-0,00047	-0,63	0,012968	27,80	0,95301	4,04				
2,8723	40,5	2	0,021916	0,002498	0,004417	0,97	-0,00058	-0,63	0,013137	26,98	0,94896	3,19				
2,8723	40,5	3	0,021640	0,002498	0,004522	0,99	-0,00047	-0,63	0,012971	28,99	0,94812	3,51				
2,8723	40,5	4	0,021529	0,002866	0,004943	0,97	-0,00079	-0,65	0,014807	27,09	0,96812	3,08				